Master of Science Thesis

Methodology for Prediction of the Fatigue Life for Lug Joints Subjected to Combined In-Plane and Out-of-Plane Loading

R.C. Kuipers

Faculty of Aerospace Engineering · Delft University of Technology

TU Delft Delft University of Technology

Methodology for Prediction of the Fatigue Life for Lug Joints Subjected to Combined In-Plane and Out-of-Plane Loading

Master of Science Thesis

For obtaining the degree of Master of Science in Aerospace Engineering
at Delft University of Technology

R.C. Kuipers

March 9, 2018

Faculty of Aerospace Engineering · Delft University of Technology

The work in this thesis was supported by GKN Fokker Aerostructures. Their cooperation is gratefully acknowledged.

Delft University of Technology
Faculty of Aerospace Engineering
Department of Aerospace Structures and Materials

GRADUATION COMMITTEE

Dated: March 9, 2018

Chair holder:

Dr.Ir. R.C. (René) Alderliesten

Committee members:

Ir. T. (Tim) Janssen

Dr. C.D.(Calvin) Rans

Dr. B. (Boyang) Chen

Abstract

In aerospace engineering different joining methods are available to assemble the complex structures known as aircraft. One of these methods is the joining via a pin-type joint element, of which one type specifically is the lug joint. Lug joints are used in aircraft for the attachments of flaps and ailerons (aircraft movables) to the wing. With the next-generation aircraft comes the use of new aircraft movables. These new methods for aircraft movables introduce different loads on lugs like oblique- and out-of-plane loads. With the introduction of oblique and lateral (out-of-plane) loads on lugs the need rises for more detailed fatigue life prediction method that take these conditions into account.

Therefore, in light of this need, the thesis research focused on creating a methodology for predicting the fatigue life for lug joints subjected to combined in-plane and out-of-plane loading. The research has been performed in co-operation with GKN Fokker Aerostructures. The current fatigue prediction methods are all based on axially loaded lugs. In concept, this method applies the Larsson relation, which relates the nominal stress of an arbitrary lug to a reference lug through certain correction factors. The nominal stress of the lug is then implemented in S-N curves resulting in the number of cycles till failure (fatigue life). Fokker describes this method in their Technical Handbook 3 (TH3). However, Larsson nor TH3 take oblique and/or out-of-plane loaded lugs into account for the prediction of the fatigue life. Some research has been performed on oblique loaded lugs but the main focus of these studies has been peak stress location and calculation of the Stress Concentration Factor (SCF). Information for out-of-plane loaded lugs has not been found in public reported research.

After performing Finite Element Analyses (FEA) on different loaded lugs a methodology for predicting the fatigue life is proposed. Using ABAQUS/CAE from SIMULIA by Dassault Systèmes a Finite Element (FE) lug model has been created. Using the FE model the stress distribution for in- and/or out-of-plane loaded lugs has been analysed from which the nominal stress of each load case has been determined. By adding taper angle, load angle and lateral loads (out-of-plane component) in the FEA, additional correction factors for the Larsson relation have been proposed to take these parameters into account for the fatigue life prediction.

From the FEA of the axially loaded lugs, the influence of eccentricity on the Larsson relation became apparent. The eccentricity, which is solely defined by the geometry of the lug, required the addition of the eccentricity correction factor K_{ecc}. The analyses on tapered lugs showed that no taper correction factor was required. Changing the load angle in the FEA allowed for the creation of the load angle correction factor K_{α}. To combined in- and out-of-plane loading in the FEA, a lateral load has been added to the FE model. For the combined in- and out-of-plane load a bending factor is introduced. The bending factor is the ratio between the lateral load and the in-plane load. The results of the combined load FEA lead to the creation of the lateral correction factor K_L.

Combining the Larsson relation with the factors K_{ecc}, K_{α}, and K_L resulted in a methodology for predicting the fatigue life for various in- and out-of-plane loaded lugs. Although the method is verified, experimental test have to be performed in order to validate the results and the proposed correction factors. To further expand the research recommendations are made for the inclusion of transverse loaded lugs and the expansion of the out-of-plane load condition in the FEA with the inclusion of variable taper and load angles.

Nomenclature

Abbreviations

3D	Three Dimensional
BC	Boundary Condition
FE	Finite Element
FEA	Finite Element Analyses
HSB	Handbuch Struktur Berechnung
NS	Net Section
SCF	Stress Concentration Factor
TH3	Technical Handbook 3

Greek Symbols

α	Load angle	$^\circ$
β	Taper angle	$^\circ$
γ	Load ratio transferred to another sheet	$-$
δ	Deflection	mm
ϵ	Correction factor	$-$
ζ	Correction factor	$-$
θ	Load angle	$^\circ$
θ	Cycle correction factor	$-$
σ	Stress	MPa
σ_a	Nominal stress of an arbitrary lug	MPa
σ_A	Nominal stress of the reference lug	MPa
σ_{br}	Bearing stress	MPa
σ_{max}	Maximum stress	MPa
σ_{nom}	Nominal stress	MPa
$\sigma_{nom_{ref}}$	Nominal stress of the reference lug	MPa
σ_{peak}	Peak stress	MPa

Roman Symbols

a	Distance between top of the hole edge and the top of the lug	mm
A	Net section area	mm^2
B	Width of the lug	mm
c	Horizontal distance between the side of the lug and the hole edge	mm
d	Diameter of the hole	mm
D	Diameter of the hole	mm
E	Young's modulus	GPa
e	Distance between top of the lug and the centre of the hole	mm
F	Applied load	N
F	Lateral load	N
h	Distance between top of the lug and the centre of the hole	mm
H	Geometry factor	$-$
I	Second moment of area	mm^4
k	Bending factor	$-$
K_{ecc}	Eccentricity correction factor	$-$
K_L	Lateral correction factor	$-$
K_t	Stress concentration factor	$-$
K_{tb}	Bearing stress concentration factor	$-$
$K_{t,br}$	Bearing stress concentration factor	$-$
$K_{t_{hole}}$	Stress concentration factor open hole	$-$
$K_{t_{joint}}$	Stress concentration factor of the joint	$-$
$K_{t,ns}$	Net section stress concentration factor	$-$
$K_{t_{pin}}$	Stress concentration factor pin loaded hole	$-$
K_{t1}	Top side stress concentration factor	$-$
K_{t2}	Bottom side stress concentration factor	$-$
K_α	Load angle correction factor	$-$
K_β	Taper angle correction factor	$-$
k_1	Shape factor	$-$
k_2	Size factor	$-$
L	Length	mm
M	Moment	Nm
N	Number of cycles	$-$
P	Applied load	N
r	Radius	mm
R_i	Hole radius of lug	mm
R_o	Outer radius of lug head	mm
$S_{bending}$	Bending stress	MPa
$S_{tensile}$	Tensile stress	MPa
t	Thickness of the lug	mm
v	Poisson's ratio	$-$
W	Width of the lug	mm

Table of Contents

List of Figures

List of Tables

Preface

Dear Reader,

This thesis report is the conclusion for my master Aerospace Engineering on the University of Technology Delft, the Netherlands. The research topic was provided by Fokker Aerostructures, the Netherlands in collaboration with the university. The research was into the effects of taper angles, load angles and lateral load on the fatigue life of lug joints. For over a year I worked on this topic in providing a preliminary prediction method into the fatigue life of an in- and out-of-plane loaded lug. I want to use this opportunity to thank the people who helped me along the way.

I want to thank my supervisors, Tim Janssen and Guido van Gool from Fokker in providing me with the opportunity to do my thesis work at Fokker. I want to thank them for their support and feedback during my work at the company and for the advise they gave me along the way. I want to thank my supervisor at the university, RenÃľ Alderliesten for his insight on and guidance of my thesis work and for the discussions we had during the meetings. Finally, I would like to thank all my friends and family for their continuous love and support.

I am gratefully for the opportunities I had working on this research project and will take these experiences with me in future endeavours.

Delft, University of Technology — R.C. Kuipers
March 9, 2018

"Slow and steady wins the race."
— *Aesop*

Chapter 1

Introduction

An aircraft is a large complex structure, which consists of many smaller components assembled together. Building an aircraft is based on the principle of joining elements together. In aerospace engineering three joining methods have been widely used throughout the ages. These joining methods are the joining by pin-type elements, the use of adhesive bonding, and welding. For a pin-type joint element there exists a large variety in bolts and rivets that can be used. A special case within the pin joints is a lug joint presented in Figure 1.1 and Figure 1.2. A lug joint is a joint that consists of a single pin and is connected to a 'fork structure' via the pin. This fork structure is also referred to as a female lug. The lug connected to the female lug is referred to as the male lug. While in other pin-type joints the load is carried by and transferred through multiple pins, in a lug joint all the load is carried by and passed through a single pin.

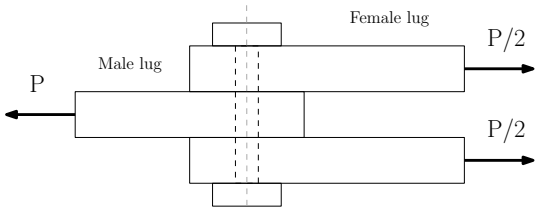

Figure 1.1: Representation of a lug joint

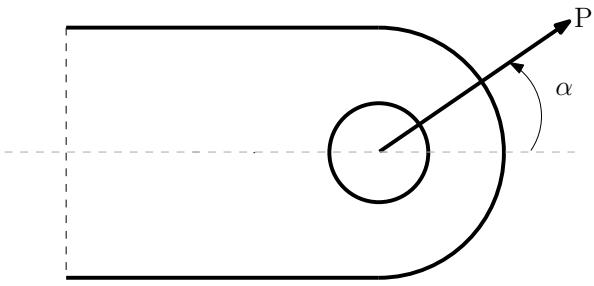

Figure 1.2: Lug with load P acting with load angle α

Some key examples where lug joints are used in aerospace is in the engine pylons for the attachment of the engines, and for connection of ailerons or flaps (aircraft movables) to the wing. The need for more detailed fatigue assessment on lugs rises due to the increasing complexity of aircraft movables in newer aircraft. For example, the new A350 aircraft series of Airbus have new state-of-the-art flaps, which deploy in a 'stream-wise motion'. Stream-wise motion means that the flaps deploy in the direction of the airflow (stream) over the wing.

Figure 1.3 shows the representation of a A350 wing with the locations of the high lift devices. The flaps are directly positioned against the inboard aileron mounted under the same sweep of the trailing edge of the wing. Conventional flaps open in perpendicular direction of the trailing edge sweep angle. The new flaps open in stream-wise direction, meaning they open under an angle compared with the conventional flaps. In Figure 1.3 a representation of the stream-wise flap motion and the conventional motion is displayed.

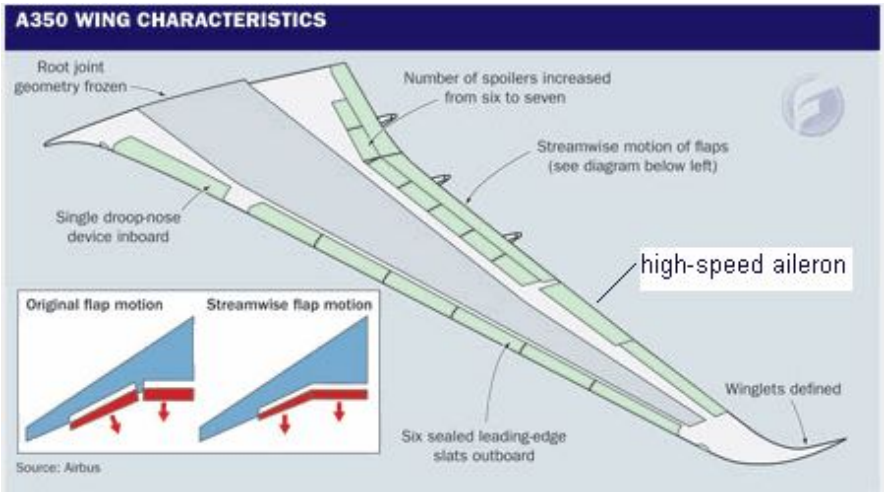

Figure 1.3: Representation of the A350 wing with high lift devices and an illustration about the stream-wise motion[1].

In order to accommodate for this stream-wise motion of the flap, the attachment points of the flap to the wing are not in the same line of action with each other, compared to the conventional flap designs. This misalignment induces oblique and lateral loads on the lug. An oblique load is a load acting under a load angle α measured from the axial direction of the lug. A lateral load is an out-of-plane load acting on the lug. In order for the flaps to extend in a stream-wise-motion, the strut attached to the flaps has to be mounted under an inclination, resulting in a swinging motion. These swinging motions introduce side loads (out-of-plane) on the attachment lugs of the flap and generate small oblique load component as well.

With the increasing complexity of aircraft movables structures the need arises for more detailed fatigue prediction models, which take out-of-plane loads and other (in-plane) load directions into account. The current fatigue life prediction models are based on axially loaded non-tapered lugs. Many studies and experimental testings have been performed on the fatigue life of axially loaded straight-sided lugs [1–15]. The scientific gap lies when the load angle changes and lugs are obliquely loaded or when lugs are laterally loaded. Some research has been performed for changing load angle [16–21] however for laterally loaded lugs no publicly reported research has been found.

[1] URL:http://www.airliners.net/forum/viewtopic.php?t=527647&start=200 [Cited: 12-01-2017]

The objective of the thesis is to create a methodology for predicting the fatigue life for a lug subjected to a combined in-plane and out-of-plane loading. By using a Finite Element (FE) program a preliminary prediction methodology has been proposed, which includes varying lug geometries, load angles, taper angles, and lateral loads.

This report contains the work done and conclusions of the thesis project for the faculty Aerospace Engineering on the Delft University of Technologies in cooperation with GKN Fokker Aerostructures. The report commences with the research questions and objectives in Chapter 2. Following is an overview of the literature review performed for the thesis project in Chapter 3. In Chapter 4 the lug parameters are defined and the FE model for the in-plane and the out-of-plane analyses are presented. The verification of the FE model is found in Chapter 5. Here, the model is compared with two Stress Concentration Factor (SCF) calculation methods, Technical Handbook 3 (TH3) of Fokker and Handbuch Struktur Berechnung (HSB). Then in Chapter 6 the results of Finite Element Analyses (FEA) are introduced in the calculation methods in order to investigate and verify the use of the relations. Load and taper angles are introduced in Chapter 7 and the FEA results are presented. This results in a new proposed relation, which includes effects of taper and load angles. The proposed method is verified with more FEA on lugs subjected to varying load and taper angles in Chapter 8. The Chapters 6 to Chapter 8 all resolve around the in-plane loaded lugs. In Chapter 9 the FEA for out-of-plane loaded lugs are presented. Here, the effects on a lateral load on a lug using the proposed method are discussed and a methodology to include lateral loads is suggested. The conclusions of the thesis project is found in Chapter 10 and recommendations for further research is presented in Chapter 11.

The thesis report includes a variety of appendices. In Appendix A the convergence study for the FE model is presented. Then in Appendix B the results of the TH3 SCF diagrams are replicated to verify the FE model results. The nominal stress calculated from FEA, which are used in the Larsson relation, are shown in Appendix C. The verification of the out-of-plane model is presented in Appendix D. Here, the deflection of the lug is compared with deflections of standard cases. In Appendix E the different Net Section (NS) paths, used to find the nominal stress, of the out-of-plane FEA are presented.

Chapter 2

Research Scope

This chapter contains the research objective and questions for the thesis project. A research road map is presented on procedure of the thesis project. The objective and question have been split in several sub-levels to help obtain the objective or answer the questions.

2.1 Research objective

The research objective is defined as:

Determine a methodology to predict the fatigue life of a lug, which is subjected to combined in-plane and out-of-plane loading by varying the load angle and the shape of the lug by use of finite element analyses.

2.2 Research questions

The research question that needs to be answered, following from the research objective is:

"What are the effects of varying the shape of the lug and the load angle on the fatigue life of a lug, subjected to combined in- and out-of-plane loading?"

2.3 Research approach

In order to find an answer for the research question several sub-questions have been formulated. These sub-questions are listed in Section 2.3.1. The sub-questions act as a guide to check the different sub-objectives, which are formulated to come to the research objective. The sub-objectives serve as the road map for the research procedure on completing the thesis project. The sub-objectives are presented in Section 2.3.2.

2.3.1 Sub-questions

The sub-questions follow from the literature review that has been performed for the thesis project and is presented in Chapter 3. The sub-questions are defined as:

- What are the current prediction methods on the fatigue life of lugs?
- What is the effect of the shape of the lug on the fatigue life?
  - How does varying the ratio $\frac{a}{c}$ influence the fatigue life?
  - How does varying the taper angle influence the fatigue life?
- What is the effect of changing the load angle on the fatigue life of a lug?
- What is the effect of load reversal on a lug?
- What is the effect of an out-of-plane load on the fatigue life of a lug?

2.3.2 Sub-objectives

The sub-questions provide answers to fulfill sub-objectives, which are defined as:

- Define a relation between the stress concentration factor and the fatigue life of a lug.
- Create a finite element model to analyze different in-plane load cases for different lug geometries.
- Define a relation to relate in-plane load cases to the fatigue life
- Create a finite element model to analyze different out-of-plane load cases on a lug.
- Define a relation to relate an in-plane and out-of-plane loaded lug to the fatigue life.

Chapter 3

Literature Review

For the thesis project a literature study has been conducted into the current knowledge of lug joints and defining the scientific gap, which the thesis project addresses. This chapter presents an overview of the literature study performed and provides the background information for the thesis research.

3.1 Lug parameters

Lug joints are a special case of lap joints were the entire load is transferred through a single pin. Lugs are geometrically defined by the following parameters shown in Figure 3.1.

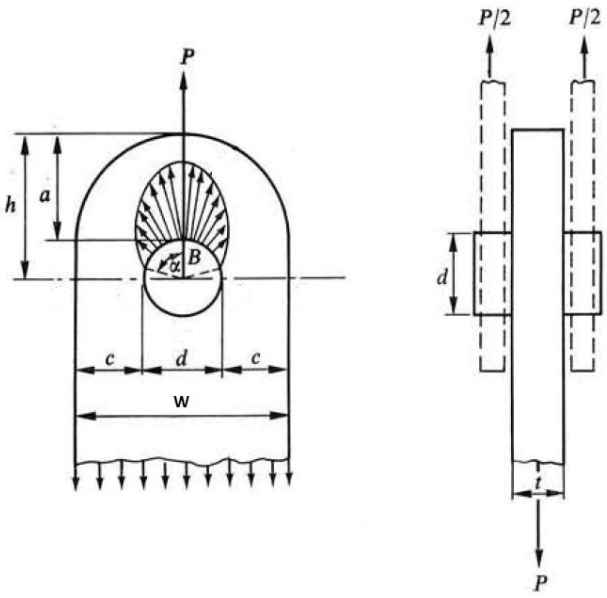

Figure 3.1: Lug parameters and geometry modified from [1].

The lug is loaded with an axial load P. The height of the lug is defined by distance h, width is defined by distance W, and d for the diameter of the hole. The distances a and c are related via the following relations, respectively:

$$a = h - \frac{d}{2}, \quad c = \frac{W - d}{2} \tag{3.1}$$

When the lug is axially loaded stress locations around the hole occur resulting in a peak stress (maximum stress) around the circumference. For axially loaded lugs the peak stress locations are predefined [1, 2, 18]. The peak stresses for an axial load are located at the hole circumference at the dashed line displayed in Figure 3.1. This area for axially loaded lugs is also defined as the net section area. For an axially loaded lug the net section area A is defined by:

$$A = (W - d) \cdot t = 2 \cdot c \cdot t \tag{3.2}$$

Here, the t stands for the thickness of the lug. At the net section area the net section stress is defined. The net section stress is the average of the stress distribution along the net section area. For the remainder of the report the net section stress is referred to as the nominal stress σ_{nom}. The nominal stress is given by:

$$\sigma_{nom} = \frac{P}{A} = \frac{P}{2 \cdot c \cdot t} \tag{3.3}$$

Bear in mind that the net section area changes when the load angle changes. As such the relations presented in Equation 3.2 and Equation 3.3 are for the nominal stress for axially loaded lugs.

Another option to define the stresses on a lug joint is via the radial or bearing stress σ_{br}. The radial pressure caused by the axial load is displayed the marked area in Figure 3.1. The bearing stress is calculated by:

$$\sigma_{br} = \frac{P}{d \cdot t} \tag{3.4}$$

3.2 Load cases

In total four load cases are defined, which are of interested. These cases are the axially, transversely, oblique and laterally loaded lug. It is important to note that axial, transverse and oblique represent an in-plane load condition, while lateral is an out-of-plane load condition.

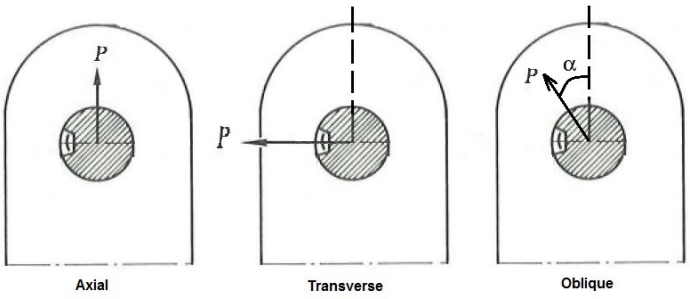

Figure 3.2: In-plane lug load cases.

Figure 3.2 the different in-plane load cases are represented. An oblique load is dependent on the load angle, defined as α. A lug is subjected to an oblique load case when the angle α does not match the angle for an axial (0° and 180°) or a transverse load (±90°) case.

Lugs subjected to a lateral load or side load have a bending moment acting on them. A lateral load case is illustrated in Figure 3.3. Here, The lateral load F acts on the pin of the lug joint.

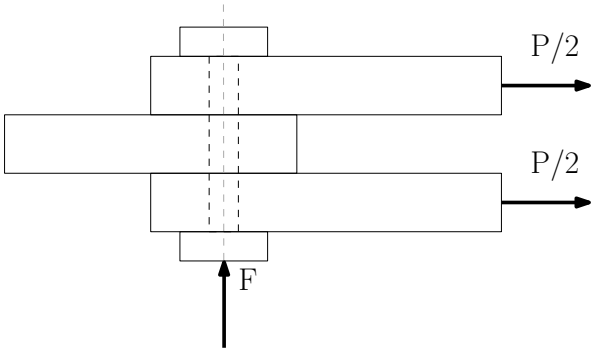

Figure 3.3: Lateral load case

3.3 Phenomena occurring in lug joints

With the lug parameters defined, phenomena occurring in lug joint are detailed. Schijve [1] explained in detail about the complex fatigue life of lugs and describes a couple phenomena occurring in lug joints. These phenomena are responsible for the complexity in determining the fatigue life for lug joints. The phenomena presented in this section are the load reversal behaviour and fretting.

Load reversal behaviour

Load reversal is when the load shifts from a tensile force to a compression force (from +P to a -P load acting on the pin). Obviously when load reversal occurs, the load transmission from the pin to the lug changes. When the lug is loaded in pure axial tension load, the load transmission is along ABA, as seen in Figure 3.4 [1]. For compression the load transmission is along ACA.

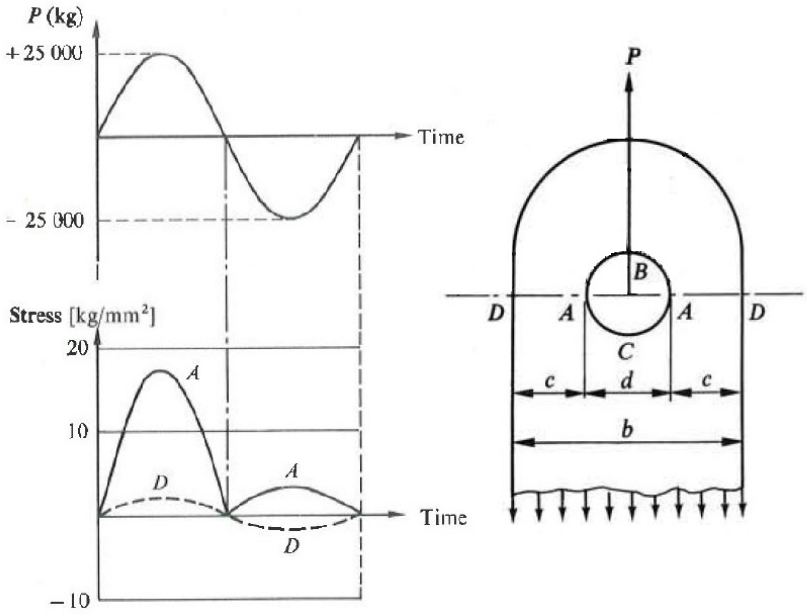

Figure 3.4: Stresses during a tension-compression cycle modified from [1]

In Figure 3.4 a tension-compression cycle is presented showing the peak stresses at two locations. Here, it shows that the peak stress of the tension load is significantly larger than the compression peak stress. Since the compression peak is generally smaller compared with the tensile peak, the compression part of the load cycle is hardly "damaging" the lug joint compared with the tension part. Therefore, in fatigue strength calculation the compression loads are neglected [1, 13, 14].

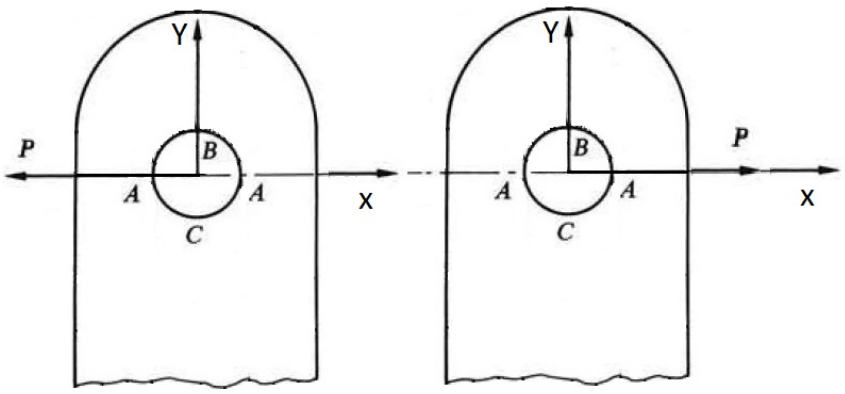

Figure 3.5: Load reversal example on a transverse loaded lug. Figure modified from [1]

For axially loaded lugs the assumption of neglecting compression forces in fatigue calculations is widely used. However, when the load angle changes and the lug is not axially loaded than the question remains if the compression part can be neglected from the calculations. Assume a transverse load instead of the axial load on the symmetrical lug displayed in Figure 3.5.

When a pure transverse load has a tension-compression cycle, the situation remain similar as before only that the load direction is changed by 180°. Both the tension and compression transverse load with the same magnitude produce the same peak stress at the locations B and C on the hole edge. Neglecting the compression load in fatigue strength for the transverse load does seem counter intuitive since both cases generate similar peak stresses at the same location. For oblique loads the same can be said as with the transverse load to a certain extend. Oblique loads can be split into an axial and transverse component. The challenge for oblique loads is to identify under which load angles the compression load can be neglected and when it affects the fatigue strength prediction. Load reversal has a greater impact on the fatigue life of non-axial loaded lugs and is an important phenomena to take into account.

Fretting

Fretting is a phenomenon, which occurs between two materials as a result of small cyclic movements between the materials [1,3,6]. In a pin-type joining like a lug, fretting occurs due to the movement of the pin on the hole edge. Due to the small cyclic movements chaffing of the material occurs. These chaffing locations act as initiation locations for fretting corrosion. It is called fretting corrosion because in normal air corrosion plays a primary role at the initiation locations. Fretting corrosion is primarily a surface damage phenomenon.

Fretting can cause a significant reduction in the fatigue properties of a structure. Fretting increases the probability of crack initiation zone, which in turn increases the chance for a shorter fatigue life. The fatigue life of a structure covers a crack nucleation phase and a crack propagation phase. Since fretting is a surface phenomenon, fretting assists the crack nucleation phase. Fretting is not expected to affect the crack growth phase because cracks

grow away from the surface on which fretting occurs.

Fretting nucleation is primarily noticed in structures for which the number of cycles before failure are in the order of millions. In low cycle fatigue, fretting damage has hardly developed and will not lead to a large reduction in fatigue life. Different studies on the effects of fretting on the fatigue life have been done [11,12]. Schijve [11] looked at the effect of fretting in aluminum lugs and at means to improve the fatigue strength. Bush [12] looked at the difference in fatigue and fretting for lugs with and without an interference fit. The effects of fretting can be reduced by implementing the following principles [6]:

1. Separation of contact surfaces
2. Eliminate the relative motion
3. Reduction of the surface tensile stresses
4. Anti-fretting measurements like inserts, surface treatment or anti-fretting compounds

In most lug joints used in aerospace a bush is implemented in order to reduce fretting effect. With a bush the load transmission occurs through the bush from a pin to lug (principle 1). The bush is placed via interference fit (principle 2) into the hole, causing the introduction of residual stresses (principle 3). Special wear resistant material can be selected for a bush in order to further reduce the fretting between pin-bush and bush-lug (principle 4). One can note that the implementation of a bush within a lug joint uses the principles 1 to 4 for reduction of fretting. Using a bush reduces fretting damage on the hole surface reducing the number of nucleation sides occurring on the hole surface. Now the relative motion is between the pin and the bush instead of the hole edge and fretting on the hole edge surface is largely reduced. In reality a bush will be present in a lug joint for these reasons.

Theories based on stress concentrations of a lug like Heywood [6] or Larsson [2] do not take a bush in the pin into account. Instead, both assume the pin has a 'tight fit' with the hole. The effects of fretting are generally empirically included within the calculations methods. It is to note that, in the theory for stress calculations [1,3,6,8], the diameter of the hole is taken in order to calculate stresses. In reality the diameter of the pin is smaller than the diameter of hole because of the presence of a bush or other joining components. As such the diameter of the hole has to be taken into account and not the diameter of the pin for fatigue calculations.

3.4 Axially loaded lug

Lugs are predominately loaded in axial direction. Many studies [1–3,6,8–10] and tests [11–14] have been performed on axially loaded lugs throughout the years. The result is that the stress distribution and crack initiation for axially loaded lugs are well known and prediction methods for axially loaded lugs are well established. This section gives insight into the stress concentrations of an axial loaded lug.

During an axial (tensile) load the pin generates a radial pressure on the bore of the hole presented in Figure 3.4 by the distribution. Net section failure for axially loaded lugs occurs between DD. Critical net section implies that the pressure loads on the hole is near the root of the notch [3]. The root of the notch is located at point A. Looking at the stress distribution around the hole than point A contains the highest (peak) stresses measured around the hole periphery. Therefore, crack nucleation is expected under cyclic loading for purely axially loaded lugs at point A. From point A crack nucleation shall start and under sustained cyclic loading expand into crack growth, which eventually leads to failure.

Stress Concentration Factor

In order to express the stress concentration around notches or holes the Stress Concentration Factor (SCF) was introduced. The SCF expresses the ratio between the maximum (local) stress and the nominal (usually net section) stress. Expressing the SCF K_t via the net section stress is given by:

$$K_t = \frac{\sigma_{peak}}{\sigma_{nom}} \tag{3.5}$$

Take note that K_t is a dimensionless factor. All deformations are supposed to be elastic since K_t is an elastic concept [3]. Looking at the K_t for lugs it is good to realize that the net section stress is often taken as the nominal stress. The SCF based on the net section is sometimes indicated by $K_{t,ns}$. Another option to express the SCF is via the bearing stress (radial pressure). The SCF based on bearing stress is defined by:

$$K_{t,br} = \frac{\sigma_{peak}}{\sigma_{br}} \tag{3.6}$$

Both SCF based on net section or bearing are used but remain consistent. Generally $K_{t,ns} \neq K_{t,br}$. Calculation methods for the SCF define if they use the net section stress or the bearing stress. The equation for σ_{nom} defines if the SCF is based on bearing or net section. The K_t for lugs under pure axial loads are well known and were first documented by Frocht and Hill in the 1940s [9].

Using photoelastic and strain-gauge measurements test Frocht and Hill determined the K_t values for riveted or bolted joints in its simplest form, a lug joint. The influence of the $\frac{d}{W}$ and $\frac{h}{W}$ ratio on the SCF has been studied by Frocht and Hill. In Figure 3.6 a typical stress pattern for a pin load lug is present. Using the results of the photoelastic and strain-gauge test lead to the SCF curve for a pin loaded lug displayed in Figure 3.7.

Figure 3.6: Typical stress pattern photoelastic test [9]

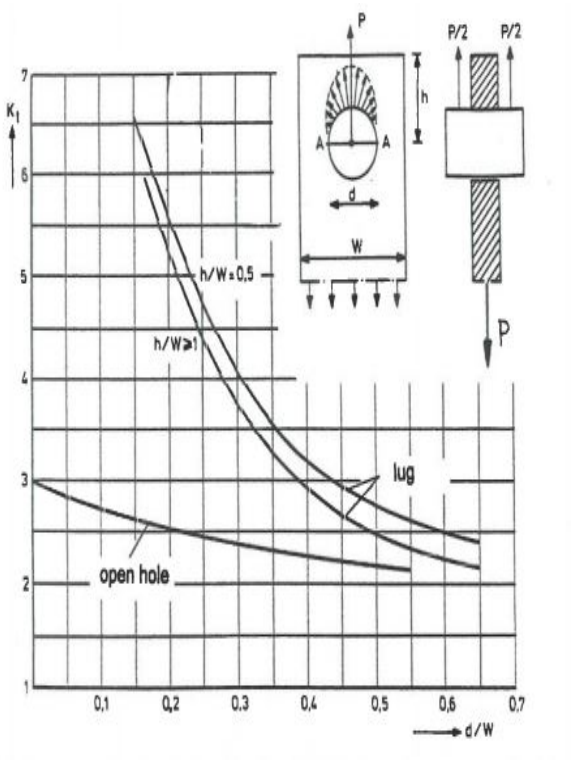

Figure 3.7: K_t values for a lug with a comparison between open unloaded hole [3,6,9].

Using Figure 3.7 a quick estimation of the SCF for an axially loaded lug is possible. When the shape or size of the lug changes a different SCF curve is required to make an estimation of the SCF. Frocht and Hill [9] for example had a square ended lug head while the lugs presented so far in the review have round ended lug heads. Estimation curves for the SCF of lugs joints are widely documented. Heywood [6], Peterson [8], or ESDU [15] are some examples to find SCF prediction curves for lug joints as well as different geometry lug joints.

3.5 Fatigue strength calculation method

Heywood [7] created a fatigue strength prediction equation for lugs. Heywood used the Frocht and Hill SCF curve for the reference lug and modified the result by a size factor and a stress concentration factor [7]. Rewriting Heywood in millimeters and keeping the notation of the relation in line with the thesis documentation, the relation is given by [2]:

$$\sigma_a = \sigma_A \cdot \frac{2.5}{K_t}\left(\frac{50}{25+d}\right) \tag{3.7}$$

Here, σ_a is the stress amplitude of the arbitrary lug and σ_A the stress amplitude of the reference lug. With $K_t = 2.5$ and $d = 25$ mm for the reference lug. The K_t stands for the SCF. From the relation it is clear that the size factor is defined by $\frac{50}{25+d}$ and the stress concentration factor by $\frac{2.5}{K_t}$.

Then Larsson [2] proposed an update to the Heywood relation. Heywood defined the relation by using the K_t of lugs. Larsson viewed the use of K_t from graphs as inconvenience and a large source of scatter [2]. Therefore, Larsson defined a relation based on the geometry of the lug. The relation is based on fatigue data of about 900 lugs to empirically proof the theory. The tested lugs were all made from aluminum. Larsson defined the primary parameters, which are of significance for the fatigue strength of lugs. These primary parameters according to Larsson are [2]:

1. Material
2. Stress cycle
3. Ratio $\frac{c}{d}$
4. Ratio $\frac{a}{c}$
5. Pin diameter
6. Shapes of lugs that (significantly) diverges from the standard geometry, the symmetrical straight-sided lugs

These parameters are combined in the Larsson relation.

3.6 The Larsson relation

By the defined primary parameters, Larsson [2] derived a calculation method for the fatigue strength defined by:

$$\frac{\sigma_a}{\sigma_A} = 1 + \theta(k_1 k_2 - 1) \tag{3.8}$$

The subscript a stands for the stress amplitude of an arbitrary lug, while capital A stands for the stress amplitude of the reference lug (more on the reference lug is explained later). The ratio between nominal stress of the arbitrary lug σ_a and the reference lug σ_A is relate to the shape, size and cycle correction factor. The shape and size factor are denominated by k_1 and k_2 respectively, with θ representing the cycle correction factor.

Larsson introduced the shape and size factor to be able to relate all straight-sided axially loaded lugs to the reference lug. The equations for the shape and size factor are respectively defined by [2]:

$$k_1 = \sqrt{\frac{a \cdot d}{c^2}} \tag{3.9a}$$

$$k_2 = \sqrt[5]{\frac{10}{d}} \tag{3.9b}$$

The shape and size factors are dependent on the lug geometry, which is clearly shown in the equations.

The cycle correction factor depends on the number of failure cycles, N. Larsson introduced this correction factor due to the fact that (allowable) stresses of the lug are dependent on whether it is a high cycle or low cycle fatigue spectrum. The cycle correction factor is given by:

$$\theta = 0.25 \cdot log(N) - 0.5 \qquad 10^3 \leq N < 10^6 \tag{3.10a}$$

$$\theta = 1 \qquad N \geq 10^6 \tag{3.10b}$$

The value of θ for low cycle fatigue ranges between $0.25 < \theta < 1$ and for high cycle fatigue $\theta = 1$. As stated before, the cycle correction factor depends on the number of cycles till failure. The number of cycles till failure is generally the unknown, which one tries to find but is required to be known in order to calculate the number of cycles till failure. Therefore, generally a value for N is assumed or fixed due to design requirements. Via an iterative

process the number of cycles till failure is then calculated. This is important to note when using the Larsson relations with the S-N curves. Fokker uses the Larsson relation as well in their Technical Handbook 3 (TH3) to relate the stresses to the S-N curve in order predict the fatigue life of lug joints [13, 14] .

The reference lug is a lug created by Larsson with a fixed geometry in order to relate the nominal stresses of arbitrary straight-sided axially loaded lugs. The reference lug is a straight-sided symmetrical lug with the geometry of $a = c = d = 10$ mm. Larsson based the reference lug on the Frocht and Hill [9] diagram presented in Figure 3.7. With the dimensions for the reference lug and using the theory of Frocht and Hill, the SCF of the reference lug equal to $K_t \simeq 3.7$. Larsson choose the reference lug because the stress concentration of the reference lug should be far greater than a stress concentration occurring most frequently in practise [2]. The SCF of the reference lug likewise accounts for the SCF within the Heywood equation, which formed the background for the Larsson relation [2].

What has to be realized with the Larsson relation is that the Larsson relation is only valid for straight-sided axially loaded lugs.

3.7 Oblique and transverse loads

So far only axially loaded lugs have been covered and these axially loaded lugs have been use for the formulations of calculation methods for the fatigue life of a lug. When the load angle changes and the load shifts to an oblique or a transverse load, the locations for the peak stresses changes. The peak stress location is important since generally crack initiation occurs around the peak stress area eventually, under sustain loading, resulting in crack growth [3].

Katherisan et al. [19] researched the stress and fracture analysis of tapered attachment lugs. Katherisan et al. presented the normalized stress distribution for an axially, oblique and transversely loaded tapered lug. The stress has been normalized with respect to the bearing stress. The distribution for the oblique loaded lug has been taken from Kathiresan et al. and is presented in Figure 3.8. The ratio $\frac{R_o}{R_i}$ corresponds to the ratio $\frac{h}{\frac{d}{2}}$ of the discussed lug parameters in Section 3.1.

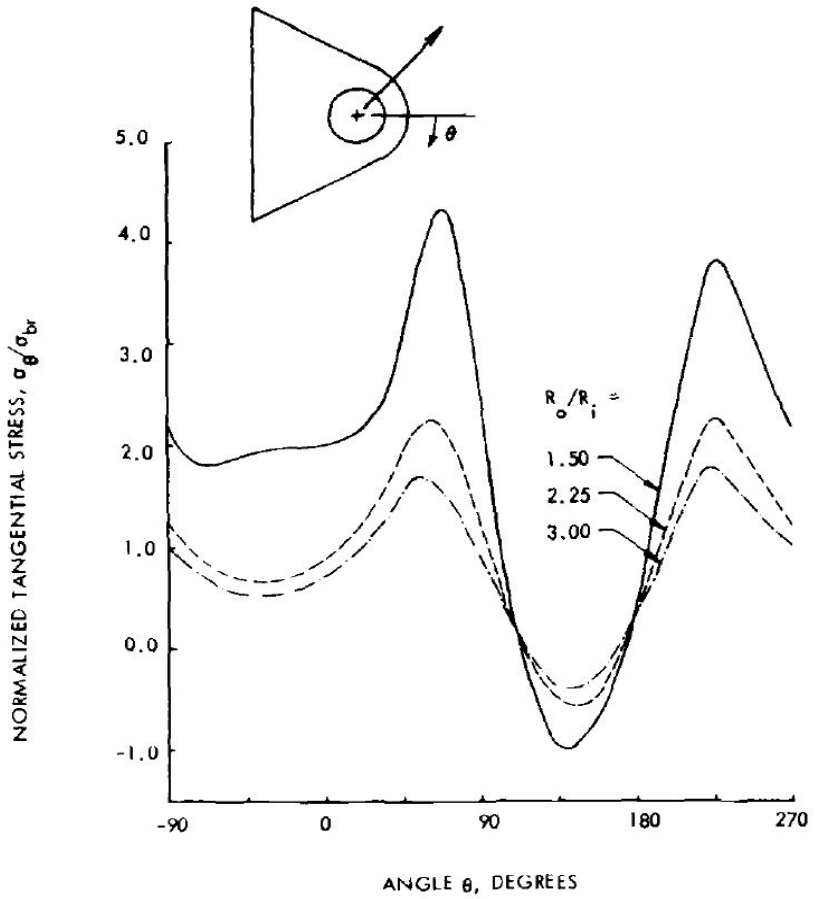

Figure 3.8: Normalized stress distribution around the circumference for an oblique loaded tapered lug [19]

From Figure 3.8 it is shown that two peak stresses are present for the oblique loaded lug. One peak stress occurs on the top side of the lug and one on the bottom side of the lug. The peak stress is located at around 65° and 225° for the $\frac{R_o}{R_i} = 1.50$ curve. The peak stresses are not exactly 180° opposite of each other like is the case with an axially loaded lug. Looking at the peak stresses for the two remain $\frac{R_o}{R_i}$ curves it shows that the peak stresses are also not 180° apart from each other. An observation made by Katherisan et al. is that the absolute maximum stress location changed from bottom side to top side when the ratio $\frac{R_o}{R_i}$ increased [19]. The shift in peak stress location is what Strozzi et al. [20] noted as well. Strozzi concluded that the maximum stress generally increased for increasing load angle and the peak stress location changed abruptly for increasing load angle [20].

The peak stress locations for the axial, oblique and transverse case of Kathiresan et al. [19] have been summarized and displayed in Figure 3.9. Figure 3.9 shows that the peak stresses for oblique loads are not located 180° from each other. Interesting to note is that the axial peak stresses are not located perpendicular to the load angle axis and are not exactly 180° apart.

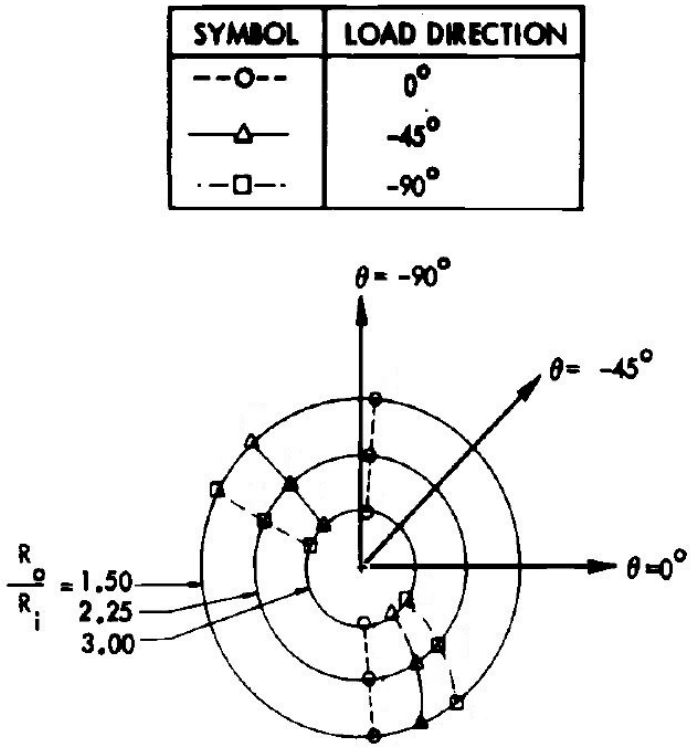

Figure 3.9: Peak stress locations for variable load angles on tapered lugs at different $\frac{R_o}{R_i}$, modified from [19]

Fokker uses TH3 [13] to calculate the SCF for oblique or transverse loaded tapered lugs. The TH3 methods calculates the SCF on the top and bottom side of the lug but does not specify the location on the circumference for the maximum SCF. Another method to calculate the SCF for oblique or transverse loaded lugs is the method of Handbuch Struktur Berechnung (HSB). The HSB method only calculates the maximum SCF occuring and does not specify the location. Both the TH3 and HSB methods are discussed in more detail in Chapter 5.

During the literature review no researches have been found for which the fatigue life of a lug subjected under an oblique or transverse load has been determined. All found studies were aimed at the SCF or the peak stress location.

3.8 Lap joint theory

Literature on out-of-plane loaded lugs have not been found in the (public) reported research. Therefore, joints that are similar are taken as a point of reference. The lug joint is comparable with a (bolted) lap joint. The main differences between the two is that a lug joint only has a single pin to transfer the load while lap joints usually has multiple pins and/or multiple rows of pins. A lug joint can be seen as a special case of lap joint. Another difference is that a lap joint is comprised of two plates while in a general lug joint the (male) lug is enclosed in the female lug. The lap and lup joint are presented in Figure 3.10 and Figure 3.11, respectively.

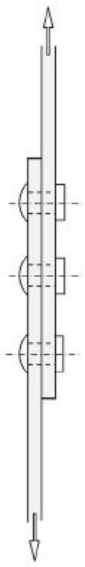

Figure 3.10: Lap joint [3]

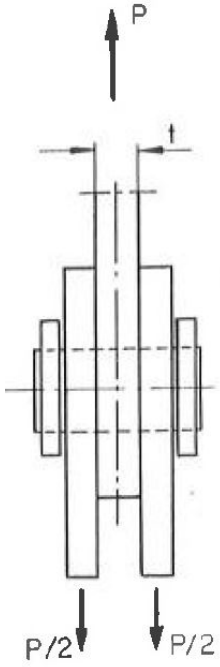

Figure 3.11: Lug joint [2]

When the lap and the lug joints in Figure 3.10 and Figure 3.11 are loaded in tension as shown. Then for the lap joint an off set between the tensile load on the two plates is present. This off set between the line of action of the tensile load is called eccentricity. As a results of the eccentricity in the lap joint, bending component is introduced on the plates. This phenomena of bending is called secondary bending. The addition of the secondary bending term increase the stress concentration around the holes in a lap joint. A lug joint under tension does not experience secondary bending, assuming symmetrical loading of the female lug, because there is no eccentricity present present in a lug joint.

Homan and Jongebreur [22] suggested a prediction method for the fatigue life of riveted lap joints under tensile loads by:

$$K_{t_{joint}} = K_{t_{pin}} \cdot \gamma + K_{t_{hole}} \cdot (1 - \gamma) + K_{t_b} \cdot k \tag{3.11}$$

Here, the γ stands for the ratio of load that is transferred to the other sheet in a rivet row. The $K_{t_{pin}}$ is the SCF for a finite width plate with a pin loaded hole in tension. The terms $K_{t_{hole}}$ stands for the SCF for a finite width plate with an open hole loaded in tension. The first two terms of the Homan and Jongebreur cover the in-plane load components.

The final term represents the bending component in a lap joint. Here, the K_{t_b} stands for the SCF for a finite width plate loaded in bending. The factor k is called the bending factor and defines the ratio of bending stress over tensile stress:

$$k = \frac{S_{bending}}{S_{tensile}} \tag{3.12}$$

Chapter 4

Finite Element Model

The stress distribution around the circular hole of the lug has been analysed by a Finite Element Analyses (FEA). The FEA have been performed using the ABAQUS/CAE package from SIMULIA by Dassault Systèmes. The lug in the FEA have been subjected under various in-plane and out-of-plane pin loads. Since a combination of an in-plane and out-of-plane loads is a potential load case, a three dimensional (3D) Finite Element (FE) model has been created. The 3D model comprises of either a straight-sided or tapered lug.

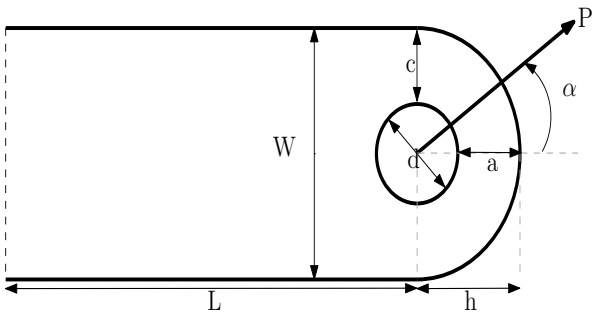

Figure 4.1: Straight-sided lug

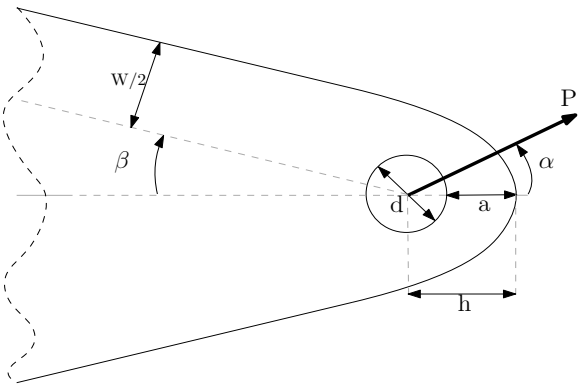

Figure 4.2: Tapered lug

Illustration of a straight-sided and a tapered lug are presented in Figure 4.1 and 4.2, respectively. The definition of the parameters for the different lugs are presented in these figures. The load angle is defined as α and is presented (in both figures) in the positive direction for the analyses. The taper angle of the lug is defined by the angle β.

Section 4.1 provides information on the FE model for the in-plane load case analyses. The FE model for the out-of-plane load cases and combinations of in- and out-of-plane load cases is described in Section 4.2.

4.1 In-plane FEA

The lugs and the pin are modelled to be rigid deformable bodies. The material properties of the lug have been modelled as aluminum. The pin has been modelled as a steel pin. This gives the pin three times the stiffness of the lug. In Table 4.1 the material properties are displayed. The pin has been assumed to be a tight fit with a frictionless lug-pin interface. A convergence study has been conducted on the axially loaded lug, which is presented in Appendix A.

Table 4.1: Idealized material properties for FEA

Material	Young's modulus E [GPa]	Poisson's ratio v [-]
Aluminum	70	0.3
Steel	210	0.3

From the convergence study a mesh size has been selected for the analyses of the (tapered) lugs. For the analyses a hexahedral element of the type C3D8R has been used. In total the lug contains 38004 nodes with a larger density of nodes around the hole, where the main area of interest is. The stress distribution around the hole (mainly the peak stresses) and the stress gradient at the net section are the relevant output data. The mesh of the straight-sided lug and the tapered lug are displayed in Figure 4.3 and Figure 4.4, respectively. The FE model have been used to simulate the in-plane load conditions on tapered and non-tapered lugs with an arbitrary geometry.

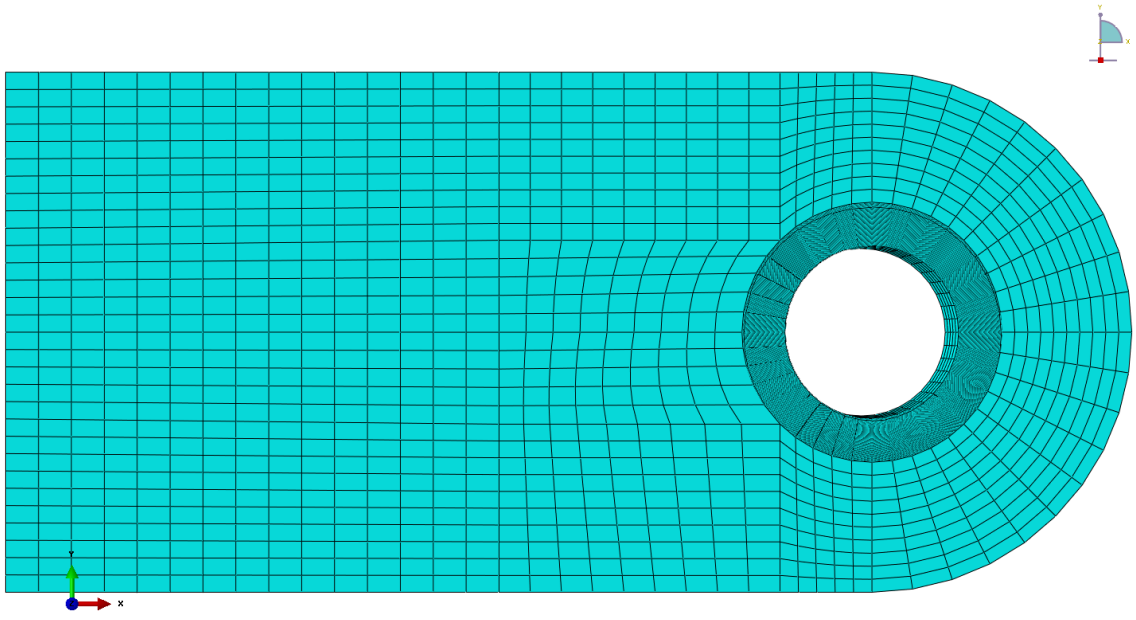

Figure 4.3: Mesh of the straight-sided lug

Both the straight-sided and tapered lug have a clamped Boundary Condition (BC) on the far end of the lug as presented in Figure 4.5. The BC on the pin is such that the z-movement has been restricted as well as all rotation in x-, y-, and z-direction. The in-plane loads are

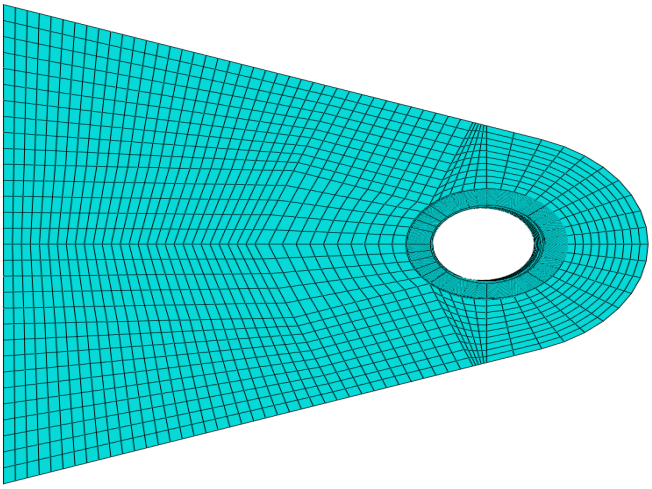

Figure 4.4: Mesh of the tapered lug

applied to the reference point, which is located on the global reference system. However, the location of the reference point is arbitrary. The lug has been constrained via a coupling constraint to the reference point. The constraint couples the reference point to the sides of the pin presented in Figure 4.6. The load for the in-plane FEA are all applied to the reference point.

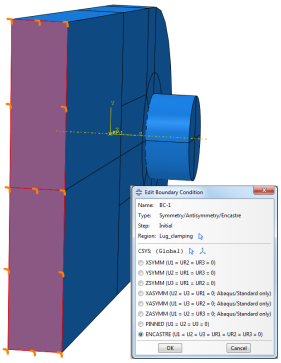

Figure 4.5: Boundary condition in-plane lug model

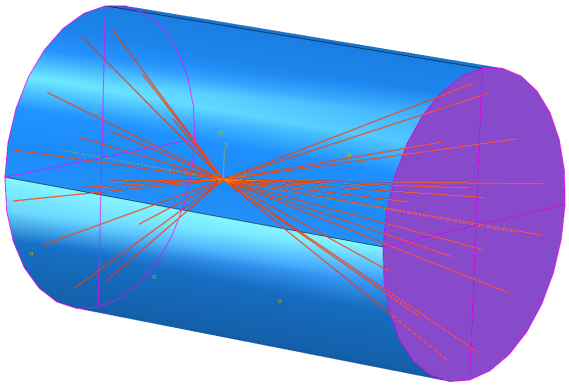

Figure 4.6: Coupling constraint of the pin to the reference point

Using the in-plane FE model the effects of taper and load angle on the lug are investigated. The results of the in-plane FEA are found in Chapter 6.

4.2 Out-of-plane FEA

For the introduction of the out-of-plane loads, the existing FE model has been modified. With the in-plane FE model the load is applied to a reference point, which is constrained via coupling constraint to the pin. With the addition of an out-of-plane component, the coupling constraint cannot be used in ABAQUS because the coupling constraint is not compatible with rotational movement.

Therefore, in order to simulate bending loads on the lug, a more detailed joint has been created. The isometric view and side view of the lug joint is presented in Figure 4.7 and Figure 4.8, respectively. Here, it shows that a female lug has been added to the existing lug model (denoted male lug) with the pin. The pin itself now contains a pin head. The pin head has been implemented due to the fact that the female lug parts would slide across the pin without the pin head present.

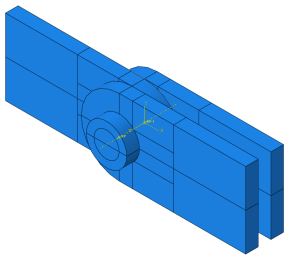

Figure 4.7: Isometric view of the out-of-plane model

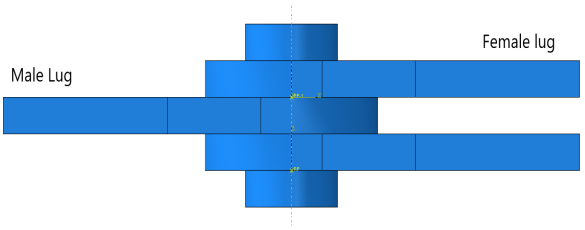

Figure 4.8: Side view of the out-of-plane model

The axial load is applied to the end of the female lugs as a distributed load. The out-of-plane load is applied as a distributed load on the pin. The male lug has a clamped BC present at the end of the lug. Between the male and the female lugs a frictionless contact interaction is implemented. The same contact interaction has been made between the pin and all the lugs as well as for the pin head and the female lugs. Figure 4.9 displays the applied lateral load and Figure 4.10 presents the applied axial load on the out-of-plane model. The boundary condition for the out-of-plane model is the same as for the in-plane model displayed in Figure 4.5.

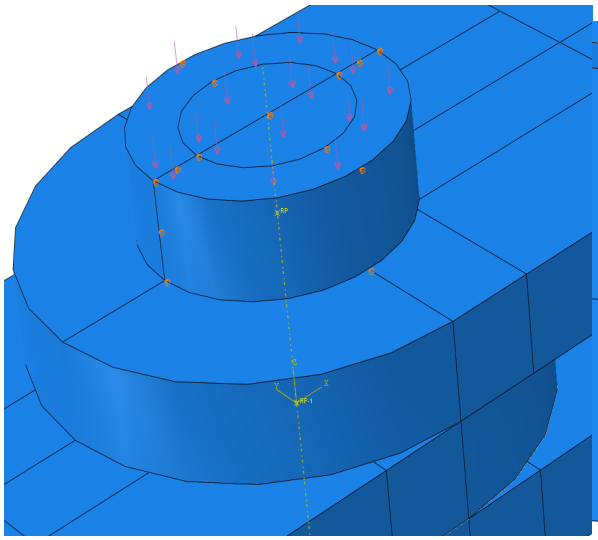

Figure 4.9: Lateral load in the out-of-plane model

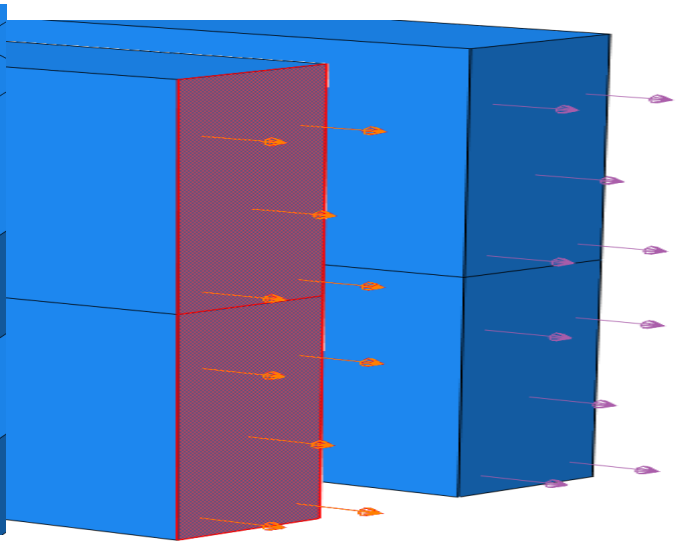

Figure 4.10: Axial load in the out-of-plane model

By applying an in-plane load on the lug and a lateral load on the pin, a new stress distribution around the lug hole is generated. Using the same principles as with the in-plane loads, the peak stresses around the hole are analysed. From these peak stresses the nominal stress is calculated. Results for the out-of-plane cases are presented in Chapter 9. The verification for the out-of-plane FE model is presented in Appendix D.

Chapter 5

Comparison FEA and Existing Calculation Methods

For the determination of the SCF two calculation methods have been compared with the FE model. One method is from HSB 34112-02 [4] and the update 26101-01 [5]. The other method is from Fokker's TH3 [13]. The comparison is made to verify the results of the FEA. Section 5.1 elaborates on the HSB method while Section 5.2 explains the TH3 method. In Section 5.3 the lug geometries used for the comparison is presented. The FEA is compared with HSB and TH3 in Section 5.4.

5.1 HSB method

The lug parameters used for HSB are illustrated in Figure 5.1. The subscript m stands for the 'male' lug. HSB makes a separation between a male and female lug in notation but the equations for the SCF apply to both types of lugs by substituting the equivalent parameter into the equation. Both female and male lug follow the same configuration of notation only the subscript differs. For the remainder of the text, the subscript m have been left out in the different equations of HSB when referring to lug parameters.

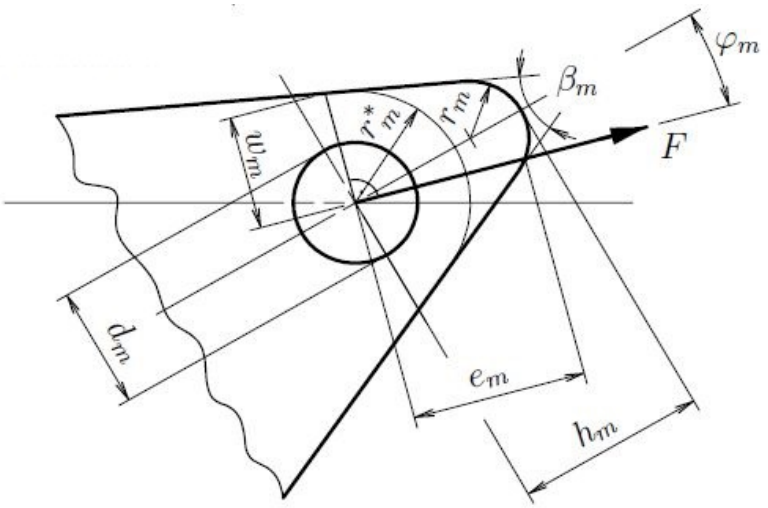

Figure 5.1: Lug definition according to HSB [4]

In Figure 5.1 two radii are listed. The radius r stands for the radius of the lug head while the radius r^* stands for a fictitious radius. Which radius is used in the calculation method is dependent on if the lug is concentric or eccentric. Concentric lug means that the centre of the lug radius coincides with the centre of the hole. For eccentric lug the two centres do not coincide. For these eccentric lugs the fictitious radius r^* is used, which creates a fictitious concentric lug.

The method of HSB is based on the theory of Ekvall [23]. Therefore, the stress concentration has been based on the bearing stress instead of the net section stress. The bearing stress is independent of the load direction and the geometry of the lug. The bearing stress is calculated by:

$$\sigma_{br} = \frac{F}{d \cdot t} \tag{5.1}$$

The applied load is indicated by F in HSB. The parameter t stands for the lug thickness. The SCF in HSB is defined as:

$$K_{t,b} = \frac{\sigma_{max}}{\sigma_{br}} \tag{5.2}$$

Here, $K_{t,b}$ stands for the bearing SCF. The equations 5.1 and Equation 5.2 form the background of the HSB method.

HSB defines a method to calculate the SCF for symmetrical isotropic lugs. This SCF relation for an arbitrary lug is defined by:

$$K_{t,b} = H \cdot K_{t,b1} \tag{5.3}$$

The parameter $K_{t,b1}$ stands for is the SCF of a special case lug where $h = r$ and H is the geometry factor. The geometry factor is dependent on the ratio between the height h and the lug radius r. The geometry factor equation depends also on the load angle α. For the load angles 0°, 45° and 90° H has a fixed equation respectively given by:

$$\alpha = 0 : H = (\frac{h}{r})^{-0.916} + 0.284 \cdot log(\frac{h}{r}) \tag{5.4a}$$

$$\alpha = 45 : H = (\frac{h}{r})^{-1.177} + 1.737 \cdot log(\frac{h}{r}) \tag{5.4b}$$

$$\alpha = 90 : H = (\frac{h}{r})^{-0.495} + 0.715 \cdot log(\frac{h}{r}) \tag{5.4c}$$

Between the angles $0° \leq \alpha \leq 45°$ and $45 \leq \alpha \leq 90°$ H follows via linear interpolation. The linear interpolation equation for H for the different angle ranges are as follows:

$$0 \leq \alpha \leq 45 : H(\alpha) = H(0) + \frac{\alpha}{45} \cdot [H(45) - H(0)] \tag{5.5a}$$

$$45 \leq \alpha \leq 90 : H(\alpha) = H(45) + \frac{\alpha - 45}{45} \cdot [H(90) - H(45)] \tag{5.5b}$$

The SCF $K_{t,b1}$ is dependent on the taper angle β and α. For straight-sided lug ($\beta = 0°$) the $K_{t,b1}$ for load angles of $\alpha = 0°$ and 90° are defined by:

$$\beta = 0, \alpha = 0 : \qquad K_{tb,1} = 2.75 \cdot [\frac{2r}{d} - 1]^{-0.675} \tag{5.6a}$$

$$\beta = 0, \alpha = 90 : 1.332 \leq \frac{2r}{d} \leq 1.723 : \qquad K_{tb,1} = 9.33 \cdot [\frac{2r}{d}]^{-1.667} \tag{5.6b}$$

$$\beta = 0, \alpha = 90 : 1.723 < \frac{2r}{d} \leq 3.400 : \qquad K_{tb,1} = 7.78 \cdot [\frac{2r}{d}]^{-1.333} \tag{5.6c}$$

Using linear interpolation the load angles between 0° and 90° for $\beta = 0°$ are calculated by:

$$K_{tb,1}(\beta = 0/\alpha) = K_{tb,1}(\beta = 0/\alpha = 0) + \frac{\alpha}{90} \cdot [K_{tb,1}(\beta = 0/\alpha = 90) - K_{tb,1}(\beta = 0/\alpha = 0)] \tag{5.7}$$

Prior equations all are limited for straight-sided lugs. When a taper angle is present, different $K_{t,br1}$ equations are required. The $K_{t,br1}$ for tapered lug is substituted in Equation 5.3. The geometry factor remains the same for tapered lugs. The taper angle for the lugs is limited by the range of $0° < \beta \leq 45°$. Tapered lugs are defined by two cases for load angles between $0° < \alpha < 90°$.

Case 1 is when the taper angle equals to 45°, $\beta = 45°$, $K_{t,br1}$ is defined by:

$$K_{tb,1}(\beta = 45/\alpha) = 2.417 \cdot [1 + 0.0063 \cdot \alpha - 0.0000815 \cdot \alpha^2] \cdot [\frac{2r}{d} - 1]^{-0.63} \tag{5.8}$$

For case 2 when the taper angle is between $0° < \beta < 45°$ than $K_{t,br1}$ is calculated via:

$$K_{tb,1}(\beta/\alpha) = K_{tb,1}(\beta = 0/\alpha) + \frac{\beta}{45} \cdot [K_{tb,1}(\beta = 45/\alpha) - K_{tb,1}(\beta = 0/\alpha)] \tag{5.9}$$

Using the HSB method a SCF is calculated for lugs of an arbitrary geometry subjected to an in-plane load. One major downside of using the HSB method is that only one SCF is calculated. It remains unexplained for which peak stress (top or bottom peak stress) the SCF has been determined. HSB does not mention which peak stress is used nor does it mention where the peak stress is located around the circumference of the hole.

5.2 TH3 method

The TH3 method [13] is based on the algorithm explained in Fokker report S-185 [16]. The algorithm of S-185 is FEA based [16]. TH3 method calculates the SCF for an arbitrary lug geometry. The lug can have an arbitrary taper angle β and be subjected to an arbitrary load angle α. In Figure 5.2 the TH3 lug parameters are defined. Important to note is that the taper angle for TH3 is defined from the axis of symmetry of the lug, while for HSB the taper angle is defined as the complete angle of the lug. Thus, $\beta_{th3} = \frac{1}{2}\beta_{HSB}$.

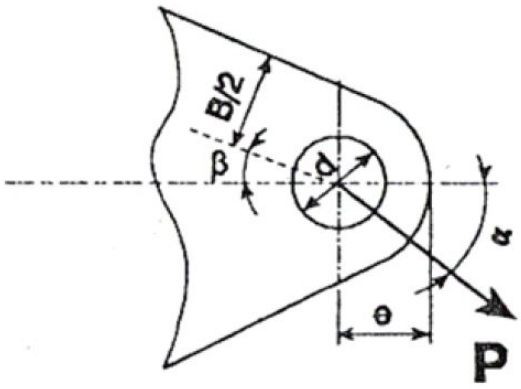

Figure 5.2: Lug definition according to TH3 [13]

TH3 computes a top and a bottom SCF factor, which are K_{t1} and K_{t2}, respectively. The the top and bottom in TH3 are defined with respect to the positive load angle (see Figure 5.2). Important to note is that the load angle for TH3 is defined as clockwise positive, while for the FEA the positive load angle is counter clockwise (see Figure 4.1). Therefore, the top SCF of the TH3 lug is compared with the bottom SCF of the FE model lug and vice verse. The SCF calculated via TH3 is based on the bearing stress of the lug. This is the same reference stress as for the HSB method. The SCF related to the bearing stress is defined in Equation 5.1.

As mentioned before, the TH3 method defines two stress concentration locations, one at the top and one at the bottom of the lug. The exact location of the maximum Stress Concentration (SC) around the circumference of the hole is not defined. TH3 only computes the magnitude of the maximum SC around the hole. Equation 5.10 defines the relation for the maximum stress concentration factors, $K_{t1(2)}$ around the circumference of the hole. The subscript 1 stands for the top side and the 2 for the bottom side of the lug.

$$K_{t1(2)} = K^*_{t1(2)} \cdot \xi \cdot \zeta \tag{5.10}$$

The magnitude of $K^*_{t1(2)}$ is dependent on the load and taper angle. The magnitude of $K^*_{t1(2)}$ are found by using their respective curve for the load and taper angle. The different curves for $K^*_{t1(2)}$ are presented in TH3 [13]. The load angle varies between 0° and 90° and the taper angle for the different curves is set at $0°, 10°, 20°, 30°$ and, 45°. The correction factor ξ is defined by:

$$\xi = 0.255 \cdot e^{4.83(1-\frac{B}{2d})} + \frac{0.1}{\frac{B}{2d} - 0.5} + 0.545 \tag{5.11}$$

The correction factor ζ is given by:

$$\zeta = 1 + 0.05 \cdot (1 - \frac{2e}{B}) \qquad ,if\, \frac{e}{B} > 0.5 \tag{5.12a}$$

$$\zeta = (1 - \frac{\alpha}{90}) \cdot \left[1 + 9.74 \cdot (1 - \frac{2e}{B})^{2.567}\right] + (\frac{\alpha}{90}) \cdot \left[1 + 0.73 \cdot (1 - \frac{2e}{B})\right] \qquad ,if\, \frac{e}{B} \leq 0.5 \tag{5.12b}$$

From the equations it is clear that ξ is a correction for the size and shape of the lug while ζ is the correction of the shape and load angle. Important to note that in Equation 5.11 the e stands for a mathematical constant, which is based on the natural logarithm as $e = 2.71828$. The e in Equation 5.12 stands for the height e defined in Figure 5.2 and is thus dependent on the geometry of the lug.

5.3 Case lug

For the initial comparison between the FE model and the two calculation methods a case study lug has been created. The case lug consists of a straight-sided and a tapered lug using the same dimensions. In Table 5.1 the dimensions for the straight-sided and the tapered lug are presented. An arbitrary lug geometry has been taken for this. The parameters in Table 5.1 are according to the parameters presented in Figure 4.1. The results of the FEA grants an insight in the compatibility of the model, as well as finding the correlation between relations. The FE results of the case lugs are verified with the two calculation methods.

Table 5.1: Dimensions of the case lug

Lug type	h $[mm]$	W $[mm]$	d $[mm]$	L $[mm]$	β $[°]$
Straight-sided	11	28	10	50	0
Tapered	11	28	10	50	20

For the analyses multiple parameters are identified. The main parameters affecting the stress distribution are the load angle, taper angle, width of the lug, height of the lug and the diameter of the lug.

The magnitude of load does affect the stress distribution, however both load and stress scale equally with respect to each other. When the load is increased by a factor two, the stresses increases with the same factor. The scaling between load and stress is valid as long as no plasticity occurs.

5.4 Comparison between FEA and calculation methods

The FE model described in Chapter 4 with the dimensions described in Section 5.3 are compared with the two calculation methods described in Section 5.1 and Section 5.2, respectively. Comparing the results of the FEA with the models provide an insight into the results of the FEA. Both HSB and TH3 are verified calculation methods and as such if the FEA produces similar results than the results produced by the FE model are verified.

Both HSB and TH3 relate the SCF with respect to the bearing stress (instead of the nominal stress). The FE model does not explicitly state or calculate a SCF. However, the FE model does provide the stress distribution around the hole for the given load. Taking the peak stress around the circumference of the hole and relating it to the bearing stress, the SCF for the FEA is calculated.

The FEA have been conducted using an applied load of 1000 N acting on the pin. The load angle varies from 0 to 90° by increments of 15°. The values for HSB and TH3 have been calculated for the same domain of load angles only with increments of 10°. Increments of 10° have been chosen to easily find the values from the TH3 graphs. The analyses has been preformed using a straight-sided lug and a tapered lug with taper angle of 20°.

First the results of the straight-sided lug for FE, HSB and TH3 are discussed in Section 5.4.1. Take note when top or bottom of the lug is mentioned, top or bottom is with respect to the positive load angle defined in the reference system of the aforementioned method. After the straight-sided lug results, the tapered lug results are compared for the different methods in Section 5.4.2 followed by a summary of both results in Section 5.4.3.

5.4.1 FEA, HSB, and, TH3 results for a straight-sided lug

The SCF for TH3, HSB and FEA (denoted by FEM) are presented in Figure 5.3. The results for the load angles 0°, 45° and 90° and the respective SCF are also displayed in Table 5.2 for convenience. Since HSB only calculates one stress thus is represented by a single SCF curve. TH3 and FEA calculate a top and bottom SCF represented by solid line for the top SCF and a dashed line for the bottom SCF.

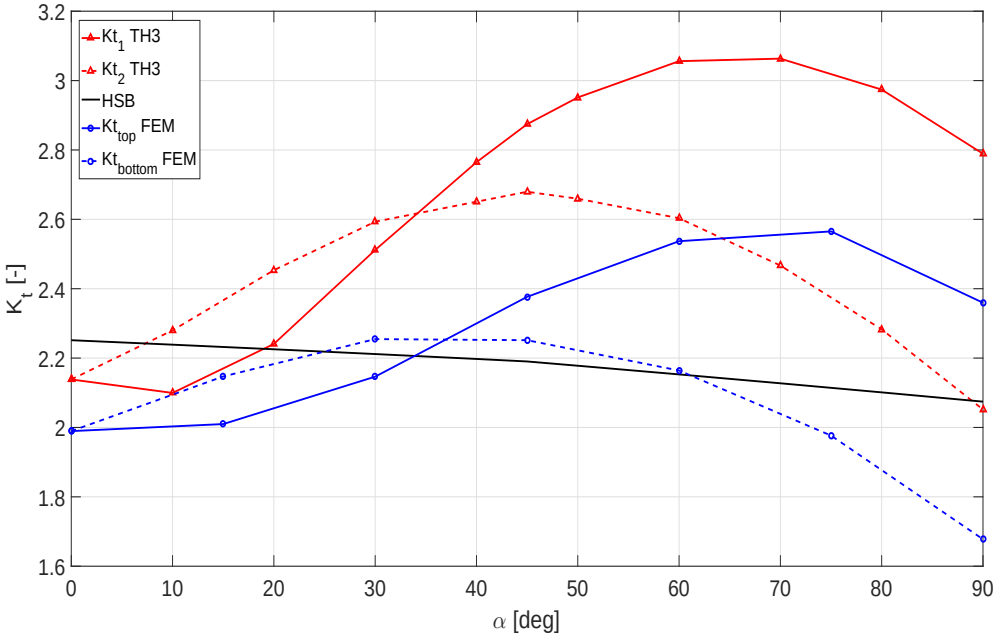

Figure 5.3: K_t for a straight-sided lug under varying load angles

Table 5.2: K_t for a straight-sided lug at certain load angles

α	0°	45°	90°
TH3 K_{t1}	2.138	2.874	2.789
TH3 K_{t2}	2.138	2.680	2.052
HSB K_t	2.252	2.190	2.074
FEM $K_{t_{top}}$	1.990	2.377	2.360
FEM $K_{t_{bottom}}$	1.990	2.252	1.678

From the results it is clear that the HSB results follow a linear relation for varying load angles. This was to be expected since HSB calculates only the load angles $0°, 45°$ and $90°$ accurately. HSB uses an interpolation principle between 0° and 45° and between 45° and 90° load angle. HSB is only limited to producing one SCF (hence only one curve present) and it is not explicitly defined if the SCF occurs on the top or bottom side of the lug. By comparing HSB with the FEA, none of the two FE curves matches with the HSB results. In fact, HSB and the FEA show different trends with respect to each other. The same applies between HSB and the TH3 method.

Both TH3 and FEM follow a non-linear relation. It shows that the $K_{t_{FEM_{top}}}$ follows the same trend as the Kt_1 TH3 while $K_{t_{FEM_{bottom}}}$ follows the trend of K_{t2} TH3. Thus, the SCF on the top side of the FE model shows similarity with the top side SCF of the TH3 method (topside according to each methods reference system). The same for the SCF on the bottom side of the lugs. When the load angle is roughly below 35° the SCF on the bottom of the lug is higher compared with the SCF of the top of the lug. The load angle at which the SCF of the top is higher in magnitude than the bottom is at $\alpha \approx 34.2°$ for TH3 and for FEM it is at load angle $\alpha \approx 36.9°$.

The magnitude of the FEA results, for every load angle are always less than the results of TH3. The reason for the difference is that the TH3 method has an added correction factor in the SCF curves displayed in Figure 5.3. The added factor is reported in S-185 [16]. In Appendix B the FE model has been used to reproduce the data of S-185. Here, the results of the FEA using the geometries of TH3 lug are compared with the TH3 SCF results.

Another point of interest is that, even though both HSB and TH3 are verified methods, both methods generate different results for the same lug at an arbitrary load angle as is presented in Figure 5.3 and Table 5.2.

5.4.2 FEA, HSB, and, TH3 results for a tapered lug

Using the same geometry as the straight-sided lug, a tapered lug with taper angle 20° has been modelled. Figure 5.4 presents the results for TH3, HSB and FEA for the SCF with respect to varying load angles.

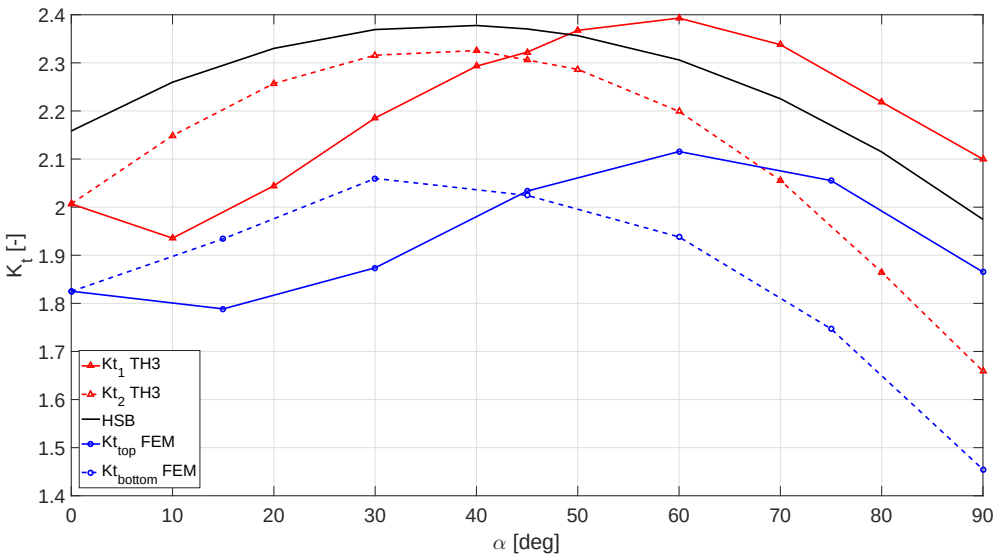

Figure 5.4: K_t for a tapered lug under varying load angles for at $\beta = 20°$

For the tapered case, the HSB method is more a second order curve for the SCF. Compared with the TH3 and FEA curves the HSB looks similar in trend to the K_{t2} and $K_{t_{FEM_{top}}}$. However, for an axially loaded lug HSB still results in the highest SCF of the three methods. For a transverse loaded lug HSB is in between the two other methods. The HSB curve shows similarity in trend with K_{t2} and Kt_{bottom} but is larger then those curves for all load angles.

The TH3 curves display the same general behaviour as with the straight-sided lug. The SCF on the bottom side of the lug (K_{t2}) is larger than the top side until a certain load angle where the curves flip. The load angle where the the curve flip is around $\alpha = 43°$. The maximum SCF for a tapered lug is far lower compared with the max SCF of the straight-sided lug. It appears that higher load angles result in lower peak stresses for tapered lugs compared with the peak stresses of a similar geometry straight-sided lugs.

Similar as in the straight-sided case, the FEM curves follow the same trends as their respective curve of TH3. The SCF on the bottom side for the FEM is larger than the top SCF at lower load angles. The FEM curves flip around at a load angle of $\alpha = 44°$. Still, the FEM curves remain smaller than the respective TH3 curve for every load angle because of the added correction factor [16].

5.4.3 Summary of results

From both the straight-sided and tapered case it is clear that the HSB method does not match with the FEA results and with the TH3 method. Therefore, the HSB has been excluded in the rest of this study.

From the comparison it became clear that both the TH3 method and FEA produced a similar trend with a discrepancy in magnitude. From Appendix B it follows that the discrepancy between the results is around 2.5%. Therefore, the results of the FEA are verified with TH3.

Chapter 6

FEA Axially Loaded Lugs

Using the FEA the SCF for the case lugs have been calculated for different load and taper angles. To calculate the fatigue life for lugs the S-N curve, which relates the amplitude stress to the fatigue life, is used. The amplitude stress is calculated by using the Larsson relations [1, 2]. Larsson created an equation to relate straight-sided axially loaded lugs to the S-N curve. In order to relate the SCF to the S-N curves, the SCF has to be related to the Larsson relations. The SCF is the peak stress divided by a nominal stress, which is set as the net section stress. The Larsson relation needs to be updated or replaced by a new methodology in order to predict the fatigue life for in- and out-of-plane loaded lugs.

6.1 Larsson relation

Larsson created an equation, which relates the amplitude stress to the number of cycles until failure using the S-N curves. For the Larsson relations, a reference lug has been selected, to which the stresses of an arbitrary lug are compared. The Larsson relation is defined as:

$$\frac{\sigma_a}{\sigma_A} = 1 + \theta(k_1 k_2 - 1) \tag{6.1}$$

Here, the subscript a stands for the stress amplitude of an arbitrary lug, while capital A stands for the stress amplitude of the reference lug. The stress amplitude are with respect to the net section stress of the lug [2]. The nominal stress σ_{nom} has been used throughout all FEA as the amplitude stress when applying the Larsson equation. Expressing the Larsson relation for the nominal stress leads to:

$$\frac{\sigma_{nom}}{\sigma_{nom_{ref}}} = 1 + \theta(k_1 k_2 - 1) \tag{6.2}$$

The ratio between nominal stress of an arbitrary lug to the reference lug is related to the shape, size and cycle correction factor. The shape and size factor are denominated by k_1 and k_2, respectively. The θ represents the cycle correction factor.

The equations for the shape factor and size factor are defined by, respectively:

$$k_1 = \sqrt{\frac{a \cdot d}{c^2}} \tag{6.3}$$

$$k_2 = \sqrt[5]{\frac{10}{d}} \tag{6.4}$$

Both the shape and size factor are dependent on the lug geometries.

The cycle correction factor depends on the number of failure cycles N and is defined as:

$$\theta = 0.25 \cdot log(N) - 0.5 \qquad 10^3 \leq N < 10^6 \tag{6.5a}$$

$$\theta = 1 \qquad N \geq 10^6 \tag{6.5b}$$

The magnitude of θ for low cycle fatigue ranges between $0.25 < \theta < 1$. For high cycle fatigue the cycle correction factor (conservatively) equals to $\theta = 1$. The number of cycles till failure is generally the unknown, which one tries to determine but is required to be known in order to use the Larsson relation. Therefore, generally a value for N is assumed or fixed following from to design requirements. Via an iterative process the number of cycles till failure are then calculated.

The Larsson relation forms the basis for a fatigue life prediction method for axially loaded straight-sided lugs. Fokker uses the Larsson relation for fatigue life predictions of lugs in TH3 [13, 14]. FEA has been performed on axially loaded lugs. The results of the FEA are used in the Larsson relation. By increasing the complexity of the FEA the Larsson relation is updated. For the Larsson relation the reference lug has been created in ABAQUS/CAE. Next to the reference lug, a couple of case lugs with variations in the a and c parameter have been created. The case lugs are compared to the reference lug according to the Larsson relation. The assumptions for the Larsson relation and geometries of the different case lugs are discussed in Section 6.2. The FEA of the reference lug is displayed in Section 6.3. The results of the case lugs compared to the reference lug by applying the Larsson relation are presented in Section 6.4.

6.2 Assumptions and FEA case lugs

The Larsson relation is based on the principle of comparing the nominal stress of an arbitrary lug with the nominal stress of the reference lug. This is done using the shape, size and cycle correction factor. In order to be able to update the Larsson relation with the option to include tapered and non-axially loaded lugs, the shape and size factor relations were investigated.

Using FEA, the nominal stress of the reference lug is referred to the nominal stress of arbitrary lugs according to Equation 6.2. In order to compare the results, an arbitrary load has been applied to the reference lug and the different lug cases. The applied load is chosen such that the stresses are always below the yield stress of the material. By applying a load for which all the stresses remain below the yield stress, all stresses are assumed to remain in the linear-elastic region. By remaining in the linear-elastic region the number of cycles till failure is assumed to be greater than 10^6. Resulting in that the cycle correction factor equals to 1, $\theta = 1$.

Rewriting the Larsson relations of Equation 6.2 using the assumption for θ results in the reduced Larsson equation:

$$\frac{\sigma_{nom}}{\sigma_{nom_{ref}}} = k_1 k_2 \tag{6.6}$$

This relation applies for the different test case lugs using the FEA. For the FEA a number of test lugs have been modelled. To further simplify the Larsson relation the diameter of the lug hole has been fixed to $d = 10$ mm. This results in that the size factor, k_2 is always be equal to 1. For the analyses of Equation 6.6, one of the geometry parameters a or c has been varied. When one is varied the other remains equal to 10 mm. For example, with the lugs a5 or a15. The distance a has been set to either 5 or 15 mm, respectively while c remained equal to 10 mm. The lugs used for the analyses are displayed in Table 6.1.

Table 6.1: FEA case lugs geometries in mm

Lug	a	c	d
Reference	10	10	10
a5	5	10	10
a15	15	10	10
a10c10	10	10	10
c5	10	5	10
c15	10	15	10

Larsson maintained an error margin between ±15%. Larsson reasoned that after eliminating scatter due to the testing procedures a ±15% variation in fatigue strength is reasonable [2]. As such when using the Larsson relation to compare the results of the lug in this thesis, a ±15% error margin is maintained.

6.3 Reference lug

Larsson created a reference lug. This reference lug has been created in ABAQUS following the geometries set by Larsson. Since the hole diameter of the reference lug equals to 10 mm combined with applying the assumption for θ, the Larsson relation reduces to:

$$\frac{\sigma_{nom}}{\sigma_{nom_{ref}}} = k_1 \tag{6.7}$$

In order to simulate the stresses, the applied load has been set to $P = 1000$ N (arbitrarily chosen). From the FEA the peak stress and stress distribution of the reference lug is calculated. Because of symmetry and an applied axial load the peak stress on the top and bottom are equal. Therefore, both the top and bottom peak stress produce the same nominal stress. Figure 6.1 presents the stress distribution of the Net Section (NS) along the top side of the reference lug. From the distribution the nominal stress has been calculated and is displayed as the horizontal line in Figure 6.1.

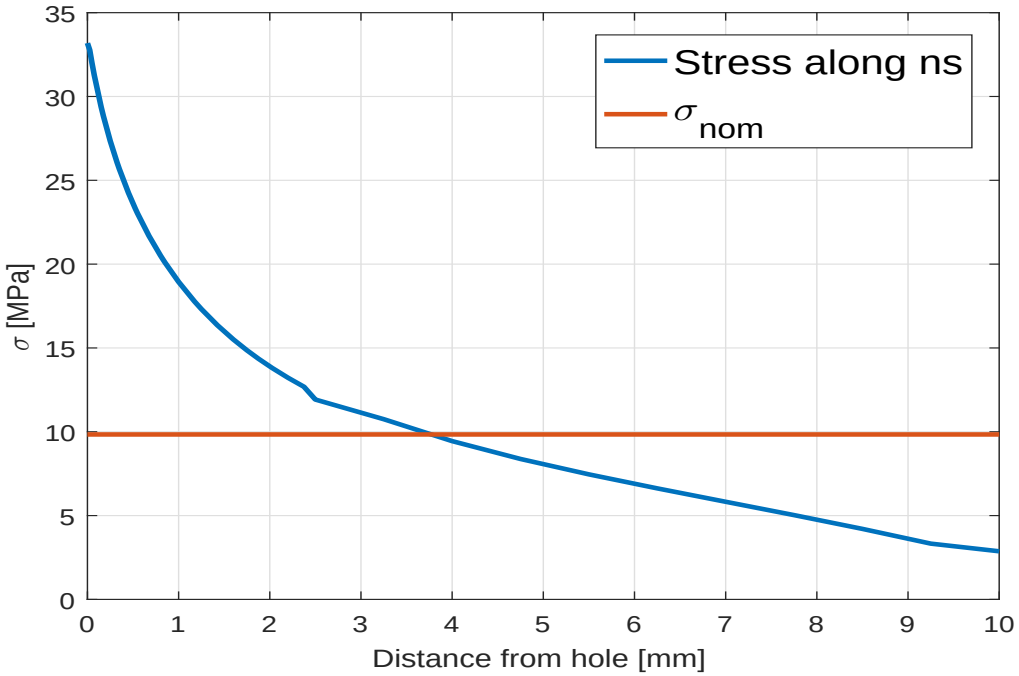

Figure 6.1: Stress along the NS of the reference lug

From Figure 6.1 it shows that the stress starts at the peak stress at the edge of the hole. Moving along the NS to the edge the stress shows an exponential decay. The second order polynomial decay for the stress distribution is along the NS, which is expected and according to theory [3]. A kink in the curve is seen around 2.5 mm. This is imposed by the applied mesh since the fine meshing ends at 2.5 mm from the hole edge and a less coarse mesh has been used for the remainder.

The nominal stress acting on the NS is the average of the stress distribution presented in Figure 6.1. The nominal stress is presented as the horizontal line and has a magnitude of $\sigma_{nom} = 9.839$ MPa. Analytically the nominal stress at the NS is calculated by:

$$\sigma_{nom} = \frac{P}{(W-d)\cdot t} = \frac{P}{2\cdot c\cdot t} \tag{6.8}$$

Filling in the dimensions of the reference lug and acting load in Equation 6.8, the analytic nominal stress equals to 10 MPa. The difference is 1.6%. The FE nominal stress is slightly lower and thus a close approximation of the analytic nominal stress along the NS. The difference between the analytical nominal stress and FEA nominal stress for a few case lugs are presented in Appendix C. From these cases the difference was around 1% between the analytical and FE. It is noted that the nominal stress calculated from FE is always lower than the analytic value. In order to be consistent, all nominal stresses are calculated from the FEA instead of using Equation 6.8. This is because when the load angle changes the location for the NS changes. When the location of the NS changes the denominator of Equation 6.8 changes as well.

The results of the reference lug for the Larsson equation are presented in Table 6.2. Here, the applied load and the magnitude for the different Larsson component are shown. The nominal stress of the reference lug has been used as the reference stress for the other case lugs during the FEA.

Table 6.2: FEA Results for the reference lug

Lug	P [N]	σ_{nom} [MPa]	k_1	k_2	$\frac{\sigma_{nom}}{\sigma_{nom_{ref}}}$	k_1k_2	Error Equation 6.6 [%]
Reference	1000	9.839	1.000	1.000	1.000	1.000	0.00

6.4 Relationship of k_1 and k_2 with the nominal stresses

From the reference lug the peak stress is obtained for the applied load. In order to compare the reference lug with the case lugs, the peak stresses of the two are set equal to each other. To do this, the applied load on the case lugs is increased or decreased. From the reference lug and the different load cases on lugs, the nominal stress of each lug has been computed using ABAQUS CAE. The applied load and nominal stress for each lug is displayed in Table 6.3.

For each of the lugs the shape and size factor are calculated since the geometry of each lug is defined. The shape and size factor for each lug is displayed in Table 6.3. According to Equation 6.6 the factor between the nominal stress of an arbitrary lug and the reference lug should equal to the shape times size factor of the lug. The factor for the nominal stress of a lug over the nominal stress of the reference lug and the shape times the size factor are presented in Table 6.3. The results of the reference lug are presented in Table 6.2.

From the results for lug a5 and c5, it is shown that these produce the largest discrepancy between the nominal stress ratio $\frac{\sigma_{nom}}{\sigma_{nom_{ref}}}$ and the k_1k_2 factor. Interesting to see is that when

Table 6.3: Results of the FEA for the case lugs

Lug	P [N]	σ_{nom} [MPa]	k_1	k_2	$\frac{\sigma_{nom}}{\sigma_{nom_{ref}}}$	k_1k_2	Error Equation 6.6 [%]
a5	800	8.731	0.707	1.000	0.887	0.707	-25.50
a15	1100	10.780	1.225	1.000	1.096	1.225	10.54
a10c10	1000	9.839	1.000	1.000	1.000	1.000	0.00
c5	780	15.360	2.000	1.000	1.561	2.000	21.94
c15	1080	7.538	0.667	1.000	0.766	0.667	-14.92

the distance a is small $\frac{\sigma_{nom}}{\sigma_{nom_{ref}}}$ is larger than the k_1k_2 factors while when c is small the nominal stress ratio becomes smaller than the k_1k_2 factor. This effect is opposite for a15 and c15 lugs.

The results show that the case lugs compared with the reference lug do not match according to the defined margin of error for the Larsson relation. All lugs used for the analyses are straight-sided axially loaded lugs close to the geometry of the reference lug. Still there is a discrepancy up to 25% between the nominal stress ratio and the correction factors, which exceeds the tolerable margin of error. From the FEA it became apparent that the eccentricity within the lug has an effect on the Larsson relation. The eccentricity is discussed in Section 6.5.

6.5 Eccentricity

Eccentricity for a lug occurs when the centre of the hole does not coincide with the centre of the lug head radius. When the centre of the hole coincides with the centre of the lug head radius than a lug is a concentric lug. A lug is concentric when the distances $a = c$, which is the case the reference lug. When the distances $a \neq c$ than a lug is eccentric. With an eccentric lug, two situations are possible. The centre of the lug hole is forwards of the centre of the lug head radius or it is backwards of the centre of the lug head radius. Figure 6.2 illustrates a concentric, an eccentric forward, and an eccentric backward lug. The arrows indicate the direction for the shift of the centre of the hole.

The lugs used for the analyses are also either concentric or eccentric. Table 6.4 shows for each lug if the lug is eccentric or concentric. The lugs have been rearranged in order of eccentricity. The table shows that the lugs a5 and c15 are eccentric forward, while a15 and c5 are eccentric backward lugs. The eccentricity of a lug is expressed by the eccentricity ratio $\frac{a}{c}$. The respective errors as found in Section 6.4, are also listed in Table 6.4.

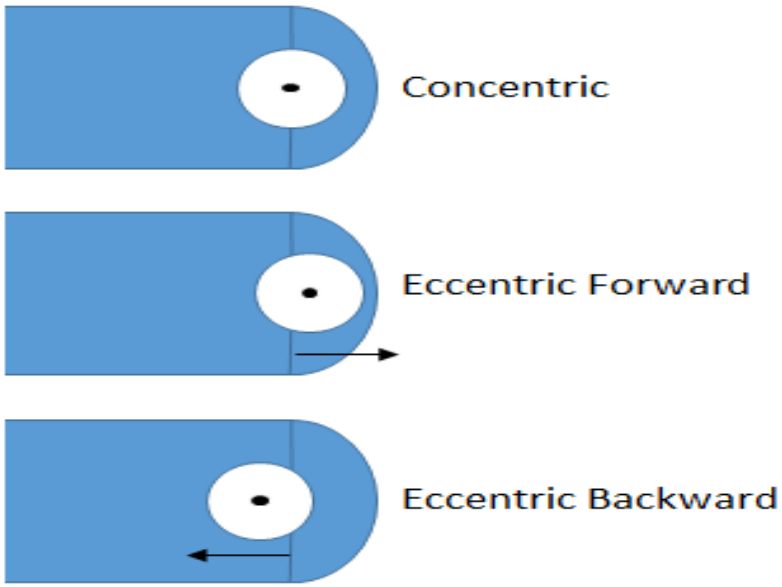

Figure 6.2: Concentric, eccentric forward and eccentric backward lugs

Table 6.4: Lug eccentricity

Lug	$\frac{a}{c}$	Eccentricity	Error Equation 6.6 [%]
a5	0.5	Eccentric forward	-25.50
c15	0.667	Eccentric forward	-14.92
a10c10	1.0	Concentric	0.00
a15	1.5	Eccentric backward	10.54
c5	2.0	Eccentric backward	21.94

The table shows that all the lugs that have eccentricity have a greater error between the nominal stress ratio and the shape/size factor compared to the concentric lugs. The minus sign in the error implies that the nominal stress ratio is larger in magnitude than the correction factors. When the eccentricity is forwards the nominal stress ratio is larger than the correction factors while this is the opposite for when the eccentricity is backwards. Even though Larsson relation should hold for an arbitrary straight-sided axially loaded lug, it appears that eccentricity does impose a discrepancy within the Larsson relation.

The error with Equation 6.2 is graphically displayed against the eccentricity ratio in Figure 6.3. From the results, a linear relations between the data points has been defined in order to create an eccentricity correction factor.

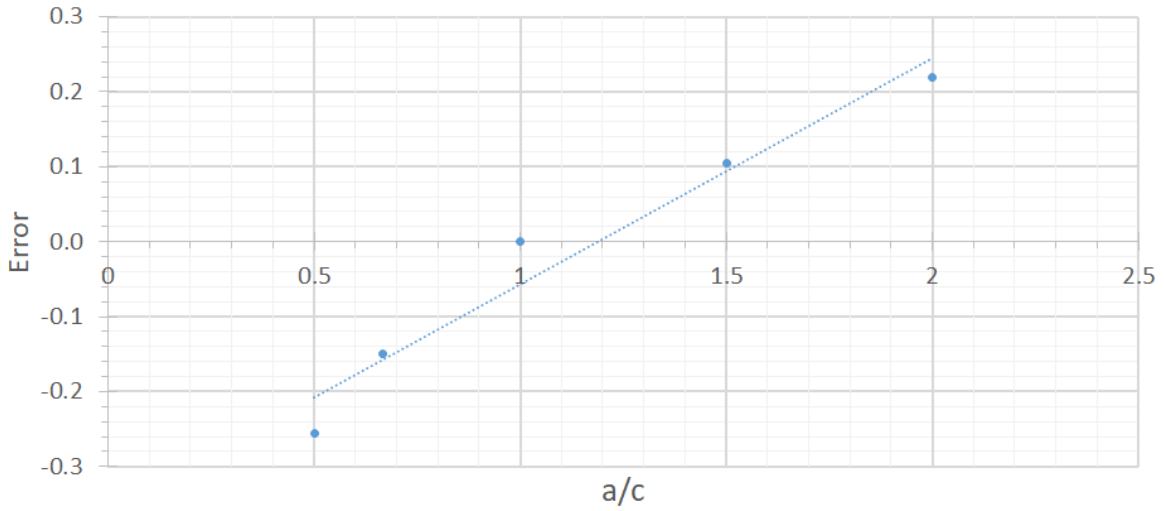

Figure 6.3: Relation between the eccentricity expressed in ratio of $\frac{a}{c}$ and the error

The eccentricity correction factor, K_{ecc} is added to the existing Larsson relation to take eccentricity into account. Factor K_{ecc} is placed on the right-hand side of the equation and is multiplied with the shape and size factor in Larsson. Multiplication has been chosen since the nominal stress ratio has to be equal to $k_1 k_2$ according to the Equation 6.2. Therefore, the existing correction factors are multiplied with K_{ecc} to take eccentricity into account. The Larsson relation with the eccentricity factor, from now on referred to as the eccentricity Larsson relation, is defines as:

$$\frac{\sigma_{nom}}{\sigma_{nom_{ref}}} = k_1 k_2 K_{ecc} \tag{6.9}$$

The correction factor K_{ecc} is a linear relation dependent on the eccentricity ratio $\frac{a}{c}$ defined from Figure 6.3. The relation for K_{ecc} is given by:

$$K_{ecc} = 1 - (0.3021 \cdot \frac{a}{c} - 0.3583) \tag{6.10}$$

The factor K_{ecc} is a normalization factor around 1 for the eccentricity. For low eccentricity ratios ($(\frac{a}{c} < 1)$ the K_{ecc} increases the correction factors while for larger eccentricity ratios ($\frac{a}{c} > 1$) the K_{ecc} decrease the correction factors.

Table 6.5 presents the results for the eccentricity Larsson relation. The error between the nominal stress ratio and the correction factors including the eccentricity factor is shown in the column error Equation 6.9.

Table 6.5: Results for Equation 6.9 and the error between the eccentricity Larsson relation

Lug	$\frac{a}{c}$	σ_{nom} [MPa]	k_1k_2	K_{ecc}	$\frac{\sigma_{nom}}{\sigma_{nom_{ref}}}$	$k_1k_2K_{ecc}$	Error Equation 6.9 [%]
a5	0.5	8.731	0.707	1.207	0.887	0.854	-3.95
c15	0.667	7.538	0.667	1.157	0.766	0.771	0.67
a10c10	1.0	9.839	1.000	1.056	1.000	1.056	5.32
a15	1.5	10.780	1.225	0.905	1.096	1.109	1.17
c5	2.0	15.360	2.000	0.754	1.561	1.508	-3.51

The results show that an initial linear correction factor for the eccentricity creates reasonable results. The discrepancy between the left and right side of Equation 6.9 is up to 5%. The largest error is for the a10c10 lug, which is the same lug as the reference lug. Since a10c10 and the reference lug have exactly the same results when axially loaded, the added eccentricity factor K_{ecc} creates the difference between the two. Taking the error margin of Larsson in account, all error margins remains between the ±15% which is deemed as valid. For the eccentric forward and backward lugs the errors have been reduced to a reasonable value of around 4% maximum.

With the addition of the eccentricity factor into the Larsson relation discrepancy between the nominal stress ratio and the correction factors fall within the error margin of ±15%. Therefore, to improve the Larsson relation the eccentricity factor is added to the equation. The implementation of factor K_{ecc} results in a closer approximation between the reference lug nominal stress and the arbitrary lug nominal stress.

The Larsson relation combined with the eccentricity factor is still limited to straight-sided axially loaded lugs. But how do the taper angles or load angles affect the eccentricity Larsson relation? In Chapter 7 the effects of changing the taper angle or changing the load angle on an arbitrary lug are compared with the eccentric Larsson relation.

Chapter 7

Taper and Load Angle Analyses

In Chapter 6 the eccentricity factor has been introduced. In order to account for more lug geometries and load cases, the taper and load angle have been varied. In reality, tapered lugs are present and the applied load is not always a pure axial load. Using the same lug geometry defined in Table 6.1 the lugs are analysed with the addition of a taper angle, load angle, and a combined case. First the results of a varied taper angle are presented in Section 7.1. Then, in Section 7.2 a varying load angle is introduced and the results are presented. Finally, in Section 7.4 the results of the combined case of taper and load angle is discussed with respect to the eccentricity Larsson relation.

7.1 Taper angle analyses

The case lugs of Table 6.1 are now analysed with an addition of a constant taper angle. The taper angle has been set at $\beta = 20°$. The lugs are subjected to a pure axial load. Following the same principles as in Chapter 6 for the simulations, the peak stress of the tapered lugs are made equal to the peak stress of the reference lug. The peak stresses of the tapered lug are always smaller than than the yield stress of the material in order to comply with the assumption made.

The results of FEA for tapered lugs are related by the eccentricity Larsson relation of Equation 6.9. This provides an indication on how the results of a tapered axially loaded lug hold with respect to the Larsson relations, since Larsson assumed only straight-sided symmetrical lugs.

Using FE for a 20° taper angle the results have been generated. Table 7.1 presents the magnitude for the different components of the eccentricity Larsson equation. The column errors represent the difference between the two sides of the Larsson relation. The first error column is with respect of the basic Larsson relation when tapered lugs are taken into account. The

second error column is for taking the eccentricity factor into account.

Table 7.1: Results Larsson relation for lugs with $\alpha = 0°$ and $\beta = 20°$

Lug	$\frac{a}{c}$	K_{ecc}	$\frac{\sigma_{nom}}{\sigma_{nom_{ref}}}$	$k_1 k_2$	$k_1 k_2 K_{ecc}$	Error Equation 6.6 [%]	Error Equation 6.9 [%]
a5	0.5	1.207	0.848	0.707	0.854	-19.90	0.68
c15	0.667	1.157	0.756	0.667	0.771	-13.40	1.98
a10c10	1.0	1.056	1.033	1.000	1.056	-3.26	2.23
a15	1.5	0.905	1.111	1.225	1.109	9.30	-0.21
c5	2.0	0.754	1.541	2.000	1.508	22.96	-2.16

From Table 7.1 it shows that the basic Larsson relation have an error up to 23% for tapered lug. When adding the correction factor K_{ecc} the error reduces with a maximum error of around 2.3%. The acceptable error margin is between ±15% for which all results of the eccentricity Larsson relation

It seems that the addition of a taper angle does not have a great effect on the discrepancy between the nominal stress ratio and the correction factors. Taking into account the eccentricity factor resolves the error between the two sides of the equation. It seems that the taper does not effect the stresses in addition to the eccentricity. The errors in Larsson follow the same trend as seen in Section 6.5 for the non-tapered axially loaded lugs. Thus, adding a taper angle does not have a large effect on the Larsson relation. Looking at the errors for the eccentricity Larsson relation are all well within the ±15%. Therefore, no taper correction factor is required in the eccentricity Larsson relation of Equation 6.9.

7.2 Load angle analyses

Larsson only took axially loaded lugs into account for his relation. In reality not all loads are purely axial and oblique loads do occur on the lug. In order to account for obliquely loaded lugs, an FEA has been conducted under a load angle $\alpha = 45°$. The same axially loaded reference lug defined in Section 6.3 has been used to determine the reference stresses for the oblique loaded lugs.

The magnitude of the load is adjusted such that the peak stress is equal to peak stress of the reference lug. Since the load angle has changed, the location of the maximum peak stress changes as well. Therefore, the NS is taken at a different location compared with the axially loaded lug.

As mentioned before when a lug is loaded, two peak stresses are present around the circumference of the hole. One at the topside and one at the bottom side of the hole. For axially loaded lugs both peak stresses are equal in magnitude and directly opposite of each other. When the load angle changes, the top and bottom peak stress are no longer equal and are not

directly opposite of each other [19]. In Figure 7.1 the peak stress locations from the FEA for a $\theta = 45°$ is presented. The load is applied the positive defined load direction. Therefore, the left peak stress is the topside peak stress and the right stress the bottom peak stress. Figure 7.1 shows that the peak stresses are not 180° from each other. The oblique peak stresses are located at 144° and 297° defined in the positive α direction, respectively. Comparing the peak stress locations of Kathiresan et al. [19], which for the oblique loaded lug were located at 65° and 225° defined in the negative α direction as positive. Rewriting the oblique FE peak stresses in the negative α direction give $-216°$ and $-63°$, respectively. Thus the peak stress location verify with literature.

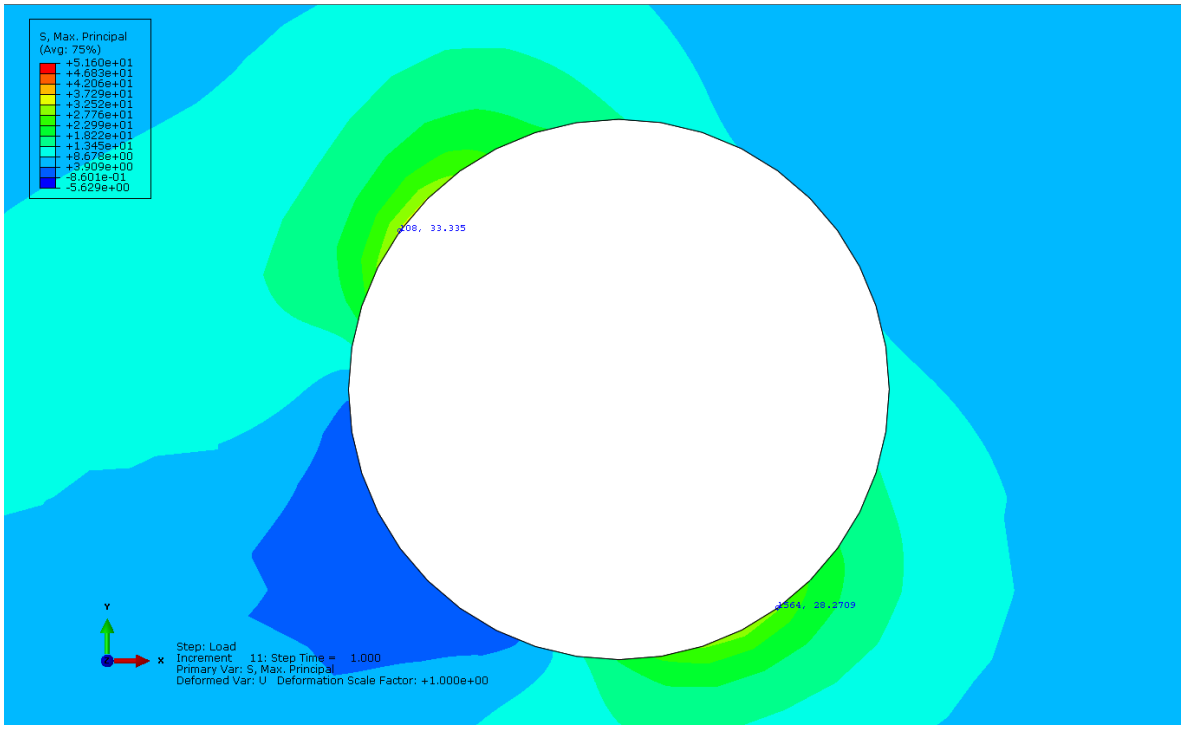

Figure 7.1: Peak stress locations for load angle $\theta = 45°$

It has been chosen to take the peak stress on the bottom side of the lug in order to find the nominal stress for an oblique loaded lug. The bottom peak stress has been made equal to the reference peak stress. Doing so makes the top peak stress always larger than the reference peak stress. The reason for taking the bottom peak stress is that when failure occurs, failure will take place at the bottom side of the lug instead failure at the topside [18, 19]. Crack initiation will start at the topside due to the larger peak stress and at a later point in time initiation starts at the bottom. Since the width at the bottom peak stress is smaller compared to the width at the top peak, failure would occur at the bottom first.

The results of the oblique loaded straight-sided lugs are presented in Table 7.2. Here, the magnitude for the different correction factors and the nominal stress ratio between the oblique loaded and reference lug is displayed. The discrepancy between the nominal stress ratio and correction factors are displayed in the error column.

Table 7.2: Results Larsson relation for lugs with $\alpha = 45°$ and $\beta = 0°$

Lug	$\frac{a}{c}$	K_{ecc}	$\frac{\sigma_{nom}}{\sigma_{nom_{ref}}}$	$k_1 k_2$	$k_1 k_2 K_{ecc}$	Error Equation 6.6 [%]	Error Equation 6.9 [%]
a5	0.5	1.207	0.983	0.707	0.854	-39.02	-15.16
c15	0.667	1.157	0.810	0.667	0.771	-21.52	-5.04
a10c10	1.0	1.056	0.862	1.000	1.056	13.83	18.42
a15	1.5	0.905	0.910	1.225	1.109	25.71	17.93
c5	2.0	0.754	1.192	2.000	1.508	40.39	20.95

The results show that the change in load angle greatly affect the Larsson relations. Using the Larsson relation (Equation 6.6), error between the stress ratio and the correction factors is up to 40%. Taking the eccentricity factor into account with Equation 6.9 than the difference between the two sides is reduced. Still the error is greater than the ±15% margin. One thing to note is that going from eccentric forward to concentric the results are quite linear in trend. While from concentric to eccentric backward the trend is quite a constant line of around 20%.

The majority of the cases fall outside the error margin of ±15%. In order to account for the load angle, a correction factor has been created.

7.3 Load angle correction factor

In order to implement a load angle correction factor into the Larsson relation, an equation is derived which is be present in the Larsson relation even if $\alpha = 0°$. The load correction factor is equal to 1 when the load angle is 0° and has to change when the load angle changes. Judging from prior results, the correction factor has to be larger than 1 for eccentric forward lugs. For the concentric and eccentric backward lugs the load correction factor should roughly stay equal for these type of lugs.

With this knowledge a load correction factor, K_α have been created. In Figure 7.2 the values for K_α for the different lug cases are presented. A trend line is provided to show the transition of the correction factor for the different eccentricity ratios.

The load correction factor is defined by the following relation:

$$K_\alpha = \alpha \cdot \left(\left(\frac{0.007}{\frac{a}{c}} \right) - 0.008 \right) + 1 \tag{7.1}$$

with the relation dependent on the load angle and the eccentricity. It is clear that when the lug is axially loaded ($\alpha = 0°$), K_α equals to 1.

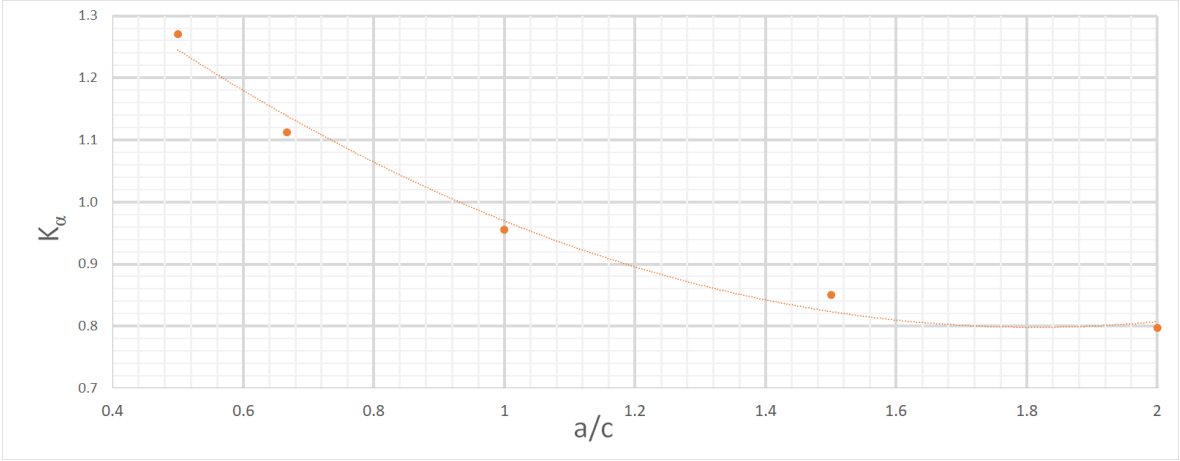

Figure 7.2: The K_α expressed against the eccentricity

The load angle correction factor is implemented in the Larsson relation in the same fashion as the eccentricity factor. The new equation which includes the load angle factor, from now on referred to as the eccentricity load Larsson relation, is defined by:

$$\frac{\sigma_{nom}}{\sigma_{nom_{ref}}} = k_1 k_2 K_{ecc} K_\alpha \tag{7.2}$$

Using K_α in the Larsson relation, the error between the left and right-hand side has been calculated again. The values for K_α and the percentile error within Equation 7.2 are presented in Table 7.3.

Table 7.3: Values K_α and the errors with Equation 7.2

Lug	K_α	$k_1 k_2 K_{ecc} K_\alpha$	Error Equation 7.2 [%]
a5	1.270	1.084	9.33
c15	1.113	0.858	5.58
a10c10	0.955	1.009	14.57
a15	0.850	0.942	3.44
c5	0.798	1.203	0.88

The implementation of the K_α factor in Larsson resulted in errors, which all fall into the $\pm 15\%$ range. The biggest discrepancy occurs for the concentric case. This is mainly because the K_α fit has the biggest discrepancy at eccentricity $\frac{a}{c} = 1$.

With the addition of the load angle correction factor, the eccentricity load Larsson relation can be used for load angles up to 45°. The question is if the eccentricity load Larsson relation is also valid for when the two cases are combined into a tapered non-axially loaded lug. More about this in Section 7.4

7.4 Combined taper and load angle analyses

The lug geometries defined in Table 6.1 have been used in combination with a taper and load angle. The taper angle has been set at 20° and the load angle has been set at 45°. The results of the FEA are presented in Table 7.4. The error with Larsson relation and the error with the eccentricity load Larsson relation are presented in the error column.

Table 7.4: Results Larsson relation for lugs with $\alpha = 45°$ and $\beta = 20°$

Lug	$\frac{a}{c}$	K_{ecc}	K_α	$\frac{\sigma_{nom}}{\sigma_{nom_{ref}}}$	$k_1 k_2 K_{ecc} K_\alpha$	Error Equation 6.6 [%]	Error Equation 7.2 [%]
a5	0.5	1.207	1.270	1.023	1.084	-44.74	5.60
c15	0.667	1.157	1.113	0.832	0.858	-24.78	3.05
a10c10	1.0	1.056	0.955	0.925	1.009	7.46	8.26
a15	1.5	0.905	0.850	0.915	0.942	25.29	2.89
c5	2.0	0.754	0.798	1.303	1.203	34.85	-8.33

It clearly shows that without the added correction factors the Larsson relation would not be valid for a tapered non-axially loaded lug. By adding the eccentricity and load angle correction factor to the equation, the error remains within the ±15% margin. So far, a lug with a combination of a taper angle and load angle are compared via the Larsson relation with the addition of the eccentricity and load angle correction factor. In Chapter 8 different taper angles, load angles and combinations between the two are investigated. The load angle is changed between 0° and 45° and taper angle between 0° and 20° in the verification.

Chapter 8

Verification In-Plane FEA

In Chapter 7 two correction factors have been added to the Larsson relation. These correction factors have been generated on the basis of a taper angle of $\beta = 20°$ and a load angle of $\alpha = 45°$. At the moment these values represent the boundaries of the correction factor. This chapter discusses the effects when the taper angle is between 0° and 20° and when the load angle is between 0° and 45°. In Section 8.1 the different combinations of load and taper angles are presented and, which lugs have been used for the analyses. Section 8.2 discusses the results of the verification analyses.

8.1 Verification lugs

For the verification different combinations of α and β have been selected. For a large part of the verification cases only the load angle is varied. Some cases included a fixed taper angle, which is different from the taper angle used for the FEA of Equation 7.2. The different options, which have been analysed are presented in Table 8.1. Since the load angle had the largest effect on the Larsson relation more cases with varying load angles have been investigated. The verification is divided into three groups. Cases 1 to 3 are for varied load angle, case 4 is for a different fixed taper angle, and cases 5 to 7 are for varied load angles at a fixed taper angle.

For each of the verification cases a selection of the different case lugs have been used for the FEA. Each of the FE lugs have been implemented with the new load and taper angles corresponding with the verification case number. The lugs used for each of the different verification cases are presented in Table 8.1 as well. The FE lugs geometries are found in Chapter 6, Table 6.1. For all these lug cases the stresses are calculated and compared using the eccentricity load Larsson relation seen in Equation 7.2. The results are displayed in Section 8.2.

Table 8.1: The verification case combinations of load and taper angle with corresponding FE lugs

Verification case	α [°]	β [°]	FE Lug
1	10	0	a5, a10c10, c5
2	20	0	a15, c15
3	30	0	a5, c15 a10c10, a15, c5
4	0	10	a5, a10c10, c5
5	10	10	a5, a10c10, c5
6	20	10	a15, c15
7	45	10	a5, a10c10, c5

8.2 Results

The verification cases are separated in three groups. A variable load angle for the cases 1 to 3, a variable taper angle for case 4 and a combination of taper and load angle for cases 5 to 7. The effects of a different load angle is discussed in Section 8.2.1. In Section 8.2.2 the effect of a different taper angle is shown. A new combination of variable load angle at a different taper angle is presented in Section 8.2.3.

8.2.1 Variable load angle

The results of the FEA for the varied load angles are listed in Table 8.2. For verification case 1 the lugs have been investigated by setting the load angle on $\alpha = 10°$. The implementation of the eccentricity and load correction factors and the comparison with the nominal stress ratio show that the errors within Equation 7.2 are within the $\pm 15\%$ error margin.

For case 2 of the verification the load angle has been set to $\alpha = 20°$. From the results it shows that the errors are within the defined margin of error. The lugs c15 and a15 have been chosen to provide confirmation that the entire spectrum of lugs complies with the Equation 7.2. In case 1 the other scenarios for eccentricity have been selected. In case 2 the inner scenarios have been selected for simulation.

In verification case 3 all the lugs have been selected for analyses. With case 3 the load angle has been set at $\alpha = 30°$. Again the error margins fall within the $\pm 15\%$. Thus, the eccentricity load Larsson relation is valid for a load angle domain of 0° to 45°.

8.2.2 Variable taper angle

With verification case 4 the effect of a different taper angle has been investigated. The effects of taper angle on the Larsson relation has been found to have negligible impact on the Larsson relation. For verification, the taper angle has been set at $\beta = 10°$. The different eccentricity lugs and the concentric lug have been selected to provide a general range for the geometry

Table 8.2: Verification results for the varied load angle cases

Case	Lug	$\frac{\sigma_{nom}}{\sigma_{nom_{ref}}}$	$k_1 k_2 K_{ecc} K_\alpha$	Error Equation 7.2 [%]
1	a5	0.932	0.905	-3.00
1	a10c10	0.974	1.046	6.82
1	c5	1.489	1.440	-3.38
2	c15	0.810	0.810	0.01
2	a15	0.998	1.035	3.55
3	a5	0.973	1.007	3.37
3	c15	0.837	0.829	-0.92
3	a10c10	0.902	1.025	11.99
3	a15	0.993	0.998	0.47
3	c5	1.262	1.305	3.24

ratios and the effect of changing taper angle. The analyses results are presented in Table 8.3.

Table 8.3: Verification results for varied taper angle case

Case	Lug	$\frac{\sigma_{nom}}{\sigma_{nom_{ref}}}$	$k_1 k_2 K_{ecc} K_\alpha$	Error Equation 7.2 [%]
4	a5	0.879	0.854	-2.94
4	a10c10	1.038	1.056	1.75
4	c5	1.608	1.508	-6.61

Using the Larsson relation to compare the results it is found that the error for the different cases falls within the margin of error. Thus, for a varied taper angle within $0° \leq \beta \leq 20°$ the eccentricity load Larsson relation is valid.

8.2.3 Variable taper angle and load angle

For the last verification cases the load angle has been varied between $0° \leq \alpha \leq 45°$ for a fixed taper angle equal to $\beta = 10°$. The load angles has been set at 10°, 20° and 45°, respectively. The results for cases 5 to 7 are displayed in Table 8.4.

Table 8.4: Verification results for variable load angle at $\beta = 10°$ cases

Case	Lug	$\frac{\sigma_{nom}}{\sigma_{nom_{ref}}}$	$k_1 k_2 K_{ecc} K_\alpha$	Error Equation 7.2 [%]
5	a5	0.996	1.084	-1.81
5	a10c10	0.951	1.009	0.76
5	c5	1.216	1.203	-8.53
6	c15	0.810	0.810	-0.85
6	a15	0.998	1.035	-3.14
7	a5	0.996	1.084	8.10
7	a10c10	0.951	1.009	5.73
7	c5	1.216	1.203	-1.23

The results for cases 5 to 7 show that all results are within the error margin of ±15%. Interesting to note is that when the load angle is 10° the c5 lug has the largest error while when the load angle is 45° the a5 lug has the largest error.

The FEA performed on the different verification case using the eccentricity load Larsson relation, shows that the Equation 7.2 is verified for varying load and taper angle within a certain range. The range for the taper angle is between $0° \leq \beta \leq 20°$. The load angle can vary between $0° \leq \alpha \leq 45°$.

In order to validate the eccentricity load Larsson relation an experimental testing campaign has to be performed. To investigate the effect of taper and load angle on the fatigue life of the lug fatigue testing of different in-plane loaded lugs have to be done. These test are mentioned in the recommendations found in Chapter 11.

Chapter 9

In- and Out-of-Plane Loaded Lugs

In the previous chapters all the lugs were in-plane loaded lugs. Chapter 9 focuses on the addition of an out-of-plane load component on the lug. These lateral loads induce bending of the lug, resulting in different stress distributions. The lateral loads are combined with an axial load creating a combined in- and out-of-plane load condition. Using FE software the stress distributions for these combined cases have been simulated. The results of FEA are given in Section 9.1. Section 9.2 discusses the shift in peak stress for increasing lateral loads. The discrepancies in the results are elaborated in Section 9.3. The nominal stresses from FEA for axially, laterally and combined loaded lugs are presented in Section 9.4. Section 9.5 presents what the predicted nominal stress for the in- and out-of-plane loaded lug is. Implementation of a correction factor for lateral loads within the Larsson relation is presented in Section 9.6. The verification for a lateral correction factor is given by Section 9.8.

9.1 Out-of-plane FEA

For the FEA an in-plane and out-of-plane loading has been applied. The axial load P has been made constant for the analyses while the lateral load F varies. This way the effects of the lateral loading on the stress distribution lug was investigated. The axial load has been set equal to $P = 1000$ N, which is in line to the axial load applied for the in-plane loaded lug analyses performed in previous chapters. The lateral load is varied from 300 to 2000 N. By keeping the axial load constant and varying the lateral load the bending factor k changes per analysis. Bending factor k illustrates the ratio between the lateral load and the axial load. The factor k is calculated with:

$$k = \frac{F}{P} \tag{9.1}$$

In a similar fashion to the in-plane FEA, the nominal stress is calculated from the peak stress location in the FEA. For the combined in- and out-of-plane loads, the peak stresses are located

at different locations compared to the in-plane peak stresses and follow different guidelines. For axially or oblique loaded lugs the peak stresses are mirrored via the line of action of the applied load. The peak stresses are directly opposite of each other by 180°. With a combined axial and lateral loaded lug the peak stresses are still mirrored by the line of action of the axial load but are not 180° apart from each other on the circumference of the hole. Figure 9.1 presents the peak stress locations of an axially and lateral loaded lug.

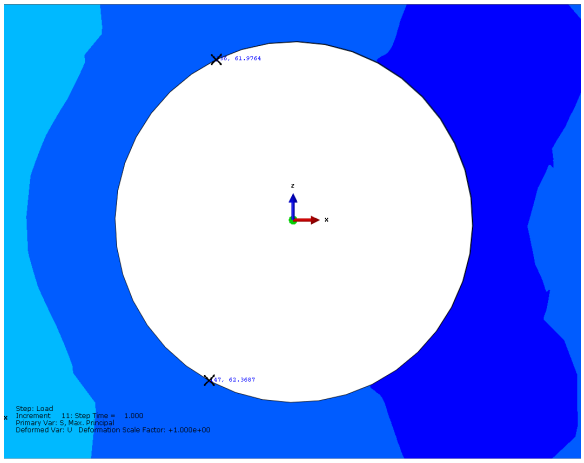

Figure 9.1: Peak stress locations of an axially and laterally loaded lug at $k = 2.0$

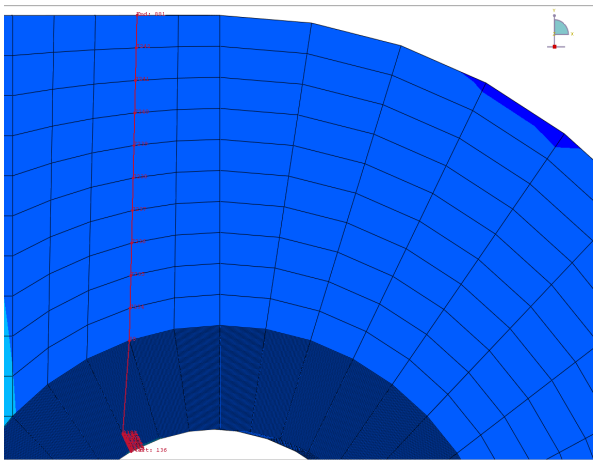

Figure 9.2: NS path in the FEA for $k = 2.0$

From the peak stress locations the nominal stress is defined by taking the stress distribution from the peak stress to the edge of the lug along a perpendicular line. The NS path is presented in Figure 9.2. Due to the way the mesh is defined the NS taken in ABAQUS is not a perpendicular line to the side of the lug as theory would dictate. The path in ABAQUS has to go along the nodes of the mesh. Since the mesh is radially defined around the hole, a perpendicular line is not possible and the closest approximation within the current mesh has been taken. The NS paths for the different k factors are displayed in Appendix E. Suggestion for improvements of the mesh are discussed in Chapter 11.

The eccentricity load Larsson relation described in Equation 7.2 has been used in order to check the effects of a lateral load component. Only the reference lug has been used for the FEA. The correction factors of Equation 7.2 are displayed in Table 9.1. The analyses has been conducted on different bending factors, each generating a different nominal stress presented in Table 9.2. The discrepancy between the two sides of the equation is presented in the error column in Table 9.2.

Table 9.1: Magnitude of the corrections factors of the Equation 7.2

Lug	k_1	k_2	K_{ecc}	K_α
a10c10	1.000	1.000	1.056	1.000

Table 9.2: Results of the combined in- and out-of-plane FEA

F [N]	k	σ_{nom} [MPa]	$\frac{\sigma_{nom}}{\sigma_{nom_{ref}}}$	$k_1 k_2 K_{ecc} K_\alpha$	Error Equation 7.2 [%]
300	0.3	11.34	1.038	1.056	1.71
500	0.5	11.91	1.042	1.056	1.33
1000	1.0	14.86	1.116	1.056	-5.63
1100	1.1	15.33	1.122	1.309	-6.26
1200	1.2	19.86	1.405	1.056	-33.05
1500	1.5	22.51	1.417	1.056	-34.19
2000	2.0	26.82	1.459	1.056	-38.17

The results show that when the bending factor is greater than 1.0 than the nominal stress ratio increases by roughly 25%. Since the correction factors remain the same for every analyses, the sharp increase in the nominal stress ratio lead to an error percentage larger than the ±15%. For bending ratios smaller than and equal to $k = 1.0$ the differences are within the error margin of ±15%.

The nominal stress ratio increases linearly for increasing lateral load. This was expected since stresses for a lateral load increase linear for increasing lateral loads. Because the axial load is kept constant a linear increase in stresses was expected. Figure 9.3 presents the nominal stress for increasing bending factor. From the results it shows that the nominal stress follows two different linear trends. There is a discontinuity in the results between $k = 1.1$ and $k = 1.2$. To understand how this discontinuity occurs the shift of the peak stress location and how the NS is defined in the FEA needs to be elaborated. This is presented in Section 9.2. After that, Figure 9.3 is discussed in more detail in Section 9.3.

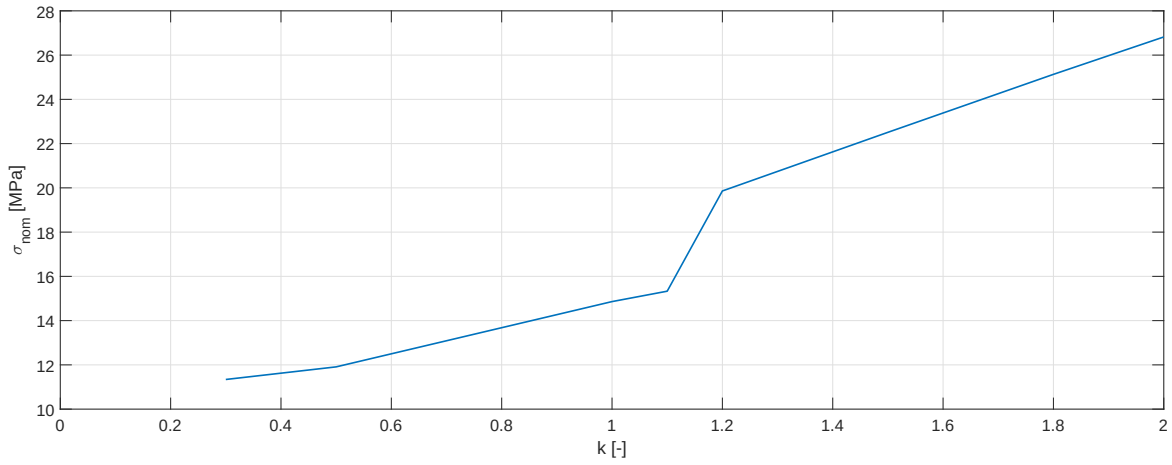

Figure 9.3: Nominal stress out-of-plane loaded lug for increasing k factor

9.2 Peak stress location shift

The FEA of the combined loaded lugs showed that for increasing bending factors the peak stress shifts further backwards compared with the peak stress location of a pure axially loaded lug. In Figure 9.4 the peak stresses for a pure axially loaded lug and a (pure) laterally loaded lug are presented. Comparing the stress locations between the two cases it is clear that the peak stresses for the lateral load have shifted towards the back of the lug.

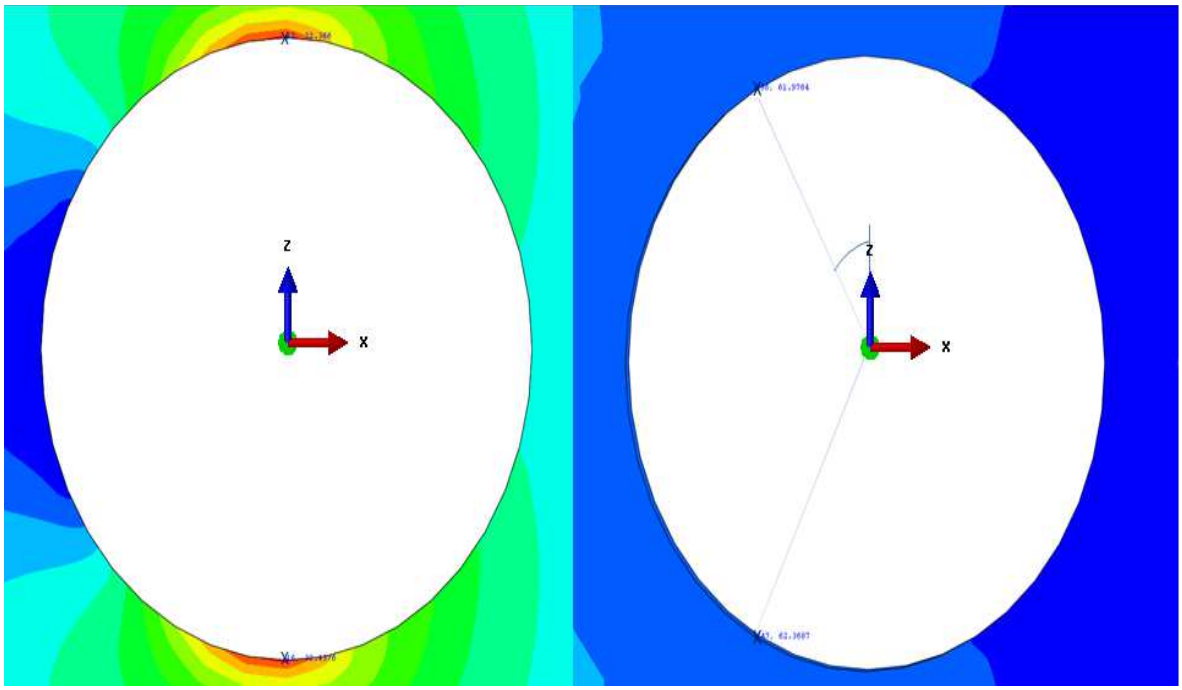

Figure 9.4: Peak stress locations for an axially loaded lug (left) and a laterally loaded lug (right)

When a lateral load is applied with an axial load, thus increasing the bending factor, a shift in peak stress location is seen from the pure axially loaded locations moving towards the lateral peak stress locations. Figure 9.5 presents the peak stress locations for a bending factor of $k = 0.5$, $k = 1.0$ and $k = 2.0$, respectively. The peak stresses show that for increasing bending factor the location shifts more and more towards the location of the lateral load peak stresses. Looking at ratios between 1.0 and 2.0 it is found that at $k = 1.1$ the peak stress location is the same as for $k = 1.0$ while for $k = 1.2$ the location are the same as for $k = 2.0$. The peak stress does not shift further than this node for the combined load cases. Because of the limitation in the number of circumference nodes present in the mesh, the shift of the peak stress location can not be followed in more detail. In Chapter 11 more about the mesh and the limitations are discussed.

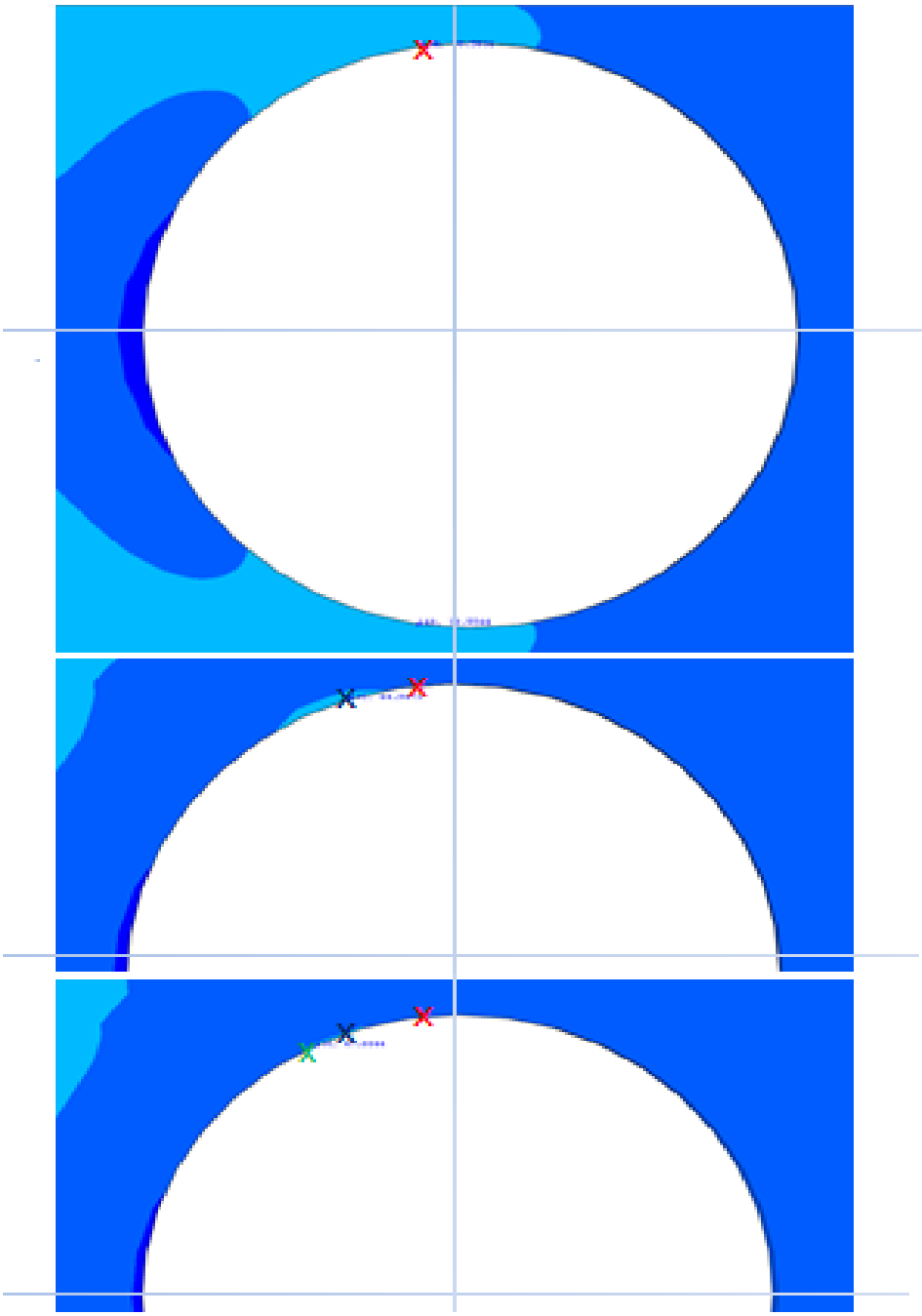

Figure 9.5: Shift of peak stress locations for $k = 0.5$, $k = 1.0$, and $k = 2.0$, respectively

As is shown in Figure 9.5 is that for increasing bending factor the peak stress shifts more towards the peak stress location for a pure laterally loaded lug. The shift in peak stress results in that the nominal stress is taken at a different location thus, the NS shifts backwards. As explained in Section 9.1 the NS can not follow a perpendicular path in the used mesh of the lug. The shift in peak stress location and the used NS path can explain the discontinuity that occurs in the nominal stress results.

9.3 Discontinuity in the FEA nominal stress

Taking a closer look at the nominal stress curve obtained from the FEA presented in Figure 9.6. The nominal stress curve is presented as the two linear trends. Knowing that a peak stress shift occurs when the bending factor increases from $k = 1.1$ to $k = 1.2$. Between these values of k the discontinuity in Figure 9.6 occurs.

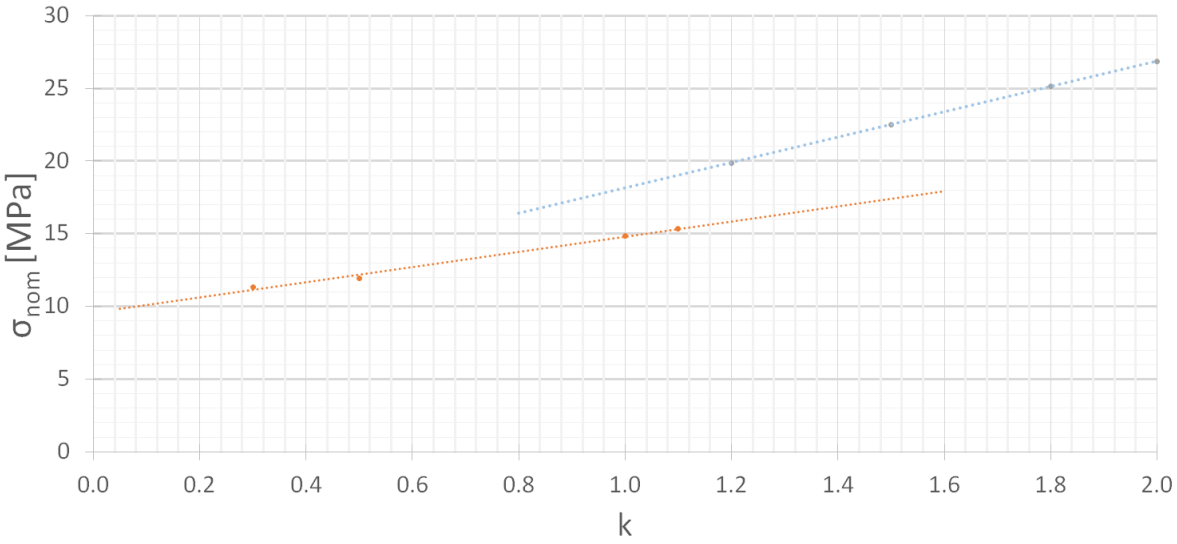

Figure 9.6: FEA Nominal stress for out-of-plane loaded lug at increasing bending factor

The different trend lines clearly indicate that the nominal stress curves before and after $k = 1.1$ are different. Since the axial load is kept constant and only a varying bending load is introduced a linear trend is expected without a discontinuity. One of the main reasons that the discontinuity occurs is because of the mesh. The mesh defined the NS path along which the nominal stress has been calculated. The NS paths used for the different FEA are presented in Appendix E.

The main difference between the analysis of $k = 1.1$ and $k = 1.2$ is the node on which the peak stress is located and the defined NS path. Beside that the starting node and the path differ, the end node is different as well. The NS path of $k = 1.1$ ends at a different node at the edge of the lug compared with the NS path of $k = 1.2$. The stresses are linearly increasing towards the clamped BC due to the applied bending. Therefore, the nodes closer to the BC have a higher stress than those further away. The stresses found via the $k = 1.2$ path are higher than those of the $k = 1.1$ path because of this. Since the loading conditions of $k = 1.1$ and $k = 1.2$ are nearly identically, the peak stresses of $k = 1.1$ are nearly equal to those of $k = 1.2$ analysis. The peak stresses and the stresses along each NS path for $k = 1.1$ and $k = 1.2$ is presented in Figure 9.7.

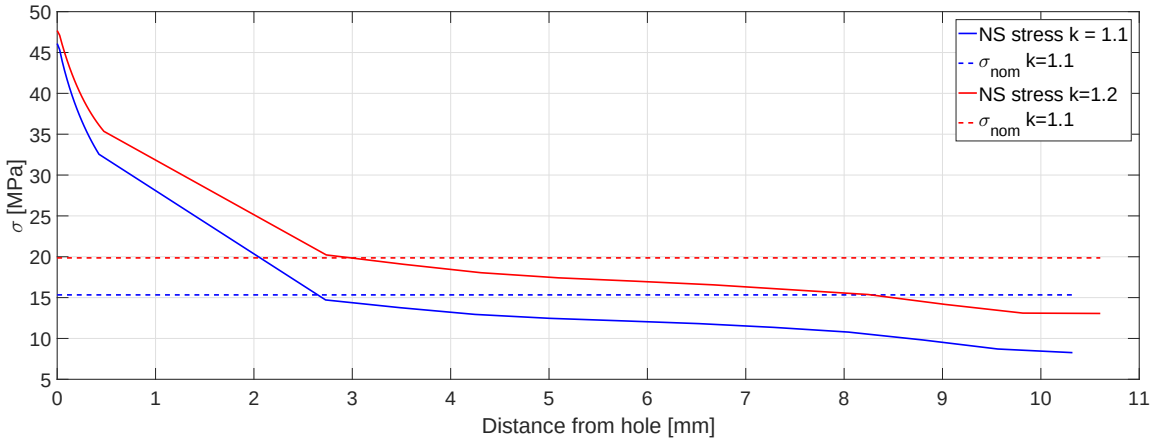

Figure 9.7: NS stress distribution and nominal stress for $k = 1.1$ and $k = 1.2$

Given the fact that the peak stresses are similar and the stresses along the path of $k = 1.2$ are larger than the $k = 1.1$ stresses result in higher nominal stresses for the analysis using the $k = 1.2$ path. This lead to the discontinuity as seen in Figure 9.6.

The results obtained with the FEA of an axially and laterally loaded lug present a nominal stress curve for increasing bending factor. These nominal stress curves are presented in Section 9.4.

9.4 Nominal stress curves

Looking at the axial and lateral component separately one would expect that the axial load is a constant nominal stress (single load condition) while the lateral load should increase linearly for increasing load. The axial and lateral nominal stresses are presented in Figure 9.8. The pure axially loaded lug nominal stress is independent of the lateral load. The nominal stresses have been calculated by performing an FEA for increasing lateral load.

For the combined load case of an axial and lateral load one would expect a combination of the two nominal stresses. This is represented in the superposition curve. The superposition curve is the superposition of the axial stress curve with the lateral stress curve. The results of the FEA for the axial and lateral loads presented in Figure 9.3 is added to Figure 9.8.

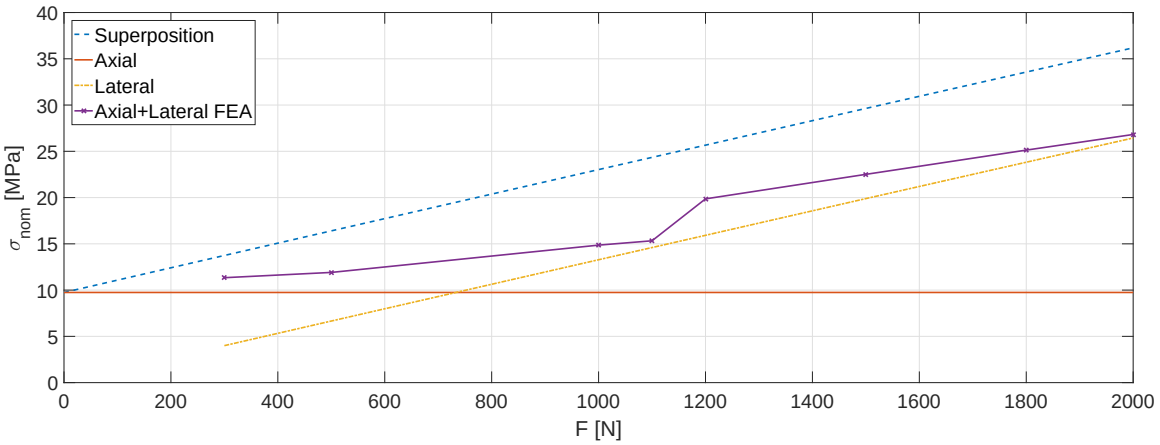

Figure 9.8: Nominal stress for axially loaded lug, laterally loaded lug, superposition, and combined axial and lateral nominal stress results

From the figure it is clear that the FE results are not the same as results calculated by superposition. Even disregarding the discontinuity, the slopes of both curves do not match, with the slope of the superposition being much steeper than the FE curve. Without experimental test it is hard to say which of the curve is a representation of reality.

From Figure 9.8 it is clear in which range the nominal stress of the combined axial and lateral load should be. The nominal stress range is above the axial nominal stress curve and between the lateral and superposition stress curve. The current FE prediction of the combined case is within this range as shown in Figure 9.8. However the slope of the ABAQUS curve does not match with the slopes of the domain boundary.

The slope difference is explained by how the loads are defined in ABAQUS. Looking at the slopes of each curve presented in Figure 9.8 it shows that the axial load has no slope since it is not dependant on the lateral load and has a constant nominal stress. The lateral load is a linear increasing line and this is the same for the superposition curve. Both these lines have the same slope. The slope of the FEA is smaller compared with the lateral or superposition slope.

A reason for the difference in slope is because of the interaction between the lateral and axial load in ABAQUS. The load for the axial and lateral load case are applied on the model as explained in Chapter 4. During the FEA the lug deforms due to the applied loads. This results in that the applied axial and lateral load will not remain a pure axial or pure lateral load since the loads are applied on a surface of the model. Because of the deflection of the lug, the surface on which the load is applied deflects resulting in a certain deflection angle between the original load position and the new position. The applied load are not acting purely in axial or lateral direction. This is represented in Figure 9.9. Breaking the loads into components shows that the horizontal lateral component counteracts the horizontal axial component. For increasing loads, deflection increase and such the misalignment under which the loads are applied on the model increase. The axial load elongates the lug while the lateral load deflects the lug. The interaction of the loads results in a different slope for the combined

load case compared with the superposition curve.

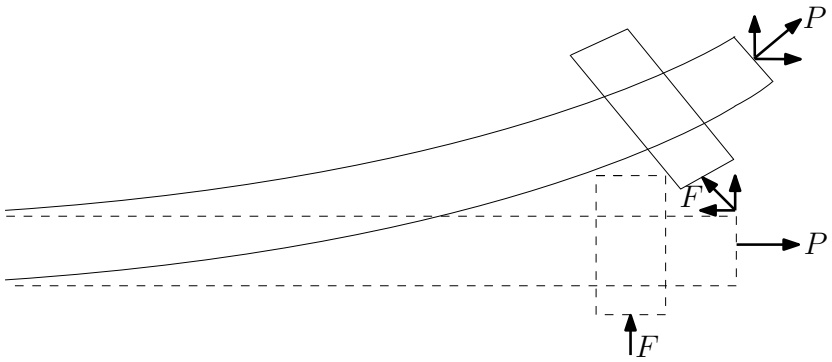

Figure 9.9: Load deflection due to the deformation of the lug

Even though the FE curve is within the domain for the nominal stress. A different more linear trend for the nominal stress of the combined load case was expected. This expected nominal stress curve is elaborated in Section 9.5.

9.5 Nominal stress prediction

The FEA shows two distinct linear relations for the combined axial and lateral load case, each resulting in a different start and end point when extrapolated. Which of the two linear trends of the combined load case is closer to reality remain uncertain without performing experimental testing. It is expected that the nominal stress curve is between the lateral and the superposition curves. The expected nominal stress curve for an axially and laterally loaded lug is presented in Figure 9.10.

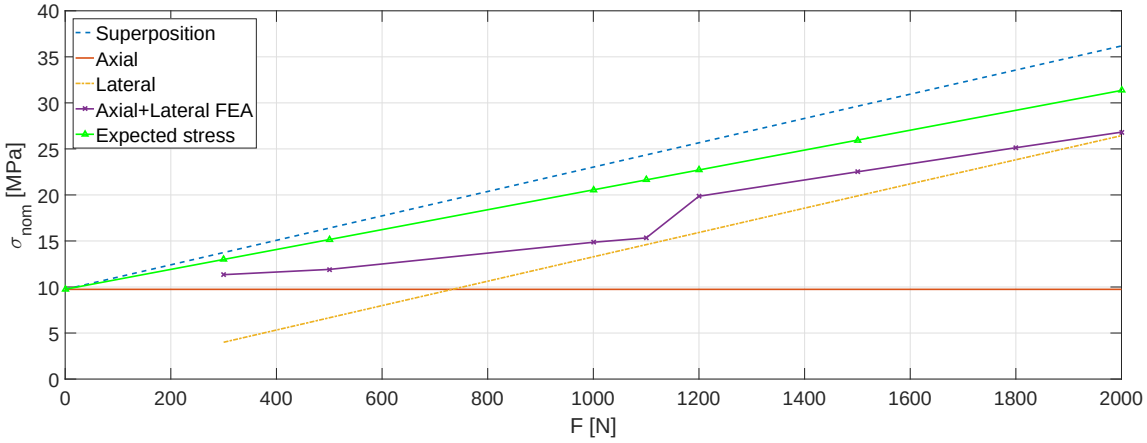

Figure 9.10: Expected nominal stress curve for axial and lateral loaded lug

The expected nominal stress curve resembles the superposition curve however, the gradient is lower. This is because the analytic curve is a direct summation of the axial and lateral nominal stress. In reality an interaction between the axial and lateral load is expected resulting in that a directed summation of the two component will be an overestimation of the stresses. Similar to the analytic and lateral curve a constant linear trend has been assumed.

The expected nominal stresses are greater than the FEA nominal stress. To remain conservative the nominal stress has been assumed to be greater than the FE nominal stress. Again, to validate that the nominal stresses are as the expected curve or the FE curve, experimental tests have to be performed. The nominal stress curve is defined by the relation:

$$\sigma_{nom_{exp}} = 0.0108 \cdot F + \sigma_{axial} \tag{9.2}$$

were F is the applied lateral load and σ_{axial} is the nominal stress for the axial load component in an axially laterally loaded lug. Since a force is multiplied by a factor in Equation 9.2, the factor 0.0108 has technically a unit of $\frac{1}{mm}$.

It is important to note from Equation 9.2 that the equation is dependent on the lateral load but also on the axial nominal stress. When the axial load varies, the nominal stress changes resulting in a different horizontal line and nominal stress range. Therefore, the expected nominal stress is dependent on the axial nominal stress and scales accordingly.

To be conservative the expected nominal stresses have been used as the respective nominal stress for the different combined load cases subjected on the lugs. The nominal stress defined by Equation 9.2 is implemented in Equation 7.2 resulting in a new error between the two sides of the equation. The results are presented in Table 9.3.

Table 9.3: Results of implementing the expected nominal stress into Equation 7.2

F [N]	k	σ_{nom} [MPa]	$\frac{\sigma_{nom}}{\sigma_{nom_{ref}}}$	$k_1 k_2 K_{ecc} K_\alpha$	Error Equation 7.2 [%]
300	0.3	12.99	1.189	1.056	-12.60
500	0.5	15.15	1.326	1.056	-25.52
1000	1.0	20.55	1.543	1.056	-46.09
1100	1.1	21.63	1.584	1.056	-49.94
1200	1.2	22.71	1.607	1.056	-52.16
1500	1.5	25.95	1.634	1.056	-54.71
2000	2.0	31.35	1.706	1.056	-61.51

The errors in Table 9.3 are larger than the errors listed in Table 9.2 when the FE results were used. Although the results are worse the nominal stresses should be closer to reality and as such calculated error is a better representation of reality. As is shown in the table the errors are increasing when the bending ratio increases. The error follows a parabolic (second order) trend. The majority of the errors are outside the ±15% error margin. Therefore, Equation 7.2 is not suitable for out-of-plane loaded lugs and a lateral correction factor is introduced.

9.6 Lateral correction factor

The lateral correction factor is created following the same principles as the other correction factors. The correction factor is a third order equation dependent on the bending factor. The lateral correction factor, K_L is defines as:

$$K_L = 1 - (k \cdot (0.19 \cdot k^2 - 0.41 \cdot k - 0.23)) \tag{9.3}$$

The lateral correction factor is a normalized factor resolving around 1, increasing for when the bending factor increases. This lateral correction factor is added to Equation 7.2. The factor is created in such a way that when the bending factor is zero the lateral factor becomes one. In order to keep consistency with the other correction factor the lateral correction factor is added in the same fashion as the other, by multiplication. Section 3.8 referred that the lug joint and lap joint showed similarity and the Homann and Jongebreur equation was presented. Looking at the lateral component in Equation 3.11 it shows that it is a summation with the in-plane load components. For consistency within Larsson, it is chosen to add the lateral correction factor by multiplication over summation. It is possible to use summation for the lateral correction factor. This shall give similar results but is not investigated in more detail.

Adding the lateral correction factor to the eccentricity load Larsson relation of Equation 7.2 results in:

$$\frac{\sigma_{nom}}{\sigma_{nom_{ref}}} = k_1 k_2 K_{ecc} K_\alpha K_L \tag{9.4}$$

Using Equation 9.4 the nominal stress ratio is compared with the combined correction factor resulting in the results presented in Table 9.4 for the different load conditions.

Table 9.4: Results of implementing the expected nominal stress into Equation 9.4

F [N]	k	σ_{nom}	K_L	$\frac{\sigma_{nom}}{\sigma_{nom_{ref}}}$	$k_1 k_2 K_{ecc} K_\alpha K_L$	Error Equation 9.4 [%]
300	0.3	12.99	1.101	1.189	1.163	-2.29
500	0.5	15.15	1.194	1.326	1.261	-5.15
1000	1.0	20.55	1.450	1.543	1.531	-0.75
1100	1.1	21.63	1.496	1.584	1.580	-0.21
1200	1.2	22.71	1.538	1.607	1.625	1.07
1500	1.5	25.95	1.626	1.634	1.718	4.87
2000	2.0	31.35	1.580	1.706	1.669	-2.22

Implementing the lateral correction factor with Larsson minimized the error between the nominal stress ratio and the correction factors. Using Equation 9.4 for the different load cases all the errors fall within the $\pm 15\%$ error margin.

9.7 Restrictions for the lateral correction factor

The lateral correction factor of Equation 9.3 has some restriction in use. The correction factor has been defined on a single geometry for a constant axial loading with a varying lateral load. The geometry used is that of the reference lug. FEA on different geometries (for example the geometries used in the in-plane analyses) under an axial and varying lateral loads have to be done to verify if the lateral correction factor applies for different geometries. Lugs with varying geometries and varying axial and lateral loads should be experimentally tested to validate the data.

For the out-of-plane loaded lug analyses the load angle has been set at zero. Therefore,the lateral load factor is valid for load angle equal to zero, $\alpha = 0°$. The same applies for the taper angle since a reference lug has been used for the FEA with has a taper angle of zero, $\beta = 0°$. Again FEA and experiments have to be conducted to verify and validate the use of the lateral correction factor for different load and taper angles.

Within the range of $0 \leq k \leq 2.0$ the use K_L is verified in the Larsson relation (presented in Section 9.8). The lateral correction factor is not designed for bending factor larger than $k = 2.0$. Since lugs are not designed for lateral loads, a bending factor of $k = 2$ should be sufficient for the lateral correction factor. When the bending factor on a lug is larger than two, the question should be if the chosen joining method is suited for the application.

9.8 Verification lateral correction factor

In order to verify the lateral relation different combinations of axial and lateral loads have been applied. This resulted in bending ratios between the $0 \leq k \leq 2.0$ for different applied loads. The geometry of the lug remained unchanged. The different load conditions are displayed in Table 9.5.

Table 9.5: The out-of-plane verification load cases

Verification case	P $[N]$	F $[N]$	k [-]
1	3000	1500	0.50
2	5000	1500	0.30
3	3000	1000	0.33
4	2000	2000	1.00
5	2000	3000	1.50
6	2000	4000	2.00
7	3000	4000	1.33
8	2000	2200	1.10
9	3000	3600	1.20

The load conditions of Table 9.5 have been implemented in the FE model for the out-of-plane analyses. From the results of the FEA it became clear that the same trend as seen in Figure 9.3 is to be expected. The nominal stress for each of the cases has been calculated using Equation 9.2. This nominal stress is than used in Equation 9.4 to find the discrepancy between the left and right side of the equation. The results for the verification cases are presented in Table 9.6.

Table 9.6: Verification results for an in- and out-of-plane loaded lug

Case	k	σ_{nom}	K_L	$\frac{\sigma_{nom}}{\sigma_{nom_{ref}}}$	$k_1 k_2 K_{ecc} K_\alpha K_L$	Error Equation 9.4 [%]
1	0.50	45.44	1.194	1.327	1.261	-5.27
2	0.30	64.95	1.101	1.190	1.163	-2.35
3	0.33	40.04	1.115	1.210	1.178	-2.71
4	1.00	41.10	1.450	1.553	1.531	-1.37
5	1.50	51.90	1.626	1.664	1.718	3.14
6	2.00	62.70	1.580	1.747	1.669	-4.70
7	1.33	72.44	1.585	1.674	1.674	-0.01
8	1.10	43.26	1.496	1.596	1.580	-0.97
9	1.20	68.12	1.538	1.657	1.625	-1.99

Table 9.6 shows that all the verification cases fall within the ±15% margin. Comparing the results with Table 9.4 it is clear that the for the same bending factor the error is roughly the same. This is to be expected since the axial nominal stress is a linear increasing function with load. The expected nominal stress curve is also a linear increasing curve for lateral load. Therefore, the nominal stress ratio for the verification cases is similar to that of the values presented in Table 9.4. The lateral correction factor is only dependent on the bending factor. This results in that the error within Equation 9.4 is roughly the same for a value of k.

From the results of Table 9.6 it is clear that by applying different loads the use of the lateral correction is verified. Within the boundaries, Equation 9.4 verifies to predict the stresses of an in- and out-of-plane loaded lug. To further expand Equation 9.4 and validate the results recommendations are presented in Chapter 11.

Chapter 10

Conclusions

Using ABAQUS, an FE model has been created in order to analyze the stresses of different lug geometries subjected to various in- and out-of-plane loads. In order to be able to predict the fatigue life of in- and out-of-plane loaded lugs for various geometries, the Larsson relation has been used. The Larsson relation is restricted for use on straight-sided axially loaded lug and has a margin of error of $\pm 15\%$. In order to apply the Larsson relation different additional correction factors have been proposed in this reports in order to take tapered non-axially loaded lugs into account.

The main research question was defined as:

"What are the effects of varying the shape of the lug and the load angle on the fatigue life of a lug, subjected to a combined in- and out-of-plane loading?"

Varying the shape of the lug has been done by changing the geometry and by applying a taper angle β. Varying the geometry introduced the effect of eccentricity. Eccentricity defined by $\frac{a}{c}$ is classified by eccentricity forward ($\frac{a}{c} < 1$) and eccentricity backwards ($\frac{a}{c} > 1$). Eccentricity in the lug resulted in errors larger than the 15% margin of error when applying the Larsson relation. To account for the eccentricity an eccentricity correction factor K_{ecc} has been introduced in the Larsson relation. Additional analyses verified the use of the eccentricity correction factor. Varying the taper angle resulted in marginal effects with respect to the results of the Larsson relation including K_{ecc}. No taper angle correction factor is required. Within the taper angle range of $0^\circ \leq \beta \leq 20^\circ$ the use of the Larsson relation including K_{ecc} has been demonstrated to be valid.

Applying the Larsson relation for varying load angle α for in-plane loaded lugs resulted in error larger than the $\pm 15\%$ error margin. In order to account for varying load angles the load angle correction factor K_α has been introduced. Implementing K_α in Larsson combined with K_{ecc} resulted in error margins within the $\pm 15\%$. The use of K_{ecc} has been verified within the range of $0^\circ \leq \alpha \leq 45^\circ$.

For combined in-plane and out-of-plane loaded lug the use of Larsson relation resulted in errors larger than the $\pm 15\%$ margin of error. Even applying the additional correction factor K_{ecc} and K_α in the Larsson relation resulted in errors larger than the margin. Therefore, the lateral correction factor K_L has been introduced. The K_L is dependent on the bending factor k, which is the ratio between the lateral load and the in-plane load. Adding the lateral correction factor to the Larsson relation with the two other proposed factors resulted in error percentiles within the margin of error. For the fatigue life of an in- and out-of-plane loaded lug only a straight-sided lug subjected to a constant axial load and varying lateral load has been investigated. This limits the use of the K_L factor for fatigue prediction purposes. Further FEA have to be performed into changing the load angle and the lug geometry to increase the range in which the K_L is applicable.

Combining the Larsson relation with the factors K_{ecc}, K_α, and K_L creates a methodology for the predition of the fatigue life, which takes various in- and out-of-plane loaded lugs into account. However, experimental testing is required in order to validate the use of the proposed correction factor in Larsson.

Chapter 11

Recommendations

For future research a couple of recommendations are formulated based on observations of the work performed. These recommendations are presented in this chapter.

- **Re-evaluating the mesh**

The large difference in number of elements in radial and circumferential direction resulted in rather long and slender (rectangular shaped) elements around the hole. Increasing the number of circumferential elements and decreasing the number of radial elements would make the elements more squared opposed to the rectangular shape in the current mesh. By decreasing the number of radial elements and increasing the number circumferential elements should results in a more vertical defined NS stress path for out-of-plane loaded lugs. This improves the accuracy of the nominal stresses calculation for out-of-plane loaded lugs.

- **Expanding the FEA for combined in- and out-of-plane loaded lugs**

Different lug geometries should added to the FEA for the combined in- and out-of-plane loaded lugs. This is to check how eccentricity and the lateral loads interact. The addition of eccentricity can result in that the current lateral correction factor be invalid for use for different lug geometries.

After the addition of more lug geometries, taper angle and/or load angle should be added into the analyses. Keep in mind the range of validity for taper and load angle. The addition of eccentricity, taper and load angle can alter the lateral correction factor. Another possibility is that there is interaction between a lateral load and eccentricity, taper angle or load angle which can results to adding interaction terms to a correction factor or addition of a new interaction correction factor.

- **Transverse loaded lugs**

In order to expand the range of viable load conditions transversely loaded lugs can be added. Increasing the load angle domain should be done following the same principle as described in the report. The correction factors proposed for the eccentricity, load angle, and lateral should be verified for the lateral load conditions and modified when required.

- **Experimental testing of lugs**

All the data used in the thesis report have all be generated by ABAQUS. In order to validate the data and the use of the proposed correction factors experimental test on lugs should be performed. The lug tested can be divided in the three categories: in-plane, out-of-plane and combined in- and out-of-plane.

For in-plane the main focus should be on lug subjected to a load angle of $0 \leq \alpha \leq 45$. Adding taper angle is optional. Here, areas of interest are the peak stress, peak location and NS stress to validate with the FEA.

Testing lug under out-of-plane loads should give an insight in the peak stress, peak location and the nominal stress. Using a number of varying lateral loads, the linear assumption of the stresses subjected to a lateral load can be validated for lugs.

Finally, lug subjected to a combined axial and lateral load should be tested in order to validate the FE results. The results of these test should provide answers to the trend of the nominal stress related to varying lateral load and constant axial load.

- **Fatigue testing of lugs**

In order to validate a fatigue life prediction using the proposed addition to the Larsson relation, fatigue testing should be performed using lugs subjected to in- and out-of-plane loads. Using Fokker's TH3.411 [14] fatigue prediction calculations can be made by substituting in the correction factors K_{ecc}, K_{α}, and K_L. When performing fatigue test on the lug do take into account that the cycle correction factor of the Larsson relation remains equal to one, $\theta = 1$ during testing. This correction factor has been assumed equal to one during the creation of the methodology but will play a factor when performing the fatigue test.

- **Distance c in the FEA of the taper angles**

During the analyses of the taper angle $\beta = 20^\circ$ in Chapter 7 the geometry parameter c has not been altered to account for the taper angle. The distance is defined from the top of the hole to the side of the lug (See Figure 4.1). However, with the inclusion of a taper angle the distance c should increase to a distance c^*. Distance c^* affects the shape function k_1 which is implemented in the Larsson relation. The effects of changing c are discussed in Appendix F.

From the results of Appendix F it is clear that the taper angle does influence the Larsson relation. With the effects of taper on Larsson and the potential relationship between α and β further analyses are required into the effect of taper. Suggested is to perform a regression study of α, β and $\frac{a}{c}$.

References

[1] J. Schijve. *Fatigue in Lugs. Contributions to the Theory of Aircraft Structures. Professor A. van der Neut Anniversary Volume.* Nijgh-Wolters Noordhoff University Press, 1972, pp. 423-440.

[2] S.E. Larsson. *The Development of a Calculation Method for the Fatigue Strength of Lugs and a Study of the Test Results for Lugs of Aluminium.* Fatigue Design Procedures, I.C.A.F. Symposium, 1969, pp. 309-339.

[3] J. Schijve. *Fatigue of Structures and Materials.* Second Edition. Springer, 2009.

[4] HSB. *Static failure loads of metallic double shear lugs*, 2010. HSB 26101-01 Issue F.

[5] HSB. *Stress concentration factors for symmetrical isotropic lugs*, 1990. HSB 34112-02 Issue B.

[6] R.B. Heywood. *Designing Against Fatigue.* Chapman and Hall Ltd, London, 1962.

[7] R.B. Heywood, Ph. D., and M. I. Mech. E. The strength of lugs in fatigue. Technical Report 182, Royal Aircraft Establishment, London, 1956.

[8] W.D. Pilkey. *Peterson's Stress Concentration Factors.* Second Edition. John Wiley & Sons, INC, New York, 1997.

[9] M.M. Frocht, and H.N. Hill. Stress concentration factors around a central circular hole in a plate loaded through pin in the hole. *J. Appl. Mech.*, 7:A5–A9, March 1940.

[10] R.J. Grant, J. Smart, and P. Stanley. A parametric study of the elastic stress distribution in pin-loaded lugs. *Journal of Strain Analysis*, 29:299–307, 1994.

[11] J. Schijve, D. Broek, and F.A. Jacobs. *Fatigue test on aluminium alloy lugs with special reference to fretting.* Nationaal Lucht- en Ruimtevaartlaboratorium, 1963. NLR-TN M.2103.

[12] A. Buch. Fatigue and fretting of pin-lug joints with and without interference fit. *Wear*, 43:9–16, 1977.

[13] Fokker. Fokker technical handbook for strength data: Elastic stress concentration factors, 2016. TH 3.281.

[14] Fokker. Fokker technical handbook for strength data: Fatigue strength of lugs, 1980. TH 3.411.

[15] IHS ESDU. *Stress concentration factors, Axially loaded lugs with clearance-fit pins.* London, 1981. ESDU Report 81006.

[16] Fokker. *S-185: Stress Concentration Factors of Transversely Loaded Lugs by Finite Element Analysis*, 1993. S-185 is a Fokker internal restricted report.

[17] Fokker. *Levensduur Bepaling van een Beslagoog onder Niet Longitudinale Dynamische Belasting (in Dutch)*, 1984. SC M-005.

[18] K. Kathiresan, T.M. Hsu, and J.L. Rudd. ***"Stress and Fracture Analysis of Tapered Attachment Lugs"**, Fracture Mechanics: Fifteenth Symposium. ASTM STP 833, R.J. Sanford, Ed.* American Society for Testing and Materials, Philadelphia, 1984, pp. 72-92.

[19] K. Kathiresan, T.M. Hsu, and T.R. Brussat. *Advanced Life Analysis Methods Volume II - Crack Growth Analysis Methods for Attachment Lugs.* Lockheed-Georgia Company, Wright-Patterson Air Force Base Ohio 45433, 1984. AFWAL-TR-84-3080.

[20] A. Strozzi, et al. Maximum stresses in a taper-shanked round-ended lug loaded by an oblique concentrated force. *Strain*, 43:109–118, 2007.

[21] A. Strozzi, A Baldini, and M. Nascimbeni. Maximum equivalent stress in a pin-loaded lug subject to inclined loading. *Journal of Strain Analysis*, 41:297–309, 2006.

[22] J.J. Homan, and A.A. Jongebreur. Calculation method for predicting the fatigue life of riveted joints. *Durability and structural integrity of airframes*, 1:175–190, 1993.

[23] J.C. Ekvall. Static strength analysis of pin-loaded lugs. *Journal of Aircraft*, 23:438–443, 1986.

[24] The James F. Lincon Arc Welding Foundation. Beam load equations. URL: http://www.sprecace.com/node/43 [cited: 07-09-2017].

[25] O.A. Bauchau, and J.I. Craig. *Structural Analysis with Applications to Aerospace Structures.* Springer, Dordrecht, 2009.

[26] B. Quimby. Chapter 9 - Combined Bending and Axial Forces. URL: http://bgstructuralengineering.com/BGSCM13/BGSCM009/BGSCM00903.htm [cited: 07-09-2017].

Appendix A

FE Convergence Study

In order to find a relation between the fatigue life of lugs and the SCF an FEA has been performed. For the FE model to produce reliable results a mesh convergence study has been carried out. By finding mesh convergence, the scatter the mesh produces on the results is limited. The convergence study has been performed on an axially loaded straight-sided lug. A straight-sided axially loaded lug is the most well-known load case on lugs. By finding mesh convergence and relating the results of said mesh with (test) data, the mesh and model are verified. In Figure A.1 the mesh of the lug is presented. Figure A.2 provides a close up of the mesh around the hole.

The lug has been partitioned in such a way that a structured mesh was applicable. Around the hole, a circle partition has been made in order to increase the number of elements around the hole. The stress distribution around the hole is an area of interest of the FEA, therefore a denser mesh is preferred around the hole. For the mesh convergence study, the number of elements around the edge of the hole and around the radial direction has been changed. The rest of the lug mesh is created in such a way that it matches and/or aligns with the mesh distribution chosen around the hole.

There are two variables for the convergence study. One of the variable has been fixed while the other variable is varied. For the convergence study the number of elements per quarter circle have been fixed on 10 elements, while the number of elements on vertical axis (net section of the lug) is increased in order to find convergence. A convergence check on the increase in number of element per quarter circle has been performed after.

The number of element in the vertical direction starts with 10 elements and are increased to 120 elements by steps of 10. A check for convergence has been performed by include 150 and 200 elements. For each iteration of the mesh, the peak stresses around the hole have been documented. In Figure A.3 the peak stresses for increasing number of elements along the net section is shown.

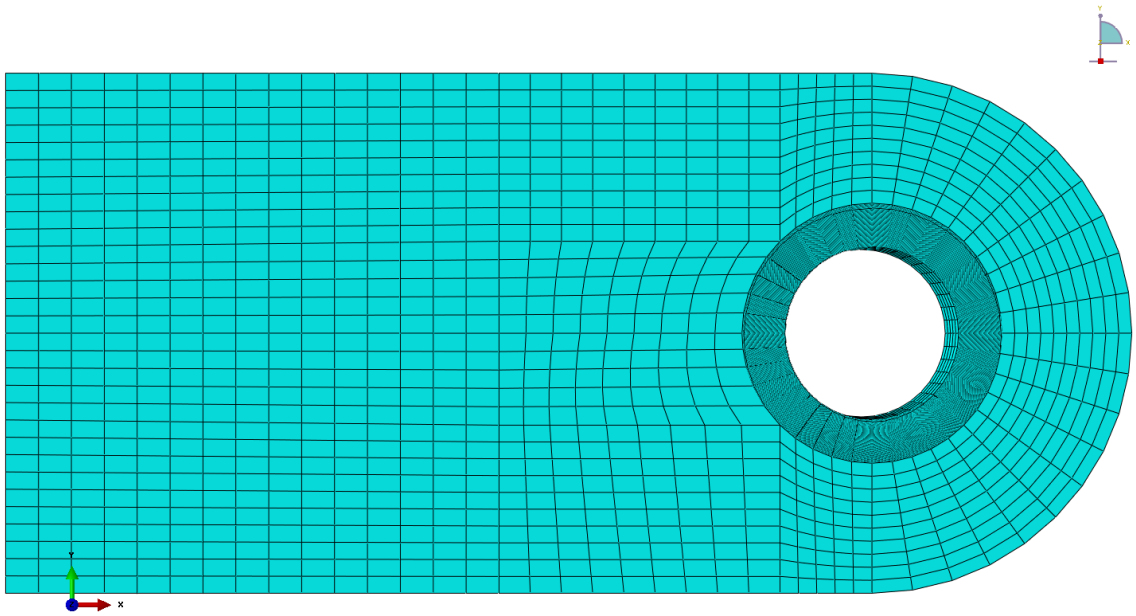

Figure A.1: Mesh straight-sided lug

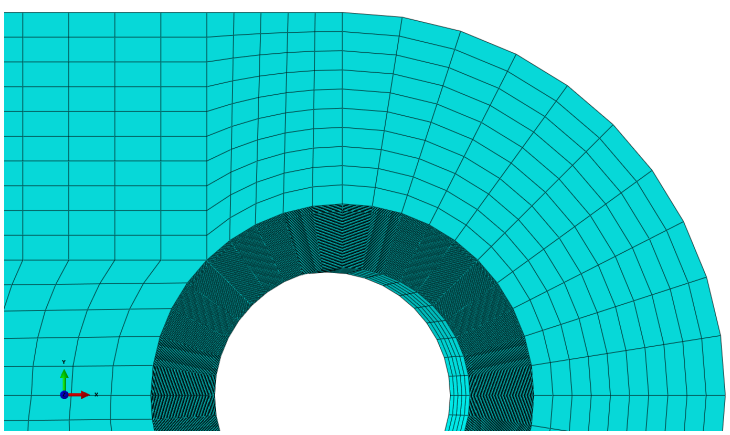

Figure A.2: Close up mesh around the hole

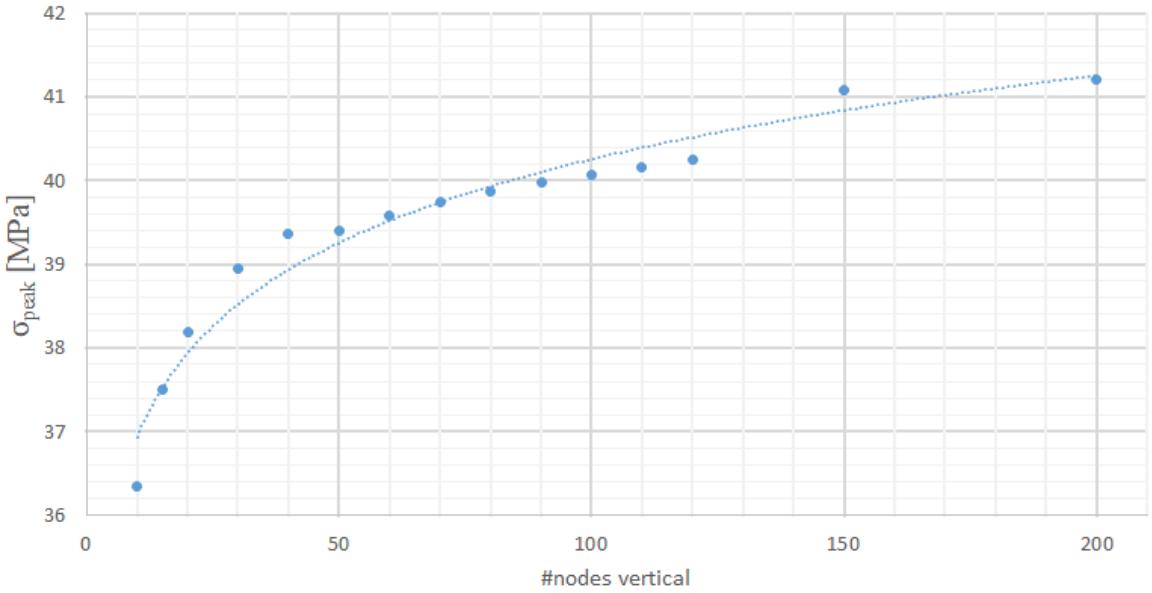

Figure A.3: Convergence study of the peak stress for increasing mesh density around the net section

When looking at the points up until 120 elements one would see a steep increase in peak stress at the beginning which gradually flattens out. The results seemed to be quite converged around 120 elements at first. By adding the control point with a far greater number of nodes (150 and 200), to see if the peak stress really had reached a limit, revealed that convergence has not been found yet. In fact the peak stress increased quite a bit from 100 to 200 elements. Further increase in the number of elements beyond 200 elements was not possible with the current model. Beyond 200 elements ABAQUS reported error messages for the mesh and were impossible to test.

In order to check the effect of the increase in number of elements along the edge, a fixed number of element in vertical direction has been chosen. The number of elements is set at 100 elements. This number of elements has been chosen because of the initial graphs (without the two outer points) showed reasonable convergence, the processing time of the calculations, and because of the limitations with the computer. During very high number of elements (when $>$ 100 nodes where used for the vertical) the ABAQUS program became quite slow in operation on the used hardware (TU desktop or laptop). In Figure A.4 the convergence study for the peak stress and variable number of elements around the hole is presented. A circle segment is a quarter of the hole circumference.

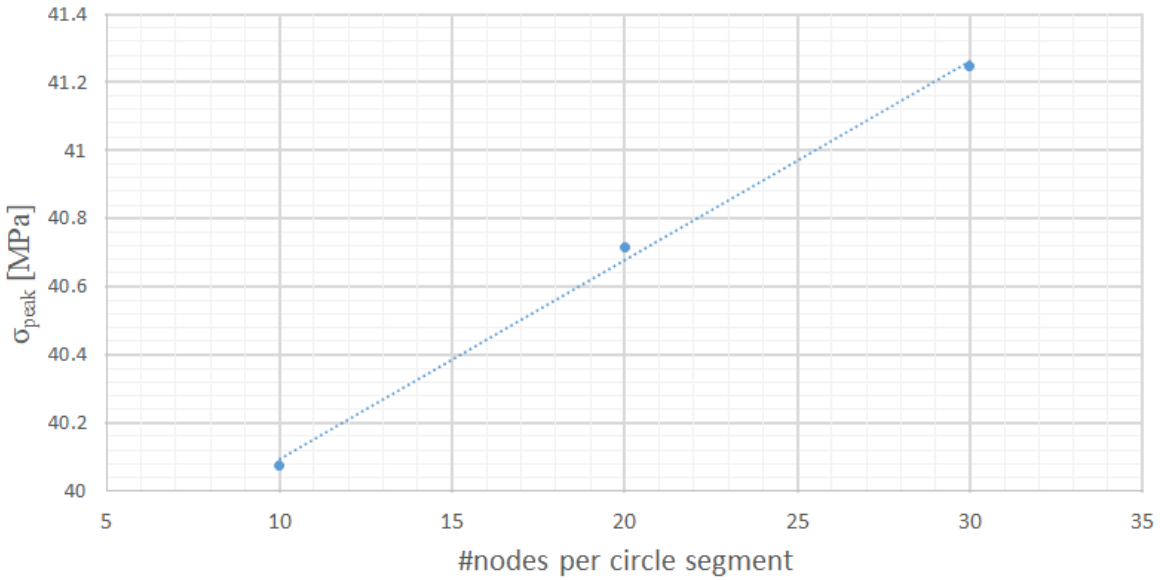

Figure A.4: Convergence study of the peak stress for increasing mesh density around the hole

When the number of elements around the hole increased, the peak stress increases as well. Still the increase of elements did not result in a converging mesh. Further increase of the elements around the hole resulted in meshing errors.

From the current convergence study no mesh convergence has been found. In order to perform the calculations in the FEA the following mesh has been chosen. The mesh has been set to 100 nodes vertical with 10 nodes along the quarter circle segments.

Appendix B

TH3 Method Verification

The method of TH3 is based on a FE model which is described in [16]. The stress concentration factor of an arbitrary tapered and loaded lug are calculated via the method described in TH3 [13]. The SCF of TH3 is calculated by taking the SCF of a special case and multiplying this by a two factors, which are dependent on geometry ratios. The SCF for arbitrary tapered and loaded lugs is given by Equation B.1 [13, 16].

$$K_{t1(2)} = K^*_{t1(2)} \cdot \xi \cdot \zeta \tag{B.1}$$

The factors ξ and ζ are dependent on the geometry ratios of the lug. The SCF $K^*_{t1(2)}$ is dependent on the load angle and taper angle. The magnitude of $K^*_{t1(2)}$ are found by reading the value from the respective curve in TH3 [13] or from Figure B.1. Please note that Figure B.1 is created from selected points of the TH3 curve and only serves as a representation.

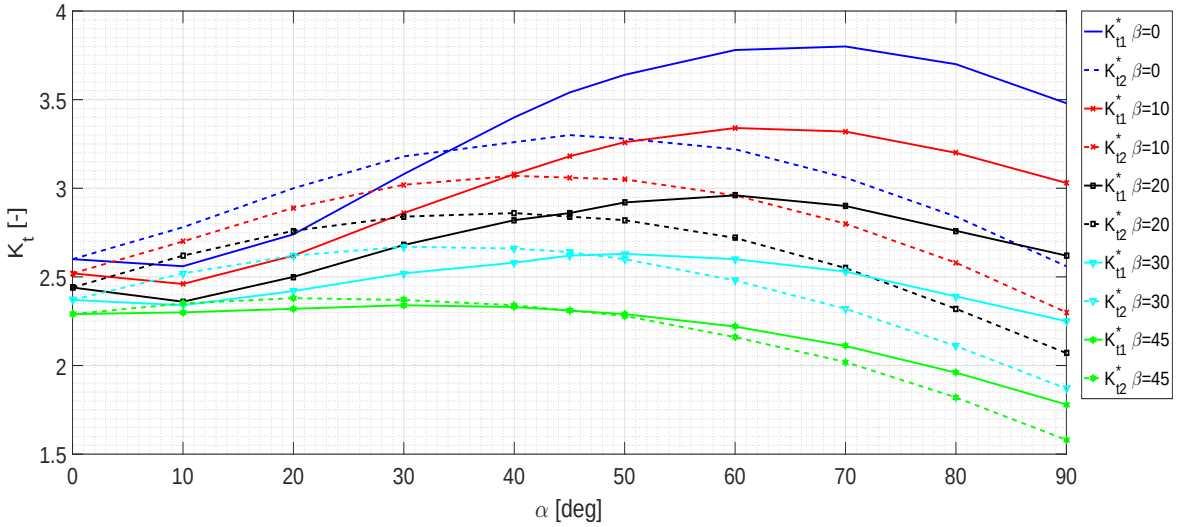

Figure B.1: Stress concentration factor for in-plane loaded lugs [13]

The curves in Figure B.1 should be reproducible by a FEA since the theory of TH3 is based on a FEA. The methods of TH3 are based on the results of the intern report S-185 [16]. The FE software used for S-185 is NASTRAN.

Using the FE model explained in Chapter 4, the S-185 curve for $\beta = 0$ is generated. This would verify that the FE model used for the calculation is comparable to the calculation method and FE model. In order to generate the curve $\beta = 0$, the factors ξ and ζ are set equal to 1. Doing so ensure that the calculated SCF from the FE equals to the K_t^* values for the $\beta = 0$ curve.

B.1 Case Lug Geometries

A couple of test cases have been made. The FEA which is compared with TH3 results in Chapter 5 has been preformed with a hole diameter fixed at 10 mm. The lugs used for the TH3 analyses have been fixed at 12 mm diameter. In order to get $\xi = \zeta = 1$ the geometry of the lug needs to change. The ξ is dependent on the ratio of $\frac{B}{2d}$ and ζ is dependent on the ratio $\frac{2e}{B}$. The equations for ξ and ζ are presented in Equation B.2 and B.3, respectively [13, 16].

$$\xi = 0.255 \cdot e^{4.83(1-\frac{B}{2d})} + \frac{0.1}{\frac{B}{2d} - 0.5} + 0.545 \tag{B.2}$$

$$\zeta = 1 + 0.05 \cdot (1 - \frac{2e}{B}) \qquad , if \frac{e}{B} > 0.5 \tag{B.3a}$$

$$\zeta = (1 - \frac{\alpha}{90})[1 + 9.74 \cdot (1 - \frac{2e}{B})^{2.567}] + (\frac{\alpha}{90})[1 + 0.73 \cdot (1 - \frac{2e}{B})] \qquad , if \frac{e}{B} \leq 0.5 \tag{B.3b}$$

For the FEA the material properties listed in S-185 have been implemented for all the different lugs. In order to satisfy the condition of $\xi = \zeta = 1$ the following case lugs have been modelled listed in Table B.1. Figure B.2 presents the geometrical parameters of the lugs.

Table B.1: Dimensions of the test case lugs and acting load

Lug name	d [mm]	h [mm]	W [mm]	t [mm]	L [mm]	P [N]
S185 lug	12	12	24	6	26.4	3000
FE lug 1	10	10	20	5	60	1000
FE lug 2	10	10	20	5	22	3000

The S-185 lug geometries presented in Table B.1 is one of the tested lugs on which the TH3 theory is based. The S185 lug is used to recreate the results presented in S-185 [16]. The FE lug 1 is comparable to the lug used for the analyses in Chapter 5. The results of FE lug 1 are compared to the results of S185. The distance h and W for FE lug 1 have been updated to uphold the applied assumptions of $\xi = \zeta = 1$. The FE lug 2 has been modelled to represent a lug with similar length as S-185 lug. The length equation used in S185 is applied to FE lug 2. The length of the lug is dependent on the diameter of the hole [16].

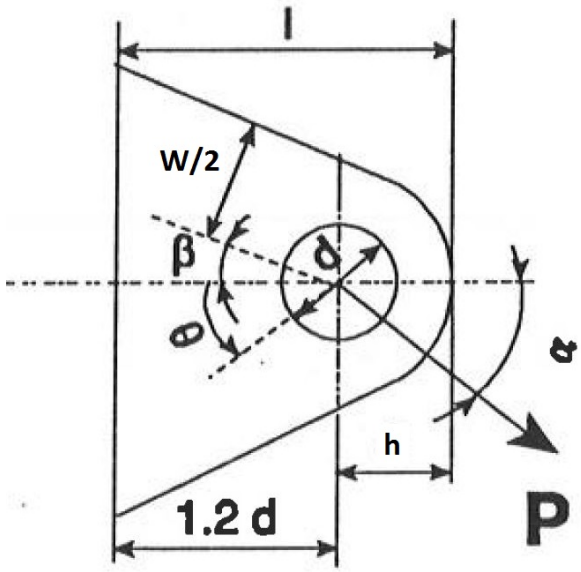

Figure B.2: Geometrical parameters of the lug

B.2 Material properties

In order to be consistent with the work of S-185 the material properties have been updated to match the properties used in S-185. The lug is an aluminium alloy 2024 and the pin is modelled as an low-ally steel pin. The material properties are displayed in Table B.2.

Table B.2: Material properties for the FEA [16]

Material	σ_B [MPa]	$\sigma_{0.2}$ [MPa]	δ_B [%]	E [MPa]	v [-]
Al 2024	450	360	18	72560	0.33
Low-alloy steel	676.5	522	20	205000	0.32

B.3 Results of the analyses

For the different case lugs the SCF has been calculated. The SCF is based on the bearing stress acting of the lug. The FE lugs 1 and 2 have been subjected to different load angles ranging from 0° to 90° in intervals of 15°. The results are listed in Table B.3. The column peak stresses listed in the table only represents the stresses occurring on the topside of the lug.

First thing to note is the result of the S185 lug. The S185 lug dimensions have been set such that the ξ and ζ equal to 1. Therefore the result for the SCF of S185 should correspond with the result listed in Figure B.1 for a taper angle of 0°. This is not the case. When one compares the results of the S185 lug with FE lug 1 and 2 similar SCFs are found but all do not match with the starting point listed in Figure B.1. The difference between the FE results and Figure B.1 is around 6%.

Table B.3: Results of the FEA

Lug	α [°]	P [N]	σ_b [MPa]	σ_{peak} [MPa]	K_t [-]
S185 lug	0	3000	41.667	102.451	2.46
S185 lug	15	3600	50	124.004	2.48
S185 lug	30	3600	50	143.924	2.88
S185 lug	45	3600	50	164.788	3.30
S185 lug	60	3600	50	173.846	3.48
S185 lug	75	3600	50	181.766	3.64
S185 lug	90	3600	50	162.055	3.24
FE lug 1	0	1000	20	48.447	2.42
FE lug 1	15	1000	20	48.936	2.45
FE lug 1	30	1000	20	56.803	2.84
FE lug 1	45	1000	20	65.711	3.29
FE lug 1	60	1000	20	69.720	3.49
FE lug 1	75	1000	20	72.107	3.61
FE lug 1	90	1000	20	67.579	3.38
FE lug 2	0	3000	60	144.277	2.41
FE lug 2	15	3000	60	145.189	2.42
FE lug 2	30	3000	60	168.234	2.80
FE lug 2	45	3000	60	192.367	3.21
FE lug 2	60	3000	60	202.928	3.38
FE lug 2	75	3000	60	210.803	3.51
FE lug 2	90	3000	60	188.881	3.15

Reading through S-185 it became clear that getting the exact same curve by assuming $\xi = \zeta = 1$ is impossible without adding the correction factor added by Fokker. On the FE results used in S-185 a correction factor of 1.06 has been applied. Fokker applied this correction factor for the following reasons.

First of all, the FE solution for the axially loaded lug is 6% lower than photoelastic and theoretical values. The FE results for the SCF are somewhat lower than the actual values [16]. The magnitude of the SCF tends to move towards the real values when mesh refinement has been preformed. A certain mesh dependency is present for the SCF. Finally an influence of lug length has been noted, which affected the SCF. The influence of length has not been investigated by S-185 [16]. It was concluded that applying the multiplication factor the length effects are covered. All these facts lead to the justification of applying a multiplication factor of 1.06 on the results.

In S-185 page 36 Figure 7.22 the FE solution curve for changing load and taper angle is presented [16]. Figure 7.22 displays the uncorrected form of the SCF curves of the TH3 curve. In Table B.4 the applied load, peak stress and SCF of the first entry from the curve in Figure 7.22 is presented.

The results of S-185 in Table B.4 match with the result of the FE lugs preformed for verifi-

Table B.4: S-185 result for axially loaded lug [16]

α [°]	P [N]	σ_b [MPa]	Peak stress [MPa]	K_t [-]
0	3000	41.667	102.29	2.46

cation presented in Table B.3. In Figure B.3 the results of the FEA with the S185 lugs are presented against the results of the S-185 [16].

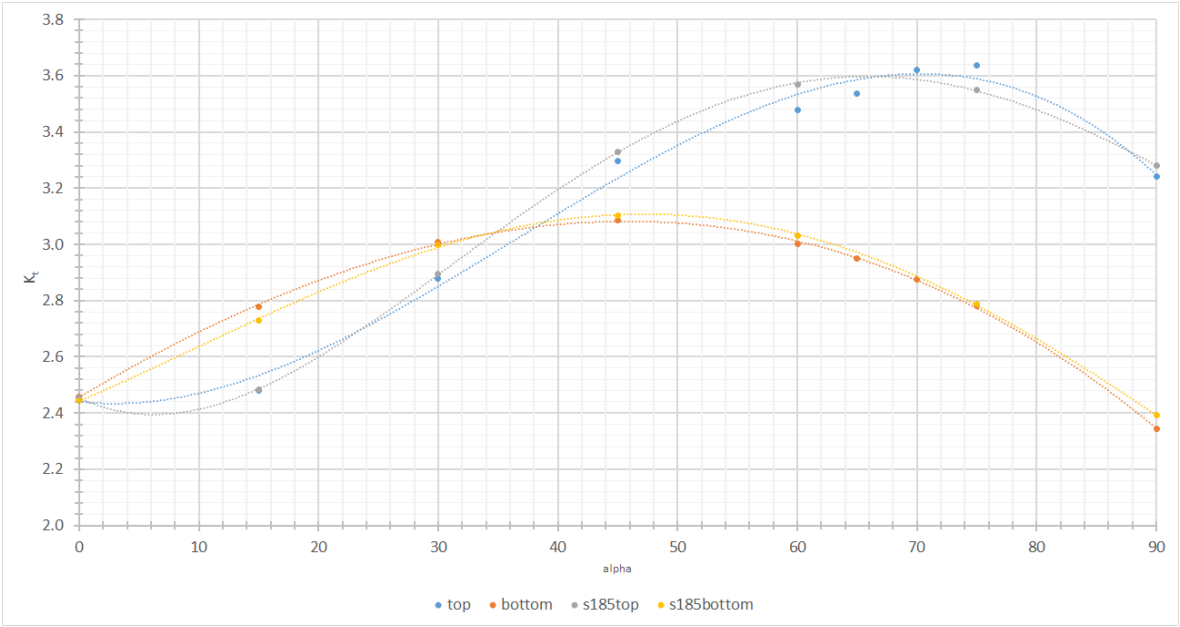

Figure B.3: Stress concentration factor of S185 lug for the different load angles and the S-185 data [16]

The curves for the bottom SCF of the FEA and the S-185 data match. The difference between the results is due to difference in meshing strategy since there is a mesh dependency for the peak stresses. The results for the top SCF are quite similar when looking at the magnitude between the two data, with a maximum error of 2.5%.

The biggest difference is the load angle for which the maximum SCF on the top side of the lug occurs. From the data presented in S-185, the maximum SCF occurs at 65° load angle, while the FEA maximum occurs at around 70° load angle. Some extra measurements have been preformed at load angles 65° and 70° in order to improve the accuracy of the FE results in this region. Still the FEA maximum remains around 70° load angle with the added points.

The SCF for FE lug 1 and lug 2 have been plotted against the changing load angle in Figure B.4 and B.5, respectively. One of the main differences between the two is that the maximum SCF for FE lug 1 is around 3.6 while for FE lug 2 the maximum SCF is around 3.4.

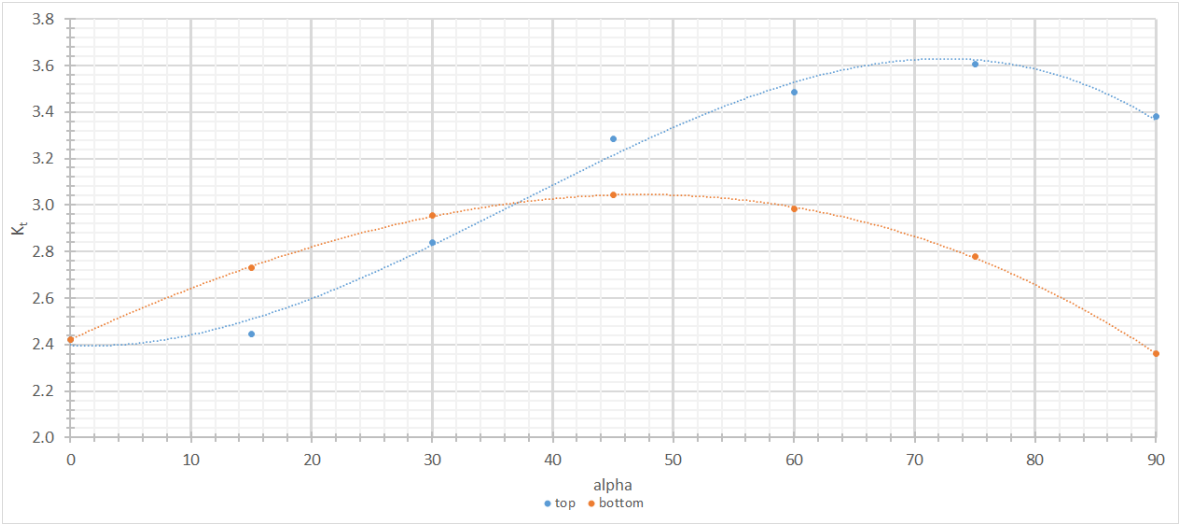

Figure B.4: Stress concentration factor of FE lug 1 for the different load angles

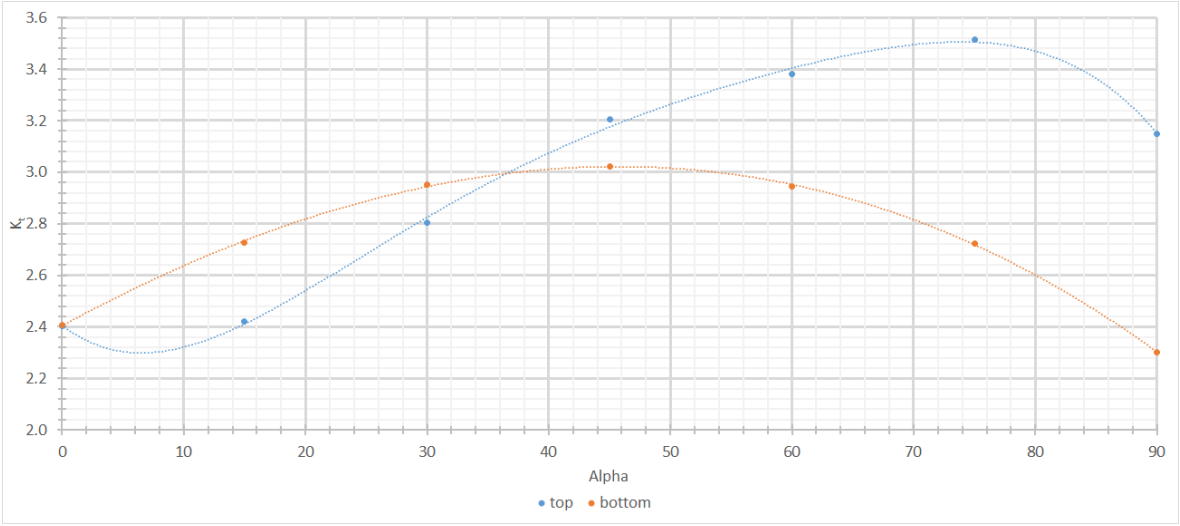

Figure B.5: Stress concentration factor of FE lug 2 for the different load angles

In Figure B.4 and B.5 a couple of key points are identified. For the SCF on the top of the lug the minimum SCF occurs around a load angle of 7°. At a load angle of 35° the SCF on the top peak stress becomes greater than the SCF of the bottom peak stress. The SCF of the bottom side has a maximum SCF around 45° load angle. All these points correspond with the data as presented in S-185.

Again for both FE lug 1 and lug 2 the maximum top side SCF occurs at around 75°. The difference between lug 1 and 2 is the overall length of the lug and the applied load. The length of the lug has an effect on the peak stresses. The effect of length influencing peak stresses has been noted by the research performed for S-185 [16]. The applied load affects the magnitude of the peak stress but the peak stress scales according. For example when the load increases

Table B.5: Dimensions of the added test case lugs and acting load

Lug name	d [mm]	h [mm]	W [mm]	t [mm]	L [mm]	P [N]
FE lug 3	10	10	20	5	22	1000
FE lug 4	10	10	20	5	36	1000

by a factor of two the peak stress increases by a factor of two.

To make a better comparison with the FE S-185 lug data and the FE lug data, two more lugs have been added for comparison. FE lug 3 has an applied load of 1000 N to show that a lower applied load produce the same curve. With FE lug 4, a lug with a length between the lengths of lug 1 and 2 has been modelled. The dimensions of FE lug 3 and 4 are presented in Table B.5. The results for the SCF for the S-185 lug and the FE lugs 1 to 4 are presented in Figure B.6.

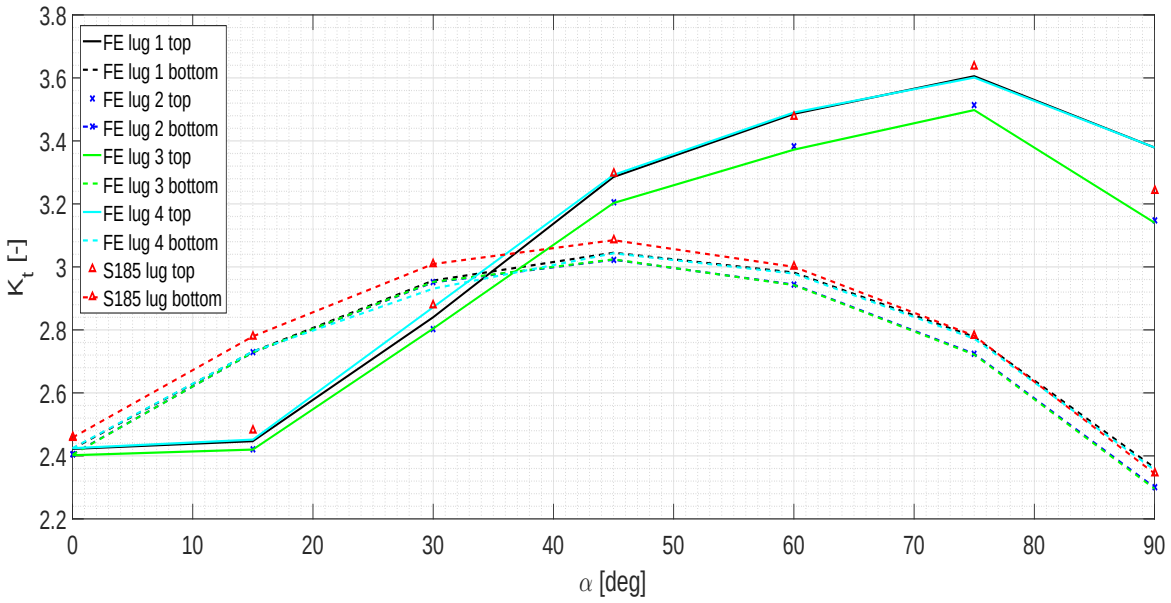

Figure B.6: SCF of the different case lugs for at different load angles

Looking at the axially loaded lug one can see that the S-185 lug has the highest SCF and that the FE lugs 1 and 4 have the same SCF and lugs 2 and 3 have the same SCF. Lugs 2 and 3 have the lowest SCF. Since the S-185 lug has a different geometry it is logical that the SCF do not match exactly. Between the results of lug 1 and 4 and the lugs of 2 and 3 one can see that the SCF of lugs 1 and 4 are always higher than the SCF of lugs 2 and 3 for the top and bottom side of the lug.

The difference in load does affect the magnitude of the SCF. If everything is kept constant and the load is increased the SCF increases with the same factor as the load is increased. As long as no plasticity occurs due to the applied load, the SCF will increase by the same factor as the load increases. S-185 gives more details on this finding [16].

The difference is occurs in the maximum SCF on the top side of the lug. For all FEA performed the maximum SCF on the top side of the lug occurs at around 75° load angle. For the S-185 data the maximum top SCF occurs at 65°. Different lugs have been modelled in FE, all resulting in the same pattern. Changing the length of the lug does show a shift in position of the curves. This is seen with FE lug 1 and lug 4 where there is an increase of magnitude at certain load angles. The only difference remaining between the S-185 data and the FEA performed is the used software.

The simulations of S-185 have been preformed using NASTRAN while the FEA has been preformed using ABAQUS CAE. The difference in simulation program can be the reason for the shift in load angle. NASTRAN and ABAQUS may simulate the responses of the model differently for the higher load angles.

An odd thing in S-185 is that for the axially loaded lug a load of $P = 3000$ N has been used. When the load angle changed the load increased to 3600 N instead of 3000 N in S-185. The change in load should not result in the load angle shift for the SCF. As explained, increasing the loading results in equal increase in peak stress when other parameters are kept constant. Dividing by the increased bearing stress for the higher load would result in roughly the same SCF.

B.4 Summary

From the FEA of the different lug cases and the comparison between the TH3 and S-185 data it shows that the FE model produces the same results as TH3. It has to be noted that the TH3 presented curve have an extra correction factor implemented in the results. As such it is not possible to reproduce the same magnitude of the curve without implementing the correction factor.

The differences in results between the $\xi = \zeta = 1$ SCF and the $K^*_{t1(2)}$ curve are due to the fact that a correction factor of 1.06 has been applied. This correction factor has been added due to the fact that the FEA provided lower SCF compared with the real values. The SCF from FE is mesh dependent. Refining the mesh results in a closer approximation of the reality. Finally, it has been noted that the lug length influenced the magnitude of the SCF.

The added factor of 1.06 is the explanation to why the initial comparison between the data of the FEA for the case lug in Chapter 5 does not match in magnitude. The verification performed indicated again that the SCF is fairly dependent on the taper and the load angle. Next to the taper and the load angle the geometry ratios, which are included in ξ and ζ, have a large influence on the SCF.

Comparison between the FEA performed and the uncorrected data of S-185 followed the same trends and resulted in the same magnitude for the SCF. For increasing load angle the SCF on the lower side of the hole is the same. For the top SCF of the FEA the maximum SCF occurs around 70° while for the S-185 data the maximum occurs at 65°. A potential reason for the difference is the use of FE software used for the analyses. The S-185 data has been generated using NASTRAN while the FEA have been generated with ABAQUS/CAE. The shift in peak can be due to the different FE software resulting to different phenomenon simulated. The FEA have been performed using a similar mesh to S-185, different lug length and equal geometry to the S-185 lug. All resulted in the same curves with the maximum SCF occurring at 70°.

Appendix C

Nominal Stress Analyses for Larsson Relation

This appendix discusses the FE results of the reference lug and the three case lugs described in Chapter 4. For the Larsson relation the amplitude stresses of all these cases were required. In order to find the amplitude stress, the stress distribution of the net-section of the lug was required. From the net section stress distribution the nominal stress has been calculated. Section C.1 the reference lug is discussed. In Sections C.2, C.3 and C.4 the results for cases 1 to 3 are discussed, respectively. Table C.1 presents the different dimensions for the different case study. All the lugs have been created in ABAQUS/CAE The analytical nominal stress is calculated by:

$$\sigma_{nom} = \frac{P}{2 \cdot c \cdot t} \tag{C.1}$$

Table C.1: Dimensions of the reference lug and the three case study lugs

	Reference lug	Case 1	Case 2	Case 3
d [mm]	10	10	6	14
a [mm]	10	6	6	6
c [mm]	10	8.68	10.67	6.67

C.1 Reference Lug Results

From the FEA the stress distribution of the reference lug has been taken. In order to compare the results, the same load of $P = 1000$ N has been. Figure C.1 presents the stress distribution along the net section of the reference lug and the nominal stress.

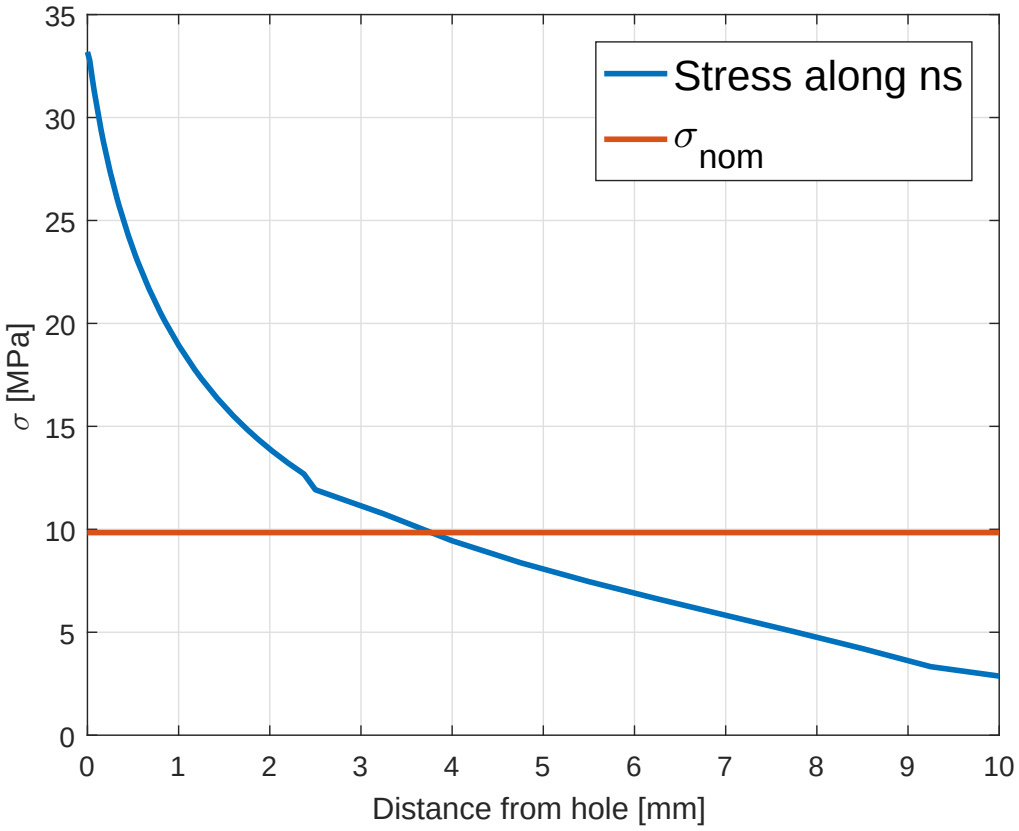

Figure C.1: Stress along the net section of the reference lug

Figure C.1 shows that the peak stress of the reference lug is equal to 33.19 MPa. Taking the average of the stress distribution of the net section grants the nominal stress of the reference lug. For the given applied load, the reference lug nominal stress is 9.838 MPa. Calculating the nominal stress of the reference lug using the analytical equation C.1 results in a nominal stress of 10 MPa. The difference between analytical and FEA nominal stress around 1.62%.

C.2 Case 1 Lug Results

The first case lug has been subjected to a load of $P = 1000$ N. The stress distribution and the nominal stress of the case 1 lug is presented in Figure C.2

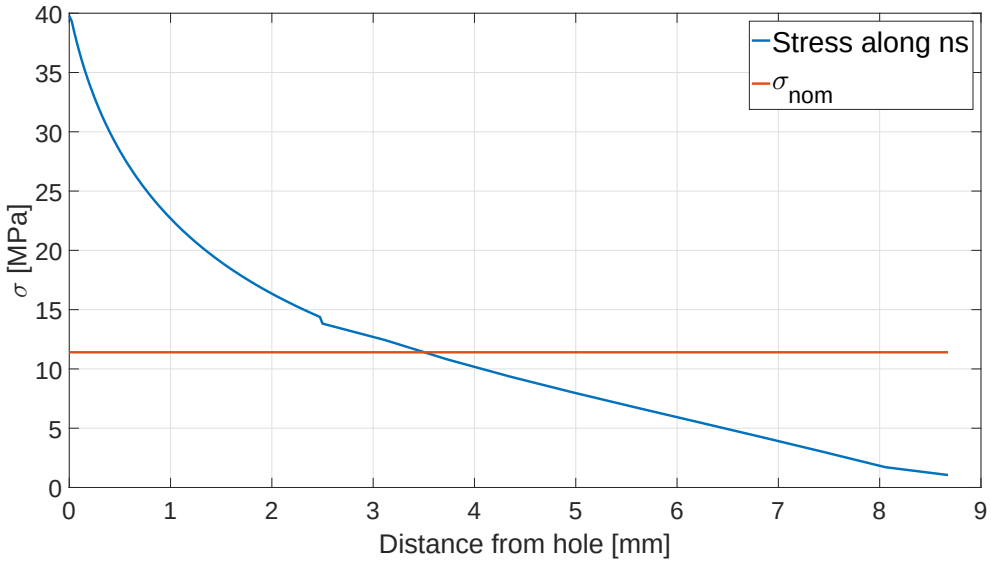

Figure C.2: Stress along the net section of case 1 at $P = 1000$ N

For the given dimensions the peak stress and nominal stress are higher than the reference lug. The FEA nominal stress equals 11.4 MPa. Calculating the nominal stress with Equation C.1 results in a nominal stress of 11.52 MPa. Here, the difference is 1.05%.

In order to compare the results, the assumption is made that the peak stress of the arbitrary lug is equal to the peak stress of the reference lug. Therefore, the load acting on case 1 has been altered such that the peak stress becomes equal to the peak stress of reference lug. From the new load condition the nominal stress has been calculated. The stress distribution and nominal stress for when the peak stress equals that of the reference lug is shown in Figure C.3.

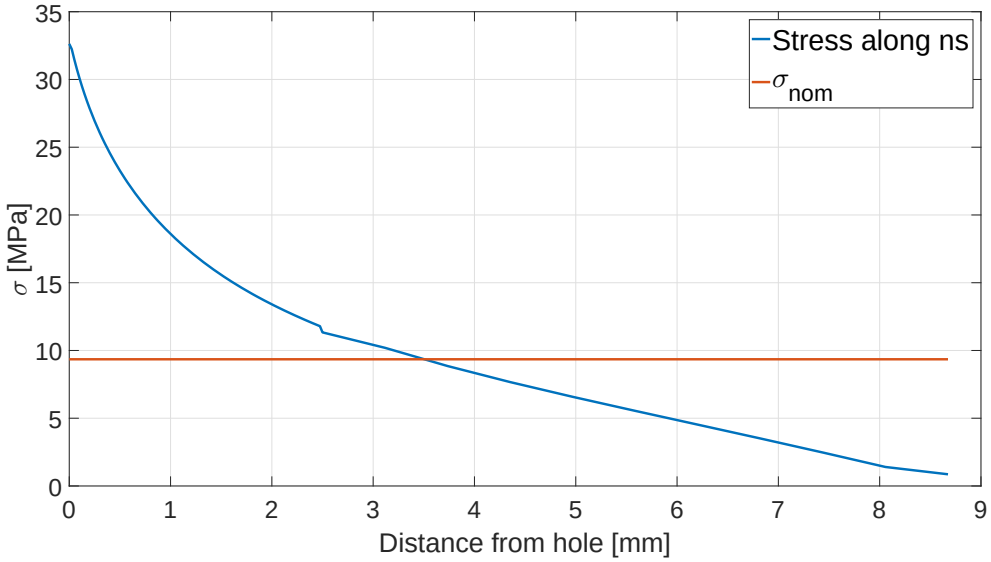

Figure C.3: Stress along the net section case 1 for equal peak stress to reference lug

At a load of 820 N, the peak stress of case 1 is comparable with the peak stress of the reference lug. The nominal stress now equals to 9.464 MPa, which is similar to the nominal stress of the reference lug. That the nominal stress is similar to the reference lug is not something that is always occurs when the peak stresses are equalized. Comparing the equal peak nominal stress with the analytical results in a difference of 1.07%

Case 2 and case 3 follow the same principle as described here for case 1. Both cases have been run for a load of $P = 1000$ N and at the load condition where the peak stress equals to the reference peak stress. The results for case 2 and case 3 are displayed in Section C.3 and Section C.4, respectively.

C.3 Case 2 Lug Results

Figure C.4 displays the stress distribution and nominal stress for a load of $P = 1000$ N. Figure C.5 presents the distribution and nominal stress for peak stress equals to reference peak stress. The small dip in the curve represents the location where the coarse mesh changes in a less coarse mesh.

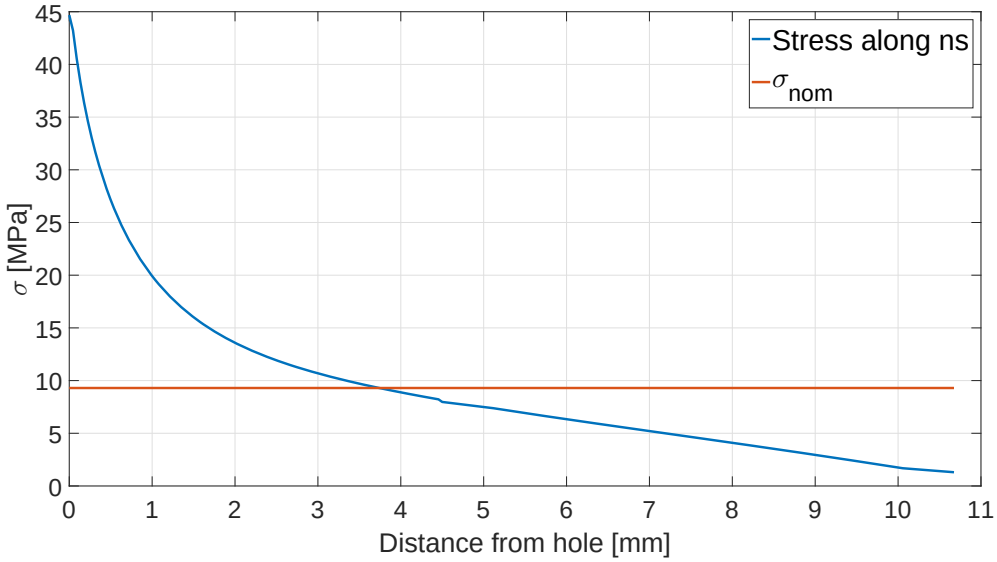

Figure C.4: Stress along the net section of case 2 at $P = 1000$ N

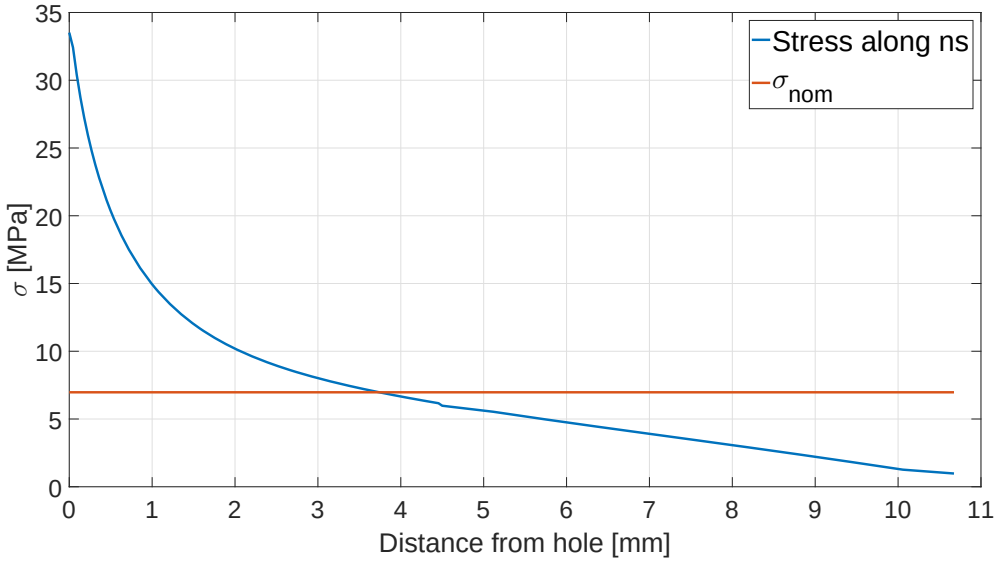

Figure C.5: Stress along the net section case 2 with equal peak stress to reference lug

The nominal stress for load $P = 1000$ N equal to 9.298 MPa and for the equal peak stress case the nominal stress is 6.973 MPa. A smaller diameter than the reference lug has been used for case 2. When the peak stress are equalized this results in a lower nominal stress compared to the reference lug nominal stress. This is mainly due to the fact that the net section area for case 2 is larger than for the reference lug. The analytical nominal stress for case 2 equals to 9.37 MPa for $P = 1000$ N. For equal peak the analytical nominal stress is 7.03 MPa. The differences between ABAQUS and the analytical are 0.79% and 0.84%.

C.4 Case 3 Lug Results

The stress distribution for case 3 for load $P = 1000$ N and for equal peak stress is presented in Figure C.6 and Figure C.7, respectively. The kink in the figure shows the location at which the mesh density changes.

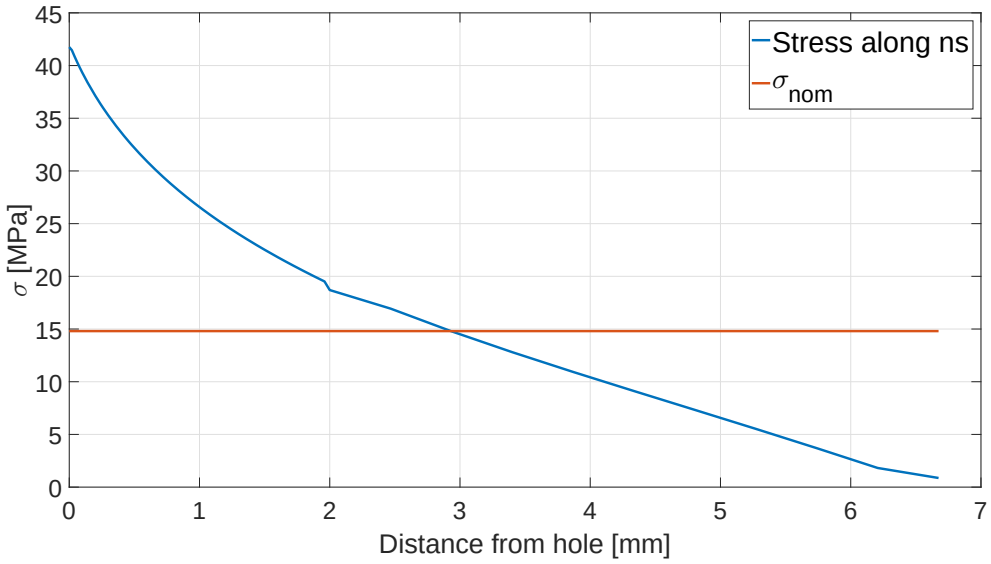

Figure C.6: Stress along the net section of case 3

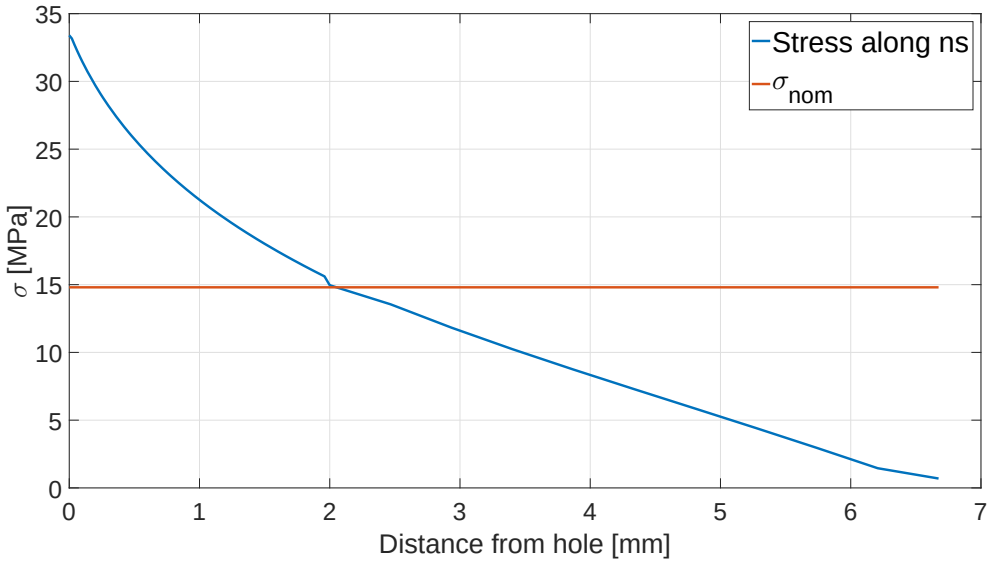

Figure C.7: Stress along the net section of case 3 for equal peak stress to the reference lug

The nominal stress for load case $P = 1000$ N equals to 14.8 MPa while for equal peak stress the nominal stress equals to 11.84 MPa. Here, the nominal stress is higher for equal peak stress due to the fact that the net section is smaller compared to the reference lug. Using Equation C.1 the nominal stress for $P = 1000$ N equals to 14.99 MPa. For the equal peak case the nominal stress is 11.99 MPa.

C.5 Summary overview of the results

The different sections presented the stress distributions and nominal stresses for the different cases. Table C.2 presents the different nominal stresses for the reference lug and the three cases. The last column represents the difference between the FE nominal stress and the analytical. Since the difference is around 1% for the nominal stress and the nominal stress calculated from Equation C.1 it has been chosen to take the nominal stress from FEA for all the analyses.

Table C.2: Nominal stress for the reference lug and the three cases for the different load conditions

Case	P [N]	FEA σ_{nom} [MPa]	Analytical σ_{nom} [MPa]	Difference [%]
Reference	1000	9.84	10.0	1.62
1	1000	11.40	11.52	1.05
1	830	9.46	9.56	1.07
2	1000	9.30	9.37	0.79
2	750	6.97	7.03	0.84
3	1000	14.80	14.99	1.28
3	800	11.84	11.99	1.28

Appendix D

Verification of the Out-of-Plane FEA using Deflections

In order to verify the results of the out-of-plane FEA, the deflection in the out-of-plane direction have been investigated. If the deflections of the out-of-plane model approximate the reality than the results produced by the out-of-plane FEA are verified. Since the SCF of the model is already verified with the TH3 method in Appendix B, the stresses of the out-of-plane model are verified when applying in-plane loads. The deflection of the FE model is compared with the deflections of the standard beam cases.

D.1 Cantilever beam with point load

A cantilever beam with a point load at the free end is one of the standard beam cases. Standard beam cases are load cases acting on beams for which the rotation and deflection of the beam can be approximated. The deflections of the standard beam cases are derived from the standard beam theory. When the deflections remain small, the standard beam theory applies to find the deflection characteristics of a beam.

Looking objectively to the out-of-plane lug model, it can be reduced to a cantilever beam subjected to a lateral point load and an axial load. First take a look at the cantilever beam with a later load at the free end. In Figure D.1 a representation of the cantilever beam with point load is shown.

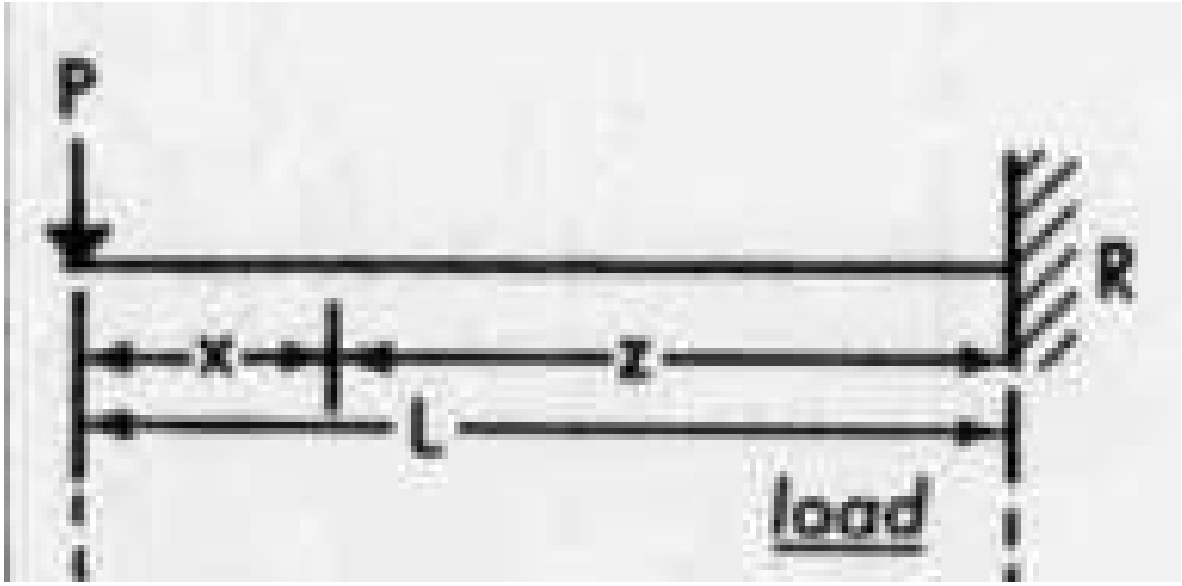

Figure D.1: Cantilever beam with a moment at the free end [24]

For the cantilever beam with a point load at the free end the displacement the standard case is defined as:

$$\delta = \frac{FL^3}{3EI} \tag{D.1}$$

Here, the E stands for the Young's modulus of the beam and the I is the second moment of area of the beam's cross-section. The moment of inertia given by:

$$I = \frac{1}{12}bh^3 \tag{D.2}$$

For simplicity, the lug is assumed to have a constant rectangular cross-section. In reality the lug has a hole present and has the rounding of the lug head which makes it so that the moment of inertia is not constant throughout the entire cross-section. The reference lug has been used for the out-of-plane models. The values of b, h and I are presented in Table D.1

Table D.1: Magnitude for the b, h, and I for beam bending

	b [mm]	h [mm]	I [mm^4]
Reference lug	30	5	312.5

In the 3D model the lateral load is applied on the pin. To simplify the lug to a cantilever beam the lateral load is assumed on the centre line of the pin. The length of the beam equals to the length of the lug to the centre of the hole.

In order to verify the displacement several simulation have been run under different applied loads. For each simulation, the U3 displacement at distance $L = 50$ mm from the clamping has

Table D.2: Lateral load cases with the deflections

	ABAQUS	Analytical	
F [N]	Deflection [mm]	Deflection [mm]	Discrepancy [%]
300	0.55	0.57	3.36
500	0.92	0.95	3.31
1000	1.84	1.90	3.18
1500	2.77	2.86	3.22
2000	3.69	3.81	3.22

been taken. The FE results are compared with the analytical result for the tip displacement. The load conditions and the deflections are presented in Table D.2.

Table D.2 shows that the deflections from ABAQUS and the analytical deflections have a 3% discrepancy between them. This is a very acceptable difference between the two results. The beam bending theory assumes a Euler-Bernoulli beam. On the beam there is a pure bending and all physical properties remain constant throughout the cross-section [25]. ABAQUS does not simulate a pure Euler-Bernoulli beam. The deflections in ABAQUS are also mesh dependent changing depending on mesh density and element type. Since a lug has been assumed to be a beam, the physical properties are in reality not constant throughout the entire cross-section. Therefore, the ABAQUS deflection are a close representation of the analytic solutions. Thus the deflection are verified.

D.2 Combined lateral and axial loaded cantilever beam

For the combined lateral and axial loaded cantilever beam the tip deflection are calculated via the standard beam theory. The combined case is separated in a lateral load case and an axial load case after lateral displacement. The lateral load deflection are presented in Section D.1. The axial load case after the lateral load is presented in Figure D.2.

Figure D.2: Cantilever beam with an axial load at the free end after lateral displacement [26]

The applied load is in tension resulting in a displacement in the opposite direction as the lateral displacement. Since there is an offset of δ between the line of action of the axial load and the clamping of the beam, a moment is induced. The moment has a magnitude of load P multiplied by displacement δ. The displacement of this induced moment is calculated by using the standard beam case of a cantilever beam with a moment on the free end illustrated in Figure D.3. The deflection equation for this load case is defined by:

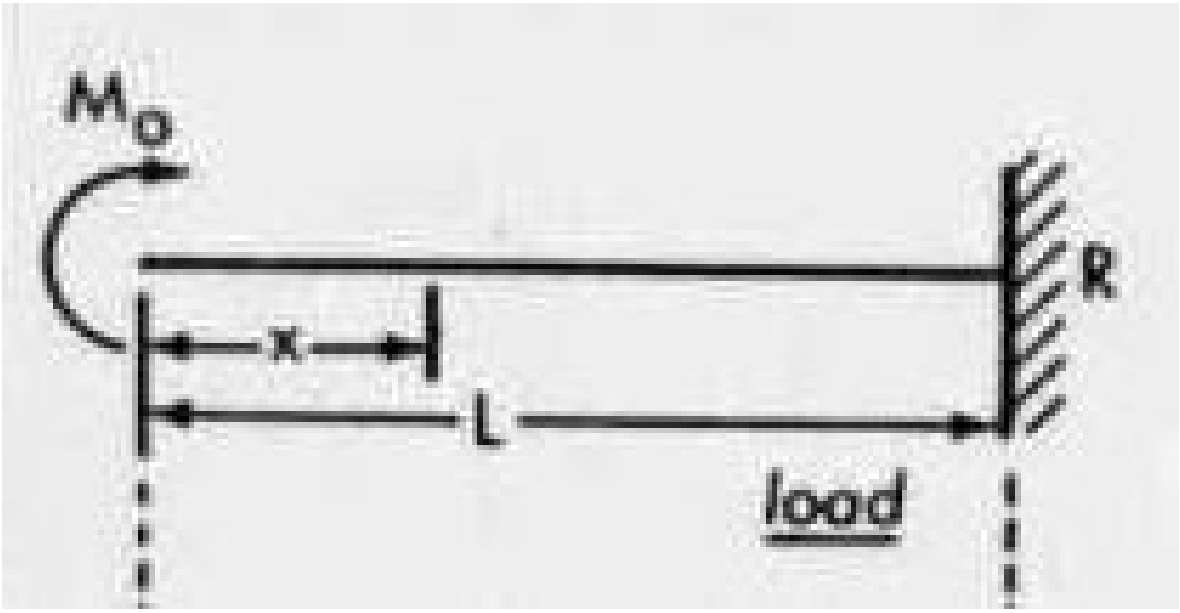

Figure D.3: Cantilever beam with a moment at the free end [24]

$$\delta = \frac{ML^2}{2EI} \tag{D.3}$$

The analytic solution for the combined axial and lateral deflection is the lateral deflection minus the axial deflection. The analytic solution is than compared with the U3 displacement in ABAQUS. In Equation D.4 the displacement equation for the combined case is presented. The axial load has been fixed at $P = 1000$ N. This axial load has been used throughout the in-plane FEA and therefore has been chosen for the out-of-plane FEA as well. The combined load cases and the deflections for each load combination are listed in Table D.3.

$$\delta_{combined} = \delta_{lateral} - \delta_{axial} = \frac{FL^3}{3EI} - \frac{(P \cdot \delta)L^2}{2EI} \tag{D.4}$$

Table D.3: Lateral and axial load case with the deflections

		ABAQUS	Analytical	
P [N]	F [N]	Deflection [mm]	Deflection [mm]	Discrepancy [%]
1000	300	0.56	0.54	3.80
1000	500	0.93	0.90	3.49
1000	1000	1.86	1.80	3.57
1000	1500	2.80	2.70	3.60
1000	2000	3.73	3.60	3.62

From the results of Table D.3 it shows that the discrepancy between the ABAQUS simulations and the analytic solution differs by around 3%. Again the same principles hold true as with only the lateral load. The deflections are mesh dependent and the simulation does not represent a perfect Euler-Bernoulli beam. Therefore, the deflections of the ABAQUS simulation are a close representation of the analytic solution and as such the results of the simulation are verified.

Appendix E

Out-of-Plane FEA NS Path

This appendix presents the different NS paths taken for the out-of-plane loaded lugs and the combined in- and out-of-plane loaded lugs. Three different paths have been used for defined the NS stresses for the FEA. The paths have been defined in the out-of-plane FE model and are on the top side of the male lug.

The NS stress path for the cases $k = 0.3$ and $k = 0.5$ are defined via the node line presented in Figure E.1. The NS stress path for the lug with bending factor $k = 1.0$ and $k = 1.1$ are presented in Figure E.2. The NS stress path for $k = 1.2$, $k = 1.5$, and $k = 2.0$ are displayed in Figure E.3.

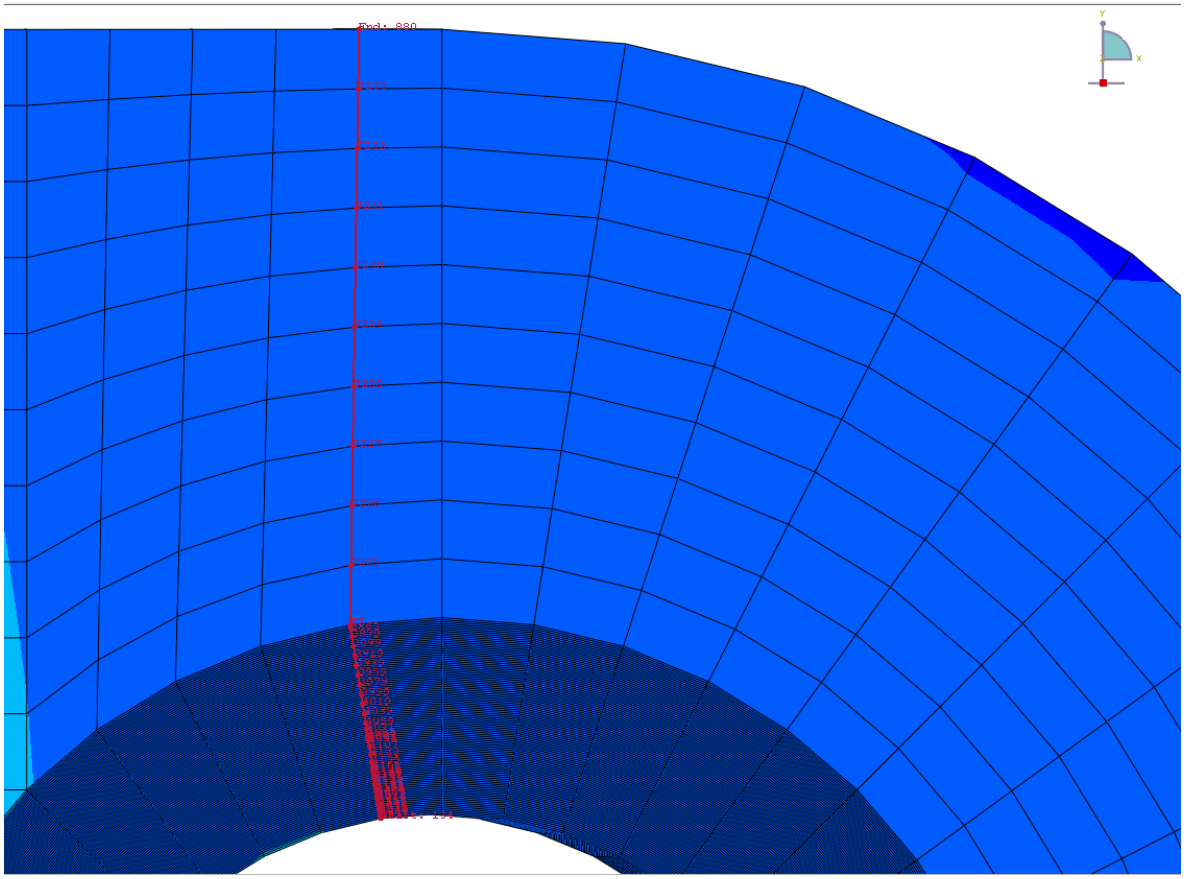

Figure E.1: NS path for $k = 0.3$ and $k = 0.5$

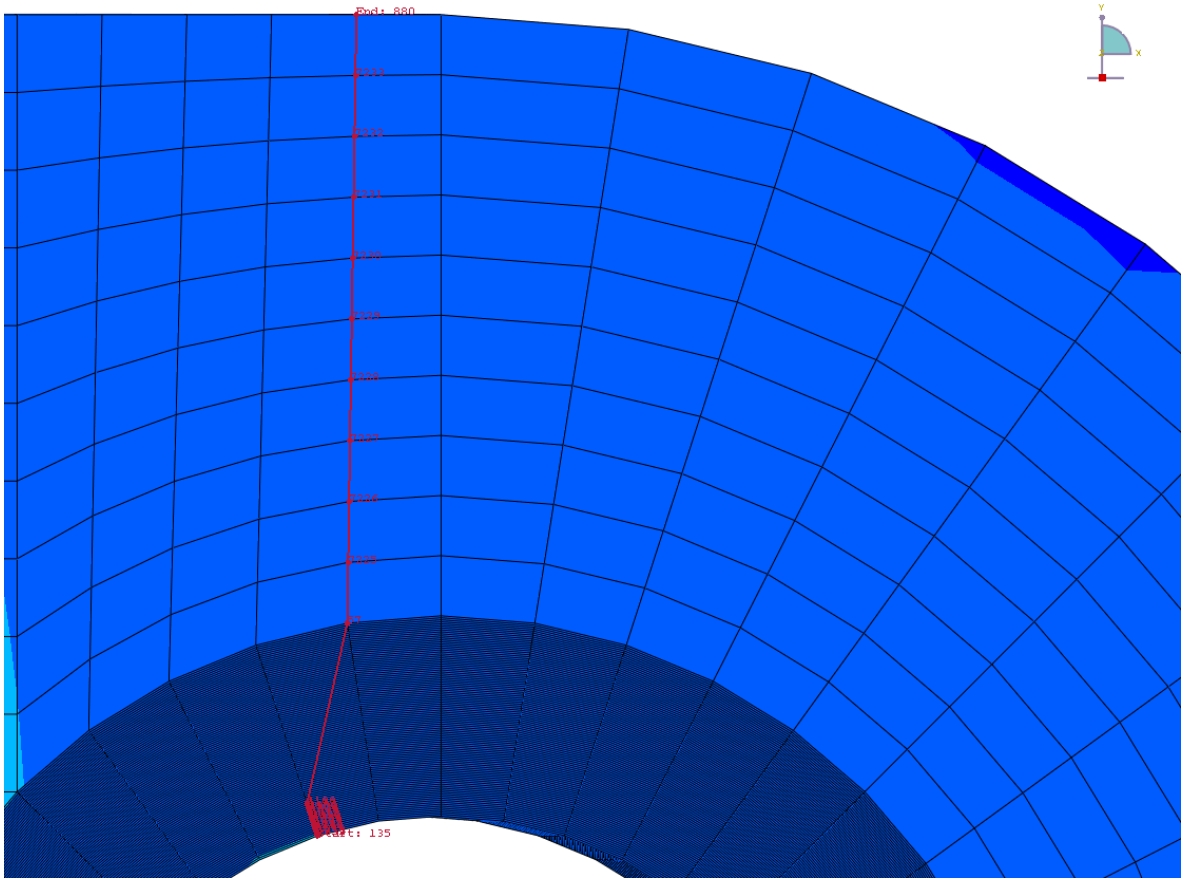

Figure E.2: NS path for $k = 1.0$ and $k = 1.1$

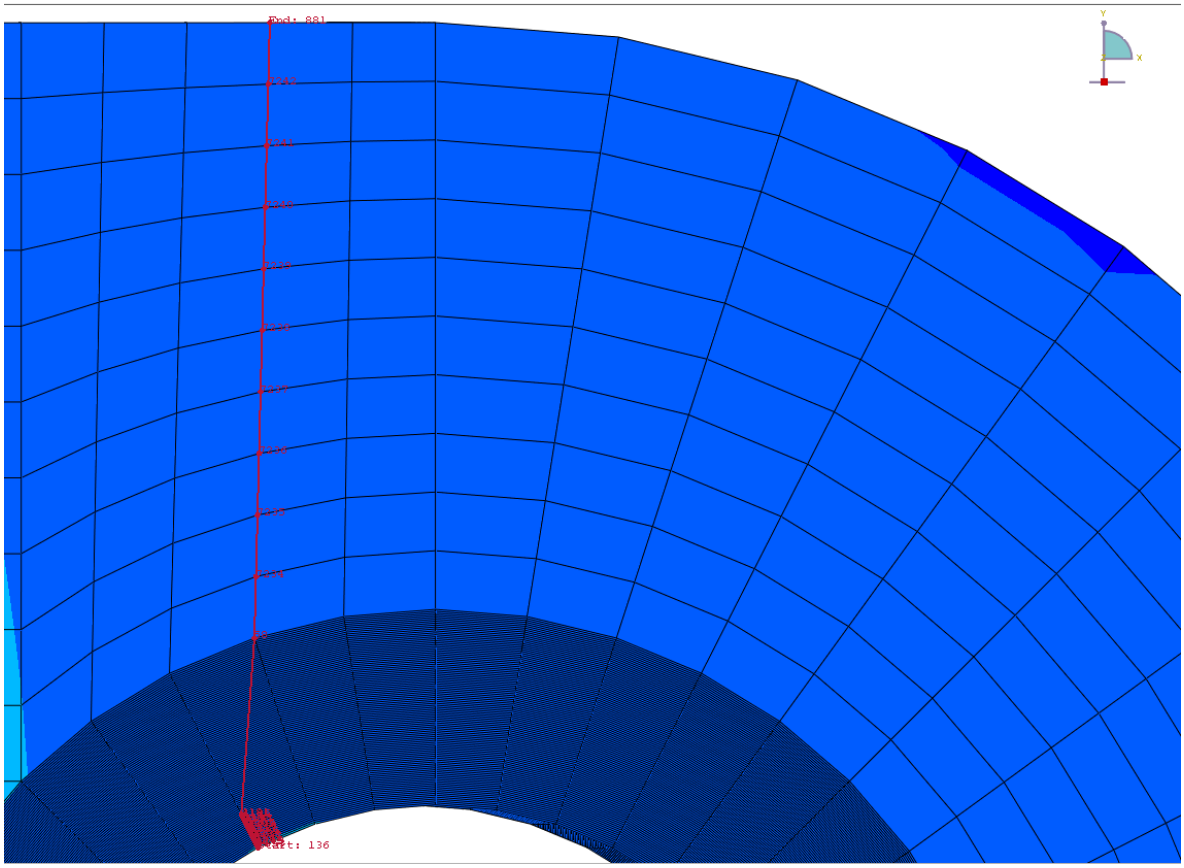

Figure E.3: NS path for $k = 1.2$, $k = 1.5$, and $k = 2.0$

Appendix F

Taper Analyses

In the taper analyses presented in Chapter 7 the geometry parameter c has not been updated to account for the taper. The distance c should increase with the addition of taper angle to a new distance c^*. Implementing c^* into the taper angle analyses and into the combined taper and load angle analyses has great consequences to the observations stated in Chapter 7.

F.1 Taper analyses results for c^*

First the distance c^* has been taken from the FE model for the different case lugs. The distance c which has been used and the distance c^* are presented in Table F.1.

Table F.1: Distance c^* for the tapered lug cases

Lug	c [mm]	c^* [mm]
a5	10	10.87
c15	15	16.28
a10c10	10	10.96
a15	10	10.96
c5	5	5.64

For every case the distance c has increased. According to the Larsson relation the distance c is used in the shape function. The shape function k_1 is defined as:

$$k_1 = \sqrt{\frac{a \cdot d}{c^2}} \tag{F.1}$$

The distance c is squared in the shape function as seen in Equation F.1. Thus when c^* is implemented, the shape function reduces in magnitude. The k_1 values using distance c and c^* are presented in Table F.2. The shape function for c^* is given as k_1^*. The size factor k_2 remains the same since the size factor is only dependent on the diameter of the hole.

Table F.2: Shape function

Lug	k_1	k_1^*
a5	0.707	0.651
c15	0.667	0.614
a10c10	1.000	0.912
a15	1.225	1.117
c5	2.000	1.773

From the analyses for the taper angle in Chapter 7 it has been concluded that no taper correction factor was required. When updating the shape factor to k_1^*, the taper analyses present something differently. The results using k_1^* are presented in Table F.3. The error as reported in Chapter 7 is presented in the column error Table 7.1. The Larsson relation including the K_{ecc} factor is defined as:

$$\frac{\sigma_{nom}}{\sigma_{nom_{ref}}} = k_1 k_2 K_{ecc} \tag{F.2}$$

Table F.3: Results using k_1^* for lugs with $\alpha = 0°$ and $\beta = 20°$

Lug	$\frac{a}{c}$	K_{ecc}	$\frac{\sigma_{nom}}{\sigma_{nom_{ref}}}$	$k_1^* k_2$	$k_1^* k_2 K_{ecc}$	Error Table 7.1 Equation F.2 [%]	Error k_1^* Equation F.2 [%]
a5	0.5	1.207	0.848	0.651	0.854	0.68	-7.96
c15	0.667	1.157	0.756	0.614	0.771	1.98	-6.38
a10c10	1.0	1.056	1.033	0.912	1.056	2.23	-7.15
a15	1.5	0.905	1.111	1.117	1.109	-0.21	-9.83
c5	2.0	0.754	1.541	1.773	1.508	-2.16	-15.24

Comparing the two errors it shows that the errors have now increased. The lug case c5 even falls outside the margin of error of ±15%. When the error is larger than ±15% a correction factor is required. Thus from these results a taper correction factor should be added.

The analyses for the combined taper and load angle concluded that no correction factor is required. When updating the shape factor to k_1^* resulted in the following results presented in Table F.4. The Larsson relation for these analyses included the load angle correction factor K_α and is defined as:

$$\frac{\sigma_{nom}}{\sigma_{nom_{ref}}} = k_1 k_2 K_{ecc} K_\alpha \tag{F.3}$$

Table F.4: Results using k_1^* for lugs with $\alpha = 45°$ and $\beta = 20°$

Lug	$\frac{a}{c}$	K_{ecc}	K_α	$\frac{\sigma_{nom}}{\sigma_{nom_{ref}}}$	$k_1^* k_2 K_{ecc} K_\alpha$	Error Table 7.4 Equation F.3 [%]	Error k_1^* Equation F.3 [%]
a5	0.5	1.207	1.270	1.023	1.204	5.60	15.00
c15	0.667	1.157	1.113	0.832	0.915	3.05	9.04
a10c10	1.0	1.056	0.955	0.925	0.972	8.26	4.80
a15	1.5	0.905	0.850	0.915	0.778	2.89	-17.58
c5	2.0	0.754	0.798	1.303	0.804	-8.33	-62.04

From the combined taper and load angle analyses using k_1^* it is clear that all the errors have increased compared with the prior results. The ±15% margin is exceeded for the a15 and c5 cases using k_1^*.

Implementing the c^* distance in the tapered lug analyses shows that a correction factor that accounts for the taper angle is required. A taper correction factor is proposed in Section F.2. The effects of the taper correction factor on the tapered lug analyses and the combined taper and load angle analyses is presented here. Recommendations are given in Section F.3

F.2 Taper correction factor

From the tapered lug of $\beta = 20°$ presented in Table F.3 the error trend for the different eccentricity ratio is found. For the taper correction factor K_β the same principle as with the load correction factor K_α is applied. The taper correction factor is dependent on the taper angle and the eccentricity and is defined as:

$$K_\beta = \beta \cdot \left(0.0031 \cdot \left(\frac{a}{c}\right)^2 - 0.0051 \cdot \left(\frac{a}{c}\right) + 0.0055\right) + 1 \tag{F.4}$$

As with the K_α, K_β equals to 1 when the taper angle equals to $\beta = 0$. The values of Equation F.4 for the different eccentricity ratios is presented in Figure F.1.

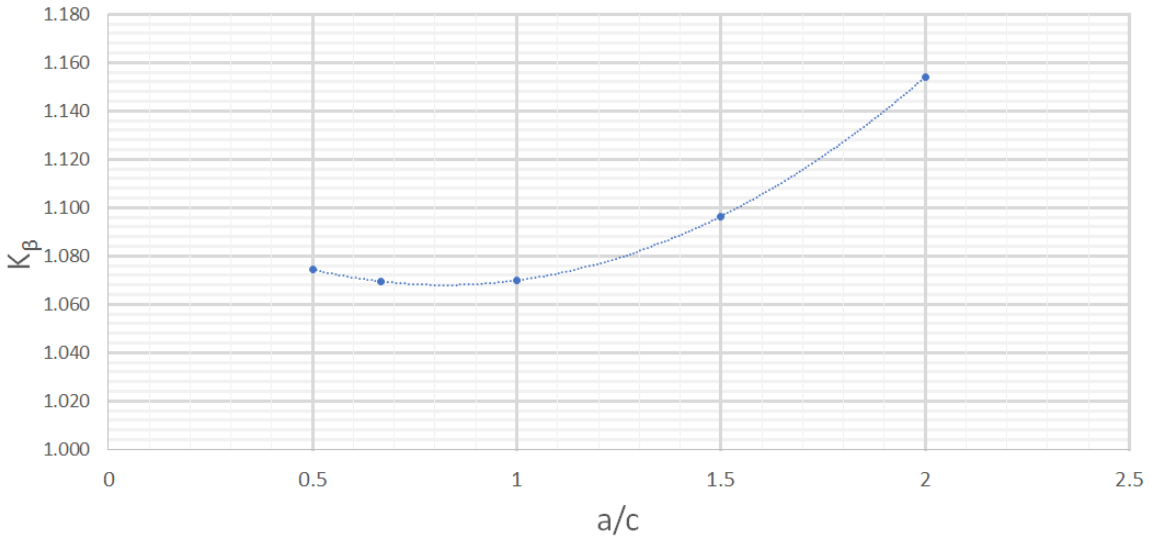

Figure F.1: The K_β expressed against the eccentricity

The K_β factor is added to the Larsson relation according to the same method as the prior correction factors. This results in a Larsson relation including the K_{ecc}, K_α, and K_β defined as:

$$\frac{\sigma_{nom}}{\sigma_{nom_{ref}}} = k_1 k_2 K_{ecc} K_\alpha K_\beta \tag{F.5}$$

Do note that for k_1 the values for k_1^* are substituted.

Applying the K_β to the tapered lug analyses reduces the error in Larsson because of the taper angle. The results are presented in Table F.5.

Table F.5: Results using k_1^* and K_β for lugs with $\alpha = 0°$ and $\beta = 20°$

Lug	$\frac{a}{c}$	K_β	$\frac{\sigma_{nom}}{\sigma_{nom_{ref}}}$	$k_1^* k_2$	$k_1^* k_2 K_{ecc} K_\beta$	Error Equation F.2 [%]	Error Equation F.5 [%]
a5	0.5	1.075	0.848	0.651	0.844	-7.96	-0.48
c15	0.667	1.070	0.756	0.614	0.760	-6.38	0.54
a10c10	1.0	1.070	1.033	0.912	1.031	-7.15	-0.14
a15	1.5	1.097	1.111	1.117	1.109	-9.83	-0.16
c5	2.0	1.154	1.541	1.773	1.543	-15.24	0.14

Introducing the K_β factor in the taper analyses reduces the error to nearly zero. Keep in mind that the factor is created on the data of $\beta = 20°$. Further analyses into the verification of the K_β should be performed.

The results of implementing the taper correction factor in the analyses for taper angle $\beta = 20°$ and load angle $\alpha = 45°$ is presented in Table F.6. The results show that with the implementation of the K_β factor for the cases a5 and c5 the error is larger than the $\pm 15\%$ error margin.

Table F.6: Results using k_1^* for lugs with $\alpha = 45°$ and $\beta = 20°$

Lug	$\frac{a}{c}$	K_β	$\frac{\sigma_{nom}}{\sigma_{nom_{ref}}}$	$k_1^* k_2 K_{ecc} K_\alpha K_\beta$	Error Equation F.3 [%]	Error Equation F.5 [%]
a5	0.5	1.075	1.023	1.294	15.00	20.89
c15	0.667	1.070	0.832	0.978	9.04	14.96
a10c10	1.0	1.070	0.925	1.040	4.80	11.03
a15	1.5	1.097	0.915	0.853	-17.58	-7.23
c5	2.0	1.154	1.303	0.928	-62.04	-40.42

Although the taper correction factor improves the taper analyses results, the combined taper and load angle is not sufficiently covered with the correction factor alone. Suggestions for improvement and further recommendations into the taper analyses are presented in Section F.3.

F.3 Recommendations

For the combined taper and load angle cases the addition of a taper correction factor in Larsson is not sufficient for all cases to fall within the $\pm 15\%$ margin. Both the factors K_α and K_β are linked by the eccentricity ratio $\frac{a}{c}$. The results in Table F.6 indicate that a potential relation between the taper angle and load angle is present. To compensate for a relation between the two angles a correction factor depending on α and β is required. To investigate this relation further analysis have to be performed over a range of different α and β.

In the current study presented in Chapter 7 the eccentricity varied via the five lug case while the taper angle is fixed to 0° or 20° and load angle is fixed to 0° or 45°. By varying the taper angle between $0° \leq \beta \leq 20°$ and load angle between $0° \leq \alpha \leq 45°$ per eccentricity lug case a range of data points is created. By performing a regression study on these data points a correction factor between α and β can be created. The regression study can be used to improve the already proposes correction factors K_{ecc} and K_α.